Abstract

Regional variation of convective structure at monsoon onset across South America inferred from TRMM observations

by Richard Barnhill

May 2010

Director: Dr. Burrell Montz

DEPARTMENT OF GEOGRAPHY

The variation of precipitation in South America is characterized by different mechanisms that both initiate and sustain precipitation. Analysis to characterize regional differences is done utilizing datasets derived from the Tropical Rainfall Measuring Mission (TRMM) satellite as well as National Center for Environmental Prediction (NCEP) Reanalysis data. Four regions were studied. These included the Amazon Basin (West), northeast coast (East), location of the South Atlantic Convergence Zone (SACZ), and extreme southeastern Brazil (South). In these regions, variables such as rain rate, feature size, lighting flash counts, updraft strength, and thermodynamic fluxes were analyzed.

Before onset in the Amazon Basin, sensible heat flux increases and is well correlated with increases in lighting flash counts that were observed using TRMM, implying thermodynamic forcing. After onset, the features become less electrified, however their frequency and rain rates increase. The East region experiences similar pre and post-onset behavior, however oceanic influence not only limits the vertical intensity of convection, but also acts to delay the timing of onset by two months, compared to the West.

Fronts are the dominant driver of precipitation in the SACZ region, increasing in

frequency as onset approaches. Time series analysis from TRMM illustrates high variability in precipitation and increases in frequency of features here that is consistent with an increase in frontal activity. Also, composite directional wind plots using NCEP 850 mb wind data, reveals interactions between the Tropics and sub-Tropics. Pre-onset MCCs dominate South time series and frontal intrusions drive precipitation in the post-onset period.

Understanding distinct regional mechanisms of precipitation can increase the predictability of monsoon onset all over South America. This is important for those who live there and depend on seasonal rains for their livelihood. Also, knowing what mechanisms are working in different regions at different times of the year and incorporating their respective contributions to the global heat budget, we can increase the accuracy of global models. The next step would be to use these observations to model the observed regional variability and timing, and identify the contributions and long-term implications of heat release from the South American Monsoon System (SAMS) on the global scale.

Regional variation of convective structure at monsoon onset across South America inferred from TRMM observations

A Thesis

Presented To

The Faculty of the Department of Geography

East Carolina University

In Partial Fulfillment

of the Requirements for the Degree

Master of Geography

by

Richard Barnhill

May 2010

Regional variation of convective structure at monsoon onset across

South America inferred from TRMM observations

by

Richard Barnhill

APPROVED BY:

DIRECTOR OF THESIS:_____

Dr. Thomas Rickenbach, PhD

COMMITTEE MEMBER:_____

Dr. Rosana Nieto-Ferreira, PhD

COMMITTEE MEMBER:_____

Dr. Jennifer Arrigo, PhD

CHAIR OF THE DEPARTMENT OF GEOGRAPHY:

_____

Dr. Burrell Montz, PhD

DEAN OF THE GRADUATE SCHOOL:

_____

Paul J. Gemperline, PhD

TABLE OF CONTENTS

LIST OF FIGURES

LIST OF TABLES

CHAPTER 1: INTRODUCTION AND REVIEW OF LITERATURE

Understanding the seasonality, distribution, and intensity of precipitation in the Tropics is important because these aspects have an influence on climate patterns all over the world. Large tropical cloud systems are responsible for massive release of heat and moisture, which is then transported toward the poles through global circulations. In South America, understanding if and when the monsoon occurs is important for the local societies who depend on the seasonal rains for farming and power. Much of the land drains into the major rivers, responsible for hydroelectricity generation, and is also subsequently used for farming, are located in regions that are affected significantly by the summer monsoon rains (Grimm and Zilli, 2008). Also, the monsoon affects the entire globe due to the heat released in these precipitating systems, which contributes to factors that drive weather patterns globally.

This research focuses on South America, and more specifically, the Amazon Basin to understand the different mechanisms responsible for the onset of the South American Monsoon and also trying to better understand its predictability. Through careful analysis of high-resolution satellite data, a storm-based characteristics dataset, and data of surface variables, the regional mechanisms for monsoon onset variability are addressed.

1.1 General Monsoon Features

Unlike the monsoons in Southeast Asia and India, the South American monsoon system is not as well understood. South America is a region that has not been as well studied as the other monsoon regions of the world and in fact, many researchers have debated whether or not South America actually has a true monsoon climate. Over the past several decades, analysis has progressed from simple empirical observations to more sophisticated satellite and model analyses.

According to the traditional definition of Ramage (1971) monsoon climates are recognized by seasonal reversals in low-level wind direction. Previous research in this region has concluded that because the winds in the lower part of the troposphere do not reverse on a seasonal time scale, South America is not a monsoon region. Many argue that the orientation of the South American continent prevents a defined monsoon climate from existing because the narrowing of the continent as it extends to the south was thought to limit the ability for large-scale circulations to form to drive the monsoon circulations (Ramage 1971).

Zhou and Lau (1998) define monsoon as a seasonal change in the continental-scale circulations due to a heating difference between oceanic and continental regions. This can be accomplished through many processes such as the land heating up much faster than the ocean due to the differences in heat capacity of land vs. water and causing a direct, onshore circulation to become established. Zhou and Lau (1998) and Kousky (1985) discuss the development of what is known as the Bolivian High, which is essentially a warm core anticyclone that is a result of heat fluxes from both the surface and also from convection in the Amazon Basin, which marks the establishment of the South American monsoon. The establishment of this large anti-cyclone in the upper troposphere over the high desert "Altiplano" region of Bolivia is a result of two factors. First, latent heat is released high in the troposphere by convection that has become established in the Amazon basin (Silva Dias et al., 1983). Second, sensible heat is released into the mid-troposphere as the high desert is heated by solar radiation (Lenters and Cook, 1997).

Until observations of this large upper atmosphere circulation, earlier work argued against a monsoon climate in South America. A paradigm shift occurred in the identification of South America as possibly having a monsoon climate after it was determined that the Altiplano Plateau in Bolivia had the ability to provide the heat that helps to establish large-scale circulations to

drive monsoon circulations (Rao and Erdogan 1989). Specifically, the heat sources that would help drive the circulation would be in for form of surface sensible and latent heat fluxes.

Equation 1 describes how latent heat flux is determined.

$$\textit{Latent Heat Flux} = C_e|V|[q_{sat}(T_s) - q_{air}] \qquad (1)$$

Where C_e is the bulk transfer coefficient for moisture, V is the wind speed, q_{sat} is the specific humidity at the surface (assumed to be the surface saturation value), and q_{air} is the specific humidity of the air (Wallace and Hobbs, 2006). Thus, latent heat is dictated primarily by the difference between the surface specific humidity and the specific humidity of the local environment. This gives the relationship that the larger the difference, the higher the latent heat flux. The optimal situations for large values of latent heat flux are a local atmosphere that is dry and a surface that is close to saturation. Another variable here that dictates the strength of the latent heat flux is the mean wind speed, which can provide a high latent heat flux value, without the condition of a large humidity difference.

Fu and Li (2004) argue that the presence of high humidity values in the lower troposphere cause a large latent heat flux that helps dictate the strength of the Bolivian High (Fu and Li, 2004). They argue higher fluxes of surface latent heat alter the thermodynamic profile of the atmosphere, causing the vertical profile to change such that there is less Convective Inhibition (CIN) and increased amounts of Convective Available Potential Energy (CAPE). This type of profile supports a more convective regime and through increased convection, even more latent heat is released from storms into the atmosphere, which eventually drives the upper level circulation over South America, the Bolivian High. However, Fu and Li (2004), note that heat fluxes do not necessarily dictate when and how strong the atmospheric circulations and that they are often influenced by external large-scale forces.

Another heat flux that is present in the Altiplano, more so during the dry season, is sensible heat flux. Equation 2 describes the relationship by which sensible heat is calculated.

$$Sensible\ Heat\ Flux = C_H|V|(T_s - T_{air}) \qquad (2)$$

Again, C_e is the bulk transfer coefficient for heat, V represents the mean wind speed, T_s is the surface temperature, and T_{air} is the local air temperature. Sensible heat flux is very much contingent upon the surface being much warmer than the local atmosphere, which drives the temperature difference upward. Also, by increasing the winds, the difference between the surface and air temperatures do not need to be as drastic as if there were no wind (Wallace and Hobbs, 2006). High values of sensible heat flux are either achieved by having large temperature differences between the surface and air without wind, or a relatively low difference with strong wind. The warming of the surface of the Earth in the dry season in the Altiplano region acts to destabilize the atmosphere (Fu et al, 1999) in the late dry season, adding to the surface sensible heat flux, altering the low level lapse rate, and increasing the convective potential. The increase in sensible heat flux during the day creates positive conditions for convective activity by altering the lower tropospheric static stability (Wallace, 1975) and contributes to the observed diurnal cycle of convection in certain regions of South America. This reduction in static stability drives convection and this convection releases latent heat into the upper atmosphere, similarly to storms driven by surface latent heat flux. Both of these fluxes help to drive convection and eventually contribute to amplifying the large-scale upper-level circulation that is commonly associated with the South American monsoon.

Fu and Li (2004) suggest that the transition from dry to wet season is partially driven by changes in surface latent and sensible heat fluxes. They argue that by altering the thermodynamic nature of the atmosphere, storms can form and rain can begin to fall even before the larger scale

monsoon precipitation mechanism is in place. These processes are observed to be important in the pre-monsoon and become more obscured by the larger scale precipitation once the monsoon is active (Fu and Li, 2004). Atmospheric dynamical adjustment to these fluxes serve to increase the available energy in the atmosphere by increasing the tendency of parcels of air to ascend, which results in rainfall increasing (Li and Fu, 2004). The increase in rainfall serves to release latent heat in the upper troposphere, which contributes to the eventual establishment of the larger scale flow that drives the monsoon regime. One other connection that Li and Fu (2004) suggest concerning surface fluxes is the relative time that it takes for the monsoon to begin (onset). They suggest that when these processes cause an early increase in rain, that the large-scale processes take over earlier than when the rain increases later in the season, thus the surface fluxes are a determining factor in when onset occurs in some regions.

Kousky (1985) utilized analysis of upper level winds and outgoing long wave radiation to diagnose upper atmospheric circulation patterns associated with the rainfall in Brazil. Outgoing long wave radiation (OLR), which is a measure of infrared radiation (converted to a temperature value) that is leaving the Earth, is a good proxy for rainfall since negative values of OLR are often associated with high clouds (which are colder than the surface of the Earth). These high clouds are often indicative of strong and vertically developed convection that has produced a large anvil cloud. The resulting assumption is that where OLR is below a given temperature threshold, it is raining heavily. Kousky (1985) identified regions over the Atlantic Ocean and South America in both the upper and lower troposphere that signaled that a monsoon regime was beginning to take shape. One of these features is an 850-mb anticyclone known as the Atlantic Sub-tropical High and its north and south movement impacts rainfall in the region, specifically in the northeast. The Atlantic Sub-tropical High is important because of its impact driving moisture

into the continent from the ocean. Fu et al (1999) note that a feature that is created from the moist onshore flow and is a key feature in the monsoon in South America is the southward turning of the easterly low-level jet known as the South American Low-level Jet (SALLJ). When the Atlantic High migrates northward and slightly westward, it acts to enhance the easterly low-level jet and results in a southerly jet coming off the eastern side of the Andes. This southward enhancement acts to draw more moisture southward into the central and southern regions of the Amazon, supplying moisture to a region that is usually thermodynamically primed for convection. One of the resulting features from this southward transport of moisture is the South Atlantic Convergence Zone (SACZ), which is a region of enhanced convection that is caused by fronts stalling and interacting with features such as the southerly moisture transport. Figure 1.1 summarizes all of the important features and circulations involved with the South American monsoon (from Zhou and Lau, 1998).

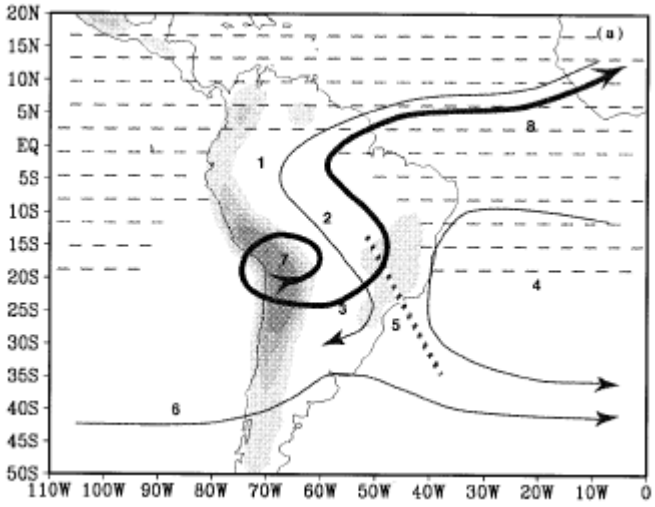

Figure 1.1: 1) low-level cross equatorial flow, 2) northwesterlies 3) Gran Chaco low 4) subtropical high 5) SACZ, 6) midlatitude westerlies, 7) Bolivian high, and 8) upper-level return flow. (From Zhou and Lau, 1998)

While it is important to know that a monsoon climate exists and how it occurs, understanding the climatology of precipitation is vital to determining regions that may be affected by the seasonal shift in precipitation pattern. Negri et al. (2000) use satellite microwave

data to analyze the precipitation climatology of the Amazon. Although Negri et al. (2000) did not specifically address the monsoon; it did identify specific features in the Amazon where rainfall occurs in large amounts yearly. One of these regions is in the northwest Amazon basin where Negri et al. (2000) suggests that the high rainfall totals are mostly caused by thermodynamically driven processes, though there are possibly other sources of precipitation such as coastal squall lines and transient Mesoscale Convective Systems (MCSs) (propagating squall lines associated with frontal systems that move across this region in a matter of days) from the sub-Tropics that also contribute to rainfall here. Another region of high rainfall is at the mouth of the Amazon River, which is also closely associated with the average position of the Atlantic Inter-Tropical Convergence Zone (ITCZ) (Negri et al.., 2000). Since these regions are climatologically favored to receive the most rain in the region, being able to identify the specific mechanisms that contribute to these totals will help tie together the monsoon as a whole because more than likely, the same mechanisms present in these regions are also at work elsewhere.

1.2 Monsoon Onset Date Determination

It is important to objectively determine the onset date of the monsoon so that one is able to characterize monsoon seasonality, regional variability, and also interannual variation. Marengo et al. (2001) address this issue by developing a definition of onset in the South American Monsoon System (SAMS) in terms of the start date of sustained rainfall. Previous work (Horel et al. 1989, Kousky 1988, and Ramage 1971) used outgoing long wave radiation, low level winds, horizontal moisture flux, as well as precipitation to develop an onset criterion. However, Marengo et al. (2001) use rainfall thresholds using rain gauge data interpolated to 2.5-degree resolution grid boxes throughout the region to define when the monsoon begins and ends.

Nieto-Ferreira and Rickenbach (2010) developed an improved definition of onset in South America, using the GPCP dataset. GPCP is a dataset that utilizes geostationary IR satellites to quantify rainfall. The main advantage of this dataset is that it is excellent for sampling temporally, but due to the limited resolution of the IR satellites, its spatial resolution is reduced, especially compared to rain gauge data. Nieto-Ferreira and Rickenbach (2010) expanded on the onset definition of Marengo et al. (2001) using GPCP because it is able to cover regions in South America that are not covered by the rain gauge network that Marengo et al. (2001) relied upon. Nieto-Ferreira and Rickenbach (2010) used a rainfall threshold and pentad averaging over a network of grids over South America, similar to Marengo et al. (2001), to define onset.

The objective onset algorithm was applied over a gridded network of boxes in South America that were 5^{o} X 5^{o}. Using the GPCP dataset, it was determined that the average rain rate over the continental portion of the study region was 4.6 mm day^{-1}. A box was determined to have reached onset if at least 75% of the future 8 pentads from a current pentad had rain rates at or above 5.1 mm day^{-1}. Also, 75% of the previous 8 pentads needed to achieve a rain rate of 4.1 mm day^{-1} or less in order for a pentad to qualify as the onset pentad. The Nieto-Ferreira and Rickenbach (2010) criteria were higher in both the maximum and minimum thresholds, compared to Marengo et al. (2001). The new maximum value is .6 mm day^{-1} higher than the 4.5 mm day^{-1} as prescribed by Marengo et al. (2001) and the new minimum value of 4.1 mm day^{-1} is again .6 mm day^{-1} higher than the old threshold. A caveat that the new definition included was accountability of variability in different parts of the study region where break periods can occur during the monsoon season. To account for this, if the original criteria were not met, then as long as 37% of the future 8 pentads had rain rate values that were double the threshold value of 4.6

mm day^{-1}, then that pentad would still qualify as the onset pentad (Nieto-Ferreira and Rickenbach, 2010). By setting the precipitation thresholds higher, some of the variability that came with the Marengo et al. (2001) definition should be smoothed out by not including dates that barely fit the original definition and only including dates where is more of a disconnect between active and break periods.

1.3 Observations of Monsoon Precipitation Structure

After objectively defining onset, the next issue to contend with is the best way to observe and subsequently analyze the regional differences in precipitation system structure and environmental characteristics over the study region. An observation platform of precipitation that improves on infrared satellite observations, utilized in previous studies, are passive microwave satellites. Microwave imagers are vital to observing precipitating systems because unlike infrared satellites, microwave imagers are able to see into clouds to observe structure rather than just the tops of the clouds. Kummerow and Giglio (1994) describe relating cloud microwave brightness temperatures to precipitation using radiative transfer models as a key to creating algorithms for these satellites to determine rain rates and the vertical structure of clouds. The ability to distinguish between a cloud that contains a large volume of ice particles compared to a cloud that contains only liquid water allows for the distinction between deep convection that can produce large volumes of rain, shallow convection with weaker updrafts, and stratiform rain which tends to be much lighter though covering a larger area. The imager is able to do this through detection of an ice scattering signature, which implies that the imager observes the microwave radiation from particles within the clouds and is able to make the determination of what is there based on known properties of specific particles (Kummerow and Giglio 1994).

One of the main advantages of the microwave imager is the 85 GHz signal from the imager, which helps reveal ice scattering processes in the tops of strongly convective clouds (Mohr et al. 1998). The 85 GHz frequency is sensitive to both liquid water and ice particles. In deep convection, which contains ice particles, microwave radiation from the earth's surface is scattered, giving a different microwave return than liquid water drops, which do not scatter the microwave energy. In what will become an important tool for future studies, Mohr et al. (1998) show a linear relationship between rainfall and ice scattering at the 85 GHz frequency. This relationship allows for the interpolation of rain rates derived solely from the microwave signal observed from the satellites.

In their study, Mohr et al. (1998) utilized the Special Sensor Microwave/Imager (SSM/I) on the Defense Meteorological Satellite, which came equipped with a microwave imager, to enhance observations of tropical rainfall characteristics using microwave data. Their objective was to understand what types of systems contributed most to Tropical rainfall, using microwave data to characterize rain system structure. The ability to observe rainfall in such a remote area with a satellite, lead to not only the microwave/rain rate relationship, but also improved correction for possible errors in ground based rain measurements.

Another conclusion that Mohr et al. (1998) discussed is that mesoscale convective systems (MCSs) are a major contributor in the overall rainfall picture in the Tropics, although they only accounted for a small percentage of the total number of precipitating systems. MCSs are responsible for releasing heat into the atmosphere, which powers regional and global circulations like the monsoons and the Hadley cells (Houze 1989). For this reason, it is important to understand the contributions to total rainfall of these systems.

1.4 Observing and Diagnosing Individual Features

Nesbitt et al (2000) expanded on the work of Mohr et al. (1998), but applied a slightly different methodology using the Tropical Rainfall Measuring Mission (TRMM) satellite. This study not only utilized the microwave imager on TRMM, but also the Lightning sensor (LIS) and the precipitation radar (PR). These instruments allow for a multi-dimensional view of precipitation systems and give researchers an ability to determine a more accurate structure of cloud systems. The PR is used because it is a direct measurement rain as opposed to the microwave imager, which infers rain rates from a temperature to rain rate statistical relationship. Nesbitt et al. (2000) describe types of rain that could be missed by a microwave imager, including shallow convection that is mainly warm and liquid water and contains little or no ice, so in regions where this type of precipitation is present, it is an issue that will need to be addressed. Also, from the PR, Nesbitt et al. (2000) were able to characterize the vertical structure of storms using radar reflectivity measurements in two ways. First, the height of the 30dBZ contour is a proxy for how strong the updrafts of the storm are because stronger updrafts loft larger particles higher, which are then measured by the radar as higher reflectivity values. Being able to determine the vertical profile of precipitation is one of the distinctive capabilities of the TRMM satellite (Zipser et al., 2006). Keenan and Carbone (1992) discuss vertical storm development and note that in their studies of monsoon systems, where higher reflectivities occur below the melting layer, warm rain is present and that where the 30 dBZ surface extends above the melting layer deeper convection and stronger updrafts exist. Also, Petersen et al. (1996) describes the boundary of the 30-dBZ contour as the "convective reflectivity core" which would indicate that outside this region the development of large hydrometeors drops off. Second, the reflectivity at 6km in height can help gauge the strength of storms relative to other regions by

indicating the highest reflectivity values present in the mid-troposphere. The Nesbitt et al. (2000) study used the PR to observe rainfall more directly, while at the same time provide groundwork for future studies by introducing the concept of a precipitation feature (discussed in detail later).

1.5 Precipitation Feature Characteristics and Environments

Petersen and Rutledge (2001) utilized the TRMM satellite to understand the regional variability of convection in the Tropics. One of the sensors that is used in this study is the Lightning Sensor (LIS) aboard TRMM. The LIS sensor is an optical imager that is able to detect prompt changes in the optical nature of clouds (Cecil et al., 2005). The detection of these flashes provides another dimension by which the inner workings of cloud systems can be diagnosed. Petersen and Rutledge (2001) argue that the LIS device helps to distinguish clouds that are mixed phase (containing both ice and water particles) from those that are not. Their argument is that high densities of lightning occurs where the strongest mixed-phase clouds exist, implying areas of deepest convection and generally correlates with higher rain rates. This argument is echoed by Cecil et al. (2005) in that the existence of lightning is dependant on the collisions of ice particles in the presence of supercooled liquid water and thus stronger updrafts should supply a cloud with more ice and supercooled liquid water. Statistically speaking, there is a strong positive correlation between lightning flash density and rainfall rate (Petersen and Rutledge, 2001) and also between lightning and maximum radar reflectivity (Cecil et al.., 2005).

Lightning can also be influenced by the availability of small cloud condensation nuclei (CCN). In the Amazon, biomass burning ejects small smoke, ash, and aerosol particles into the atmosphere that attract water vapor particles to attach to them (Roberts et al., 2003) and eventually form cloud droplets. The formation of lightning occurs when charge separation between ice and water particles within a cloud. Since these particles are very small, they are able

to be more easily lofted high into the atmosphere in strong updrafts, where large charge separation within a cloud can occur and thus high lighting flash counts.

Measuring lightning density can reveal the types of precipitation that dominates in different regions throughout the year (Petersen and Rutledge, 2001). For example, high flash count storms during the dry and burning season could be a result of the influence of these small CCN particles. Also, observing these trends in lightning density allows for the identification as to whether a region is being affected by isolated deep convection or organized convection associated with MCSs. Petersen and Rutledge (2001) observed that lightning intensity is greatest prior to monsoon season onset in South America and that it dramatically decreases once the monsoon is in place.

Observations of vertical thermodynamic profiles in South America give another perspective into precipitation structure in the region. Petersen and Rutledge (2001) argue that tropical South America is more dominated by weaker convection than other continental regions because the thermodynamic environment in the Amazon region is not as conducive to "explosive" convection as is the case for other continental tropical regions. They compare the Amazon environment to that of an oceanic location and argue that the lack of microphysics interactions that are vital in creating deep, electrified storms do not exist in the Amazon, where a plethora of moisture is available in the absence of dust, or other particles which might insight charge separation in a storm updraft (Petersen and Rutledge, 2001). The presence of more moisture, as opposed to a drier and more thermodynamically unstable environment, contributes to the structure of a vertical profile that does not support the deep convection, like what is observed in Tropical Africa.

Diagnosing intensity of convection relies on knowing the thermodynamic properties of the surrounding environment in which storms develop. Parameters such as Convective Available Potential Energy (CAPE) and Convective Inhibition (CIN) help to describe the buoyancy of air and their distributions throughout the atmosphere are necessary to diagnose the "explosive" potential of convection. Drivers of the thermodynamic fields include surface fluxes of both latent and sensible heat. Specifically, in the dry season, surface flux of latent heat is considered to be more crucial in providing moisture fluxes than other larger scale mechanisms (Fu and Li, 2004). Conversely, in monsoon climates, one defining characteristic is an atmospheric circulation reversal, which brings in and eventually erodes the monsoon, is often dominated by a larger scale mechanism such as baroclinic waves or the Atlantic ITCZ. In these transition periods, the atmospheric thermodynamic profiles can change due to advection of air from different environments (moist tropical or dry continental for example) and Keenan and Carbone (1992) suggest that in monsoon regimes that the CAPE is large, but is distributed over a deeper layer of the atmosphere. The authors suggest that the monsoon distribution of CAPE has the ability to support more organized convection in the form of MCSs and squall lines, whereas large shallow CAPE would support strong and deep isolated convection (dry season convection). While Keenan and Carbone (1992) associate the deep layer CAPE with organized convection, they also point out that this is not the sole determining factor and that vertical wind shear associated with the monsoon circulations is a necessary component.

In a follow up study to their 2001 work, Petersen et al. (2002) address the intraseasonal variability of convection in the Amazon. This study places TRMM satellite observations of rain in the context of the large scale atmospheric flow patterns. Petersen et al. (2002) describe two different regimes in the region, one consisting of dominant westerly winds and the other of

dominant easterly winds. Their analysis shows that in westerly regimes (winds coming off the Andes, out of the Tropics and toward the southeast) convection was concentrated in the southern regions around the South Atlantic Convergence Zone (SACZ) and that this regime was defined by high spatial coverage of precipitation with lower rain rates. Petersen et al. (2002) identify fronts that become stationary and intrusions of mid-latitude systems as possible aids in triggering convection in this region under this regime. Also, Rickenbach et al. (2002) identified the same SACZ occurrences in association with stalled fronts, but also noticed an enhanced northwesterly jet feature at 850-mb that implies significant convergence and moisture transport out of the Tropics and into the sub Tropics. This implied that frontal systems in these regimes extended farther into the Tropics and provided a larger scale mechanism for the enhancement of rainfall. While they did extend further into the Tropics, MCSs were much larger than their non-SACZ regime counterparts, but on average produced less rain, associated with the alteration of the thermodynamic profile of the modified atmosphere (Rickenbach et al.., 2002). The much larger MCSs that produce less rain also produced a larger stratiform rain region, which acted to block solar radiation and thus limit the ability of the lower troposphere to become thermodynamically unstable from the heating of the surface of the Earth (Halvertson et al, 2002). They note that while there was abundant moisture present with little wind shear that the CAPE produced in this regime was insufficient to support the types of convection seen during the non-SACZ regimes.

In easterly regimes (winds flowing stronger onshore in the northeast and shifting the zone of convection to the north), the concentration of convection remains in the Tropics and is drastically different (Petersen et al. 2002). This convection is dominated by stronger convection with more intense rain rates, but less spatial coverage. This regime is characterized by organized convection that propagates across the Amazon from the coastal areas in northeast Brazil. The

dynamical conditions are thought to be more ideal for organized convection when easterly regimes are present. Halverson et al. (2002) suggests that the easterly jet is a mechanism that is responsible for creating the different dynamical conditions that lead to different convective structures such as squall lines in the easterly regimes.

The Rickenbach et al. (2002) study concentrates on the variability of convection in the southwest Amazon utilizing ground based radar rather than satellite data. Key findings include identification that in westerly regimes, weaker, stratiform precipitation that covers a large area tends to dominate. Conversely, in easterly regimes, the observed thermodynamic properties change and the convection environment in these regions is altered (Rickenbach et al.., 2002). During easterly regimes the precipitation is characterized by deeper convection that can become organized into propagating squall line MCSs. This is in line with the works of (Petersen et al.., 2002, and Halverson et al.., 2002)

The works of Petersen et al. (2002), Halverson et al. (2002) and Rickenbach et al. (2002) all bring to attention the aspect of regime shifts and their importance in convection throughout South America. Identification of which regime a region is being influenced by seems to have a major impact on how much rain an area receives. It is important to better understand the influences of the wind regimes described by Petersen et al. (2002) and Halverson et al. (2002) and also how they dictate the thermodynamic structure of the atmosphere, observed by Rickenbach et al. (2002), so that a more complete picture of monsoon variability can be determined. Observing how these regimes evolve as a function of monsoon onset date over many years could provide insight as to the mechanisms that are causing this shift and also leading to the variability in when the monsoon season begins.

This study differs from these studies in that it aims to analyze the structure of convection right before, at, and after onset for different regions throughout South America. Our hypothesis is that observations of changes in the structure of convective systems as monsoon onset begins will help understand the large-scale mechanisms driving the monsoon season. Regional differences across South America in convection system properties will provide clues as to which mechanisms, such as thermodynamic priming and dynamic triggers, are controlling the spatial, vertical, and inter-annual variability of monsoon onset. Changes in feature height, frequency, and associated convective characteristics such as lighting flash count and conditional rain rates will serve as the evidence necessary to identify the mechanisms at work and how they evolve or even completely change as the season progresses. In a companion study, Ms. Emily Wright at ECU will be studying the influence of cold fronts on monsoon onset in South America.

CHAPTER 2: DATA AND METHODS

This study utilizes many different sources of data that are derived from different platforms. The most important data is derived from the Tropical Rainfall Measuring Mission (TRMM) Satellite in the form of a Precipitation Features Database (PFDB), which was developed by Dr. Stephen Nesbitt from the University of Illinois. The PFDB contains statistics about precipitation features of different vertical and horizontal dimensions in our study region over a 10-year period from 1998-2007. We will combine these data with data from National Centers for Environmental Prediction (NCEP) to form a detailed view of the regional variability of the structure of precipitation in South America. Our study region was determined by an objective analysis of 29 years of precipitation data that identified 4 regions where precipitation variability is present and distinct from other regions (Nieto-Ferreira and Rickenbach, 2010).

2.1 TRMM Satellite

The Tropical Rainfall Measuring Mission (TRMM) satellite is a low earth orbiting satellite that was launched in November 1997, with the mission to observe and measure precipitation throughout the Tropics. Onboard the satellite is a suite of instruments necessary to observe precipitation, including the TRMM Microwave Imager (TMI; Kummerow et al. 1998), the Precipitation Radar (PR; Kummerow et al. 1998), and the Lightning Imaging Sensor (LIS; Kummerow et al. 1998) (Fig. 2). These instruments will be utilized in different respects to analyze precipitation in the South American study region for this project.

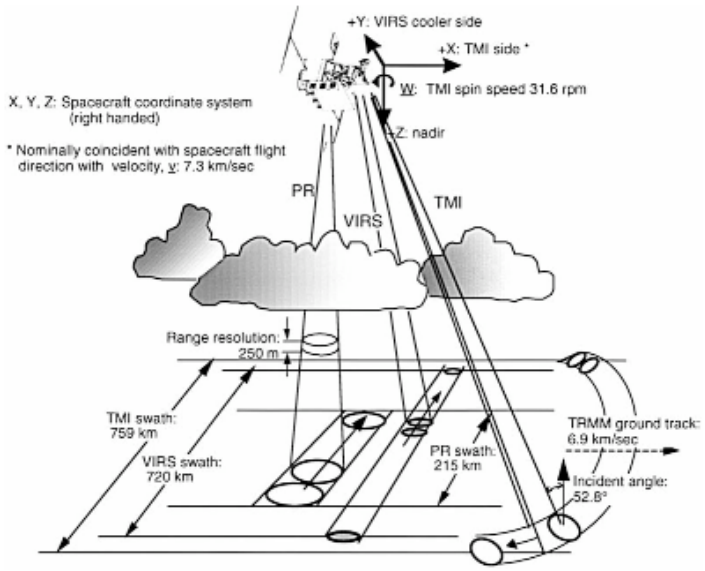

Figure 2.1: Schematic of TRMM and its 3 sensors and their scan swaths (from Kummerow et al. 1998)

The TMI is a passive microwave sensor that measures microwave radiation at multiple wavelengths. The TMI is able to scan 9 different wavelengths from 10GHz to 85GHz (Kummerow et al. 1998). Since the emissivity varies between the ocean and land and also between water and ice, these different wavelengths are necessary to fully resolve precipitating features.

The TMI is able to identify cloud top temperatures and from this can infer the types of clouds and therefore what types of precipitation are likely to be occurring. The Rayleigh-Jeans approximation to the Plank Function, expressed in Equation 3, derives this inference.

$$B_\lambda = \frac{2c\kappa T}{\lambda^4} \qquad (3)$$

In the approximation, c is the speed of light, k is the Stefan-Boltzmann constant, T is the temperature in Kelvin, and λ is the wavelength. The Rayleigh-Jeans approximation serves to describe the blackbody radiation emitted in short wavelengths, such as those used on microwave imagers (1mm-1cm). This approximation is important to understanding convection, because you

can invert the known emissivity of a source to find the equivalent blackbody temperature of a feature (Janssen, 1993).

That temperature is then used to draw the connections between feature temperature and the feature characteristics (Janssen, 1993). Kummerow et al. (1998) discusses how brightness temperatures can serve as a proxy for estimating vertical structure of a storm since the emissivity characteristics of liquid water and ice differ. One of the advantages of the 85 GHz signal is its sensitivity to ice particles and also the limited effect on the signal by background radiation from the surface of the earth (Mohr et al. 1999). At the 85 GHz wavelength, ice particles scatter radiation out of the field of view, which in turn lowers the brightness temperature that the microwave detects. Given this, if the 85 GHz signal were to detect cold brightness temperatures, then one could infer that these storms contain deeper convection and thus heavier rain. Also, if a mainly warm brightness signature is detected then an inference could be made that the storm is not vertically developed because it does not contain ice particles, synonymous with strong updrafts and deep convection, and thus the rain rates would be much less. Although the TMI cannot provide a direct measure of rain, it does give a good indication of where the heaviest and strongest storms are occurring on a regional scale.

The PR is a phased array radar that scans at a frequency of 13.8 GHz (Kummerow et al. 1998). The PR is able to scan a 215 km wide swath along the surface of the earth while being able to observe vertically to a height of 15 km above the surface. The PR does not scan in the physical sense of a moving antenna, but it scans by sending pulses at a set degree of difference from each other out across a 17-degree swath (Kummerow et al. 1998).

The PR works similarly to a ground based weather radar in that reflectivity values are derived from a relationship between the observed reflectivity and a rain rate that correlates to

that reflectivity given the radar settings. Because the particles that are being observed are smaller than the wavelength of radiation, they fall in the Rayleigh regime of scattering. Equation 4 describes this relationship:

$$\sigma = \frac{\pi^5 |K|^2 D^6}{\lambda^4} \qquad (4)$$

The coefficients of the equation are as follows: σ is the backscattering cross-sectional area of the particle, λ is the wavelength, D is the diameter of the particle, and K is a coefficient that depends on the content of the particle being detected (i.e. Ice or water). (Rinehart, 1997). This equation for detecting the reflectivity of a particle is primarily driven by the size of the largest particle being detected since the diameter of the particle is raised to the 6^{th} power. Also, the reflectivity is sensitive to the composition of the particle (ice or water), thus, the larger the particles and water coated ice particles (radar bright band) will return the highest reflectivities. The TRMM PR allows for the measurement of precipitation system structure in areas that previously were unmeasured due to lack of instrumentation in oceans and uninhabited regions throughout the Tropics.

The Lightning Imaging Sensor (LIS) is a sensor on the satellite that scans clouds in the TMI swath and acts to detect optical changes in the clouds as a way of detecting lightning flashes. The device is an optical imager that is able to observe a 360,000 km^2 area during overpass at a sampling rate of 500 frames/second and is able to detect lighting with a resolution of 3-6 km (Christian et al. 1999). The LIS works by detecting the instantaneous changes in the brightness of clouds regardless of time of day and detects all types of lightning due to the resulting change in the cloud optical brightness. The purpose of this sensor is to provide a better understanding of not only lightning but also the distribution of precipitation associated with occurrences of high

lightning flash counts (Kummerow et al. 1998). Studies such as (Nesbitt et al., 2000, Petersen and Rutledge, 2001, and Cecil et al., 2005) all emphasize the importance of the detection of lighting due to its close relationship to the development of vertically intense storms. The electrification theory for the creation of lightning requires strong updrafts to create the charge separation, thus where lighting is present, the storms are more than likely strong and vertically developed.

2.2 Precipitation Feature Dataset

The main source of analysis for this project will be a precipitation feature database that was designed using only data derived from the TRMM satellite. The data comes from scans of the TMI, VIRS, PR, and LIS sensors to develop a comprehensive database containing features of precipitating systems throughout the Tropics. Dr. Stephen Nesbitt, of the University of Illinois, produced the database specifically for this project. Its contents and methods mirror precipitation feature datasets used in his previous work (Nesbitt et al. 2006 and Nesbitt et al. 2000). Nesbitt et al. (2006) describes how storms observed by TRMM were categorized by horizontal size and also vertical structure based on VIRS, TMI, and PR observations. The PR is also used to help distinguish between stratiform rain and convective rain (Nesbitt et al. 2006).

The dataset is divided into 4 unique categories of features mainly based on TMI brightness temperature. The TMI identifies where features are present, but the specific temperatures and observed area of the features define which category the feature is in. For example, in order to be a MCS feature (the largest feature) then a TMI brightness temperature of less than 250 K must be detected for a 2000 km^2 continuous area, while within that area there must be approximately 10% of the region that has a TMI temperature below 225 K (Nesbitt et al. 2000). The dataset includes all features, shallow features with shallow convection (no TMI

temperature below 250 K), shallow features with deep convection (existence of a TMI temperature below 250K, but not large enough to qualify as an MCS), and large mid-level systems/MCSs (see above explanation) (Figure 2.2). The dataset is partitioned into arrays containing our specific 5 X 5 degree boxes throughout the region (Figure 3.1) that were used when defining when onset occurred (Nieto-Ferreira and Rickenbach, 2010). Also, the arrays contain values that are pentad averages, which is again consistent with the definition of onset since onset criteria relied on pentad rain for each box. These pentad averages suppress high frequency variability, like the diurnal cycle, and give a better representation of how the feature characteristics change on synoptic timescales. Also, due to the nature of the low earth orbit of TRMM and the two high-resolution samples it gives daily, by doing pentad averages we assure at least ten samples (Sorooshian et al. 2002). This rate of sampling does not smooth out diurnal variation, but instead smoothes out weekly/large-scale variations and over our 10-year period works to smooth out monthly variability. Using TRMM (and the precipitation feature dataset) alone will not allow us to identify one storm, but will allow us to analyze the trends in features over longer timescales.

Previous research has shown that MCSs account for a very high percentage of the rainfall observed throughout the world (Houze 1989, Negri et al. 2000, and Nesbitt et al. 2000) and more specifically in South America (Durkee et al.., 2008 and Zipser et al.., 2006). Because of this, our study will mainly focus on the MCS contributions contained in the precipitation feature dataset; however other systems will also be analyzed.

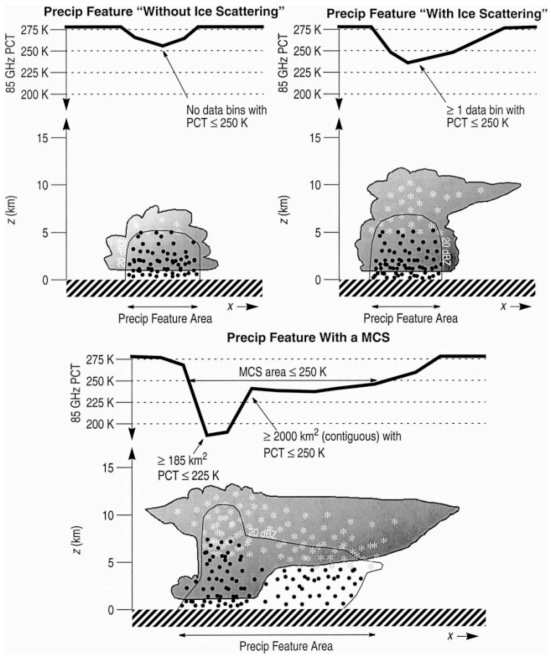

Figure 2.2: Diagram of different precipitation features included in the dataset. Black line represents temperatures observed from TMI 85GHz scan and grey outline is idealized 20 dBZ contour. Ice and rain are in the form of grey asterisks and black dots, respectively. (from Nesbitt et al. 2000)

Six parameters from the TRMM precipitation feature database have been chosen to help quantify the differences in convection structure and intensity prior to and after onset: volumetric convective rain fraction, maximum height of the 30-dBZ contour, lightning flash count, maximum reflectivity at 6 km above the surface, number of precipitation radar pixels (a proxy for storm size), and conditional rain rate. Each will be discussed in turn.

Volumetric convective fraction represents the fraction of volumetric rainfall comprised of convective rain and thus we can also derive stratiform rain fraction. In order for a part of the storm to be considered convective, the rain rates as detected by the PR radar must be greater than 5 mm hr^{-1} and occupy a relatively small area (Schumacher and Houze, 2003). Another condition that is deemed important when separating convective and stratiform rain is that convective rain typically has an inhomogeneous horizontal radar profile (Figure 2.4, left side), while stratiform rain has a homogeneous horizontal profile (Figure 2.4, center/right side). These images are a good representation of the main differences between convective features and more stratiform

features. Stratiform features consume a larger spatial region (Figure 2.3) than convective portions and contain weaker updraft speeds, which limit the overall strength of the feature and rate of precipitation. Convective features, on the other hand, typically contain much more intense rain rates, as seen in Figure 2.4, and the higher dBZ values within the convective portion because these features are driven by very unstable air that supports strong updrafts that produce high rain rates.

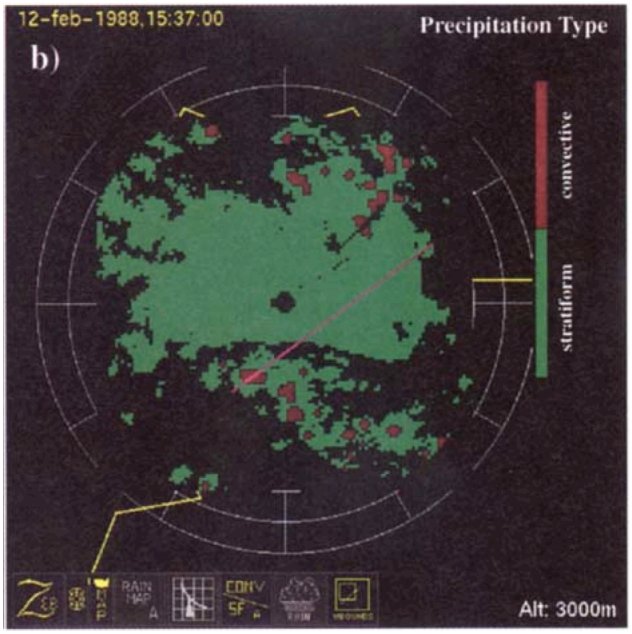

Figure 2.3: PPI Radar scan at Darwin, Australia for 12 Feb 1988 @ 0607 UTC. Returns are separated into convective (red) and stratiform (green) by objective separation algorithm (from Steiner et al. 1995)

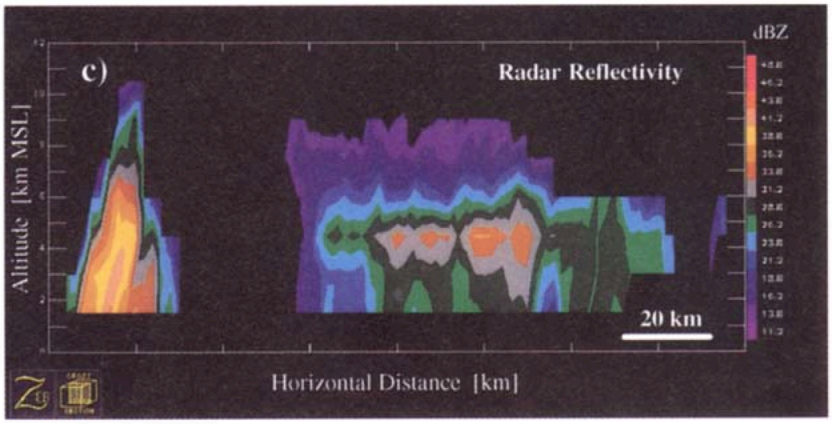

Figure 2.4: Radar volume scan at the same time as in Figure 2.3, along red line in Figure 2.3. Cross-section shows convective feature (left) and stratiform feature (center and moving right). Total cross section is 160km. Contours are in dBZ with brighter colors being higher values and darker colors being lower values (from Steiner et al. 1995)

Processes by which both types of convection develop are fundamentally different (Schumacher and Houze, 2003) and knowing what percentage of a feature consists of each type can provide insight into the thermodynamic makeup of the atmosphere. Studies have shown that changes in the convective structure of storms are indicative of distinct thermodynamic and kinematic regimes and can provide insight into mechanisms that drive precipitation at a particular point in the year (Rickenbach et al.., 2002 and Petersen et al.., 2002). For example, if a the majority of features in a pentad average are 90% convective, then we can infer that the atmosphere is set up in such a way that it supports large isolated convection with little or no organizational influence present; however, if the fraction is 40% convective then we can surmise that perhaps the conditions are right for deep convection, but also that there is sufficient vertical wind shear present to develop MCSs, which by definition have a strong leading edge of convection and a large trailing stratiform region.

Two other parameters provide information into convective intensity. The maximum height of the 30-dBZ contour has been linked to convective intensity including the strength of updrafts and the microphysical processes that produce rain (Petersen et al. 1996 and Nesbitt et al. 2000). Also, if the 30-dBZ height is above the melting level (approx 4.5 km in the Tropics), then one can infer that ice processes are present, due to strong updrafts, which is what leads to clouds becoming electrified (DeMott and Rutledge 1998; Cecil et al.., 2005).

The second field, the maximum reflectivity at 6 km above the surface, is simply the recorded reflectivity in a radar scan from TRMM at a height of 6 km. Variations in the reflectivity of this variable provide information into the vertical intensity of convection and from this provide an inference into rainfall mechanisms. The higher reflectivities are present when larger particles are present because the radar equation is a function of the largest particle present.

Where large reflectivity values above 6 km exist, more than likely strong updraft that supports lofting these large particles to this height also exist. These strong updrafts are associated with intense convection, heavy rain, and commonly lightning. Lightning, according to Zipser and Lutz (1994), is more common in strong ice processes, in reference to 6 km height, that exist at the -10^{o}C level and reflectivity values at or greater than 40 dBZ.

The lightning flash count is a tally of lightning flashes that are detected by the optical LIS sensor aboard the TRMM satellite. The flashes are recorded as specific locations per feature within each respective feature and thus are able to be counted within the 5 X 5 degree boxes. Petersen and Rutledge (2001) suggests that there is a relationship between lightning flash density and rain rates while Petersen et al. (2002) explains that there is also a correlation between lightning activity and synoptic scale wind regime. The relationship with rain rates stems from the fact that it takes deep convection to cause a cloud to become electrically charged to produce lightning and if the convection can support lightning, then theoretically it should support heavy rain. Also, when it comes to synoptic wind regime, the type of environment that is present can have an impact on the type of convection that forms (Petersen et al.., 2002 and Rickenbach et al.., 2002). Similar to the percentage of a storm that is considered to be convective, the amount of lightning present can thus give insight into the synoptic regime that is present in a region due to the necessity of ideal thermodynamic conditions, such as high CAPE, low CIN and limited vertical wind shear, in order to produce convection with strong mixed-phase clouds.

In the data set, lightning counts are presented on a per feature basis, thus giving a lightning flash density. This provides information such as when the most intense features occur as opposed to when the most lightning occurs. This will allow us to delineate regions where there are high lightning counts with many features from regions where there are high counts and fewer

features. After the regions are identified, combining these observations with rainfall will show us where rainfall is modulated by frequent, small storms or infrequent, larger storms.

Number of precipitation radar pixels (NPIXELS) is a measure of the amount of ¼ degree pixels that are filled with rain (greater than 18 dBZ, which is the minimum detectable signal on the PR) from the precipitation radar on TRMM per feature. Using this variable will allow us to compare the size of storms from region to region in an unbiased manor since the pixel sizes are equal across the domain. Also, being able to see how the size of the storms change within a region allows us to observe whether as the season progresses if storms are steadily growing larger, shrinking, or staying approximately the same size. This will allow us to correlate storm size with other feature variables to see if there is a connection to either the small-scale thermodynamics or large-scale dynamics, such as a primarily thermodynamic environment driving smaller convection as opposed to a dynamic environment driving larger systems.

Finally, conditional rain rate in the dataset is the average rain rate over the entire pentad. This variable keeps track of the rain rate only where it is raining, thus ignoring the regions that are not receiving rain. This value was recorded on a per pentad scale, thus allowing for analysis of when particular pentads become more or less rainy. Analysis of how rain rates change per pentad provides us with an indication of the approximate start and end of the rainy season.

2.3 Precipitation Feature Dataset PDFs and Means

In addition to the data in the PF dataset, we determined the Probability Distribution Functions (PDFs) of all the features in the PF dataset. A PDF describes the relative likelihood of a variable occurring in a given range of values compared to other ranges of values in the data set. The PDFs of the following variables were analyzed in the form of histograms: conditional rain, flash density, maximum height of the 30 dBZ contour, and the maximum reflectivity at 6 km.

Along with the PDFs, the dataset also contained pentad means for all variables on a per feature basis. Two variables of particular interest here were conditional rain rate and number of features. Conditional rain rate per feature showed where the frequency of high precipitation features occurred in a time series, while number of features showed when the highest occurrence of features in a pentad occurred annually. These were important here because it showed where there were few features raining heavily on average versus many features containing a lower average rain rate. Comparison showed how number of features affected to rain rate frequency throughout the year.

2.4 TRMM 3B42 data

This study uses the TRMM 3B42 data set, which is an IR-based high temporal and spatial resolution dataset, and applied them to a .25 X .25 degree box. The instantaneous rainfall estimates in the 3B42 dataset are produced on a 3-hourly time scale (Huffman et al., 2007). The precipitation field in the TRMM 3B42 data over South America provides a high-resolution look at rainfall patterns. The patterns of interest include mid latitude cyclones, fronts, the South Atlantic Convergence Zone (SACZ), the ITCZ, squall lines, and isolated convection. The 3B42 data allows the examination of a variety of timescales, from diurnal variations in convection to seasonal precipitation patterns.

2.5 NCEP Reanalysis Data

National Center for Environmental Prediction (NCEP) Reanalysis data used are a collection of meteorological variables, plotted on a daily means scale on a 2.5^{o} grid (Kalnay et al., 1996). The data are available for all the times when TRMM 3B42 and PFDB variables are plotted. Being able to connect the NCEP data with other data sources further validates any

conclusions. Variables such as sensible heat flux, latent heat flux, soil moisture, specific humidity, sea level pressure (SLP), and 850 mb winds were used.

Sensible and latent heat fluxes are important variables in understanding the local thermodynamic environment for a region. As was discussed in section 1.1, the strength of these fluxes have implications on the state of the atmosphere and its ability to support different types of convection.

Soil moisture and specific humidity are important in understanding when moisture is present and available in a region. These values are important when analyzing surface heat fluxes because soil moisture and specific humidity both play an important role in describing the moisture in a region, but also modulating the local temperature. High soil moisture, for example, can raise the specific humidity, but at the same time decrease the temperature since solar energy must go toward evaporating the moisture before heating the ground and air.

Sea level pressure (SLP) is a valuable field, especially on the daily time scale in the sub-Tropics because it can be used as a proxy for frontal passages. Fronts form in association with surface cyclogenesis in the form of a low-pressure system. Thus when a front approaches and then departs a region, there is an observed drop and then rise in SLP.

Finally, 850 mb winds are plotted to assess the mean wind speed and direction in our study area. By observing 10-year means in pentad mean wind speed, we aim to observe regional changes in both speed and direction that are consistent with previous studies of low-level wind flows (South American Low-Level Jet) and also serve to validate conclusions as to which precipitation mechanisms are at work in a particular region.

2.6 Study Region

Following the work of Nieto-Ferreira and Rickenbach (2010), our regions consisted of the four regions that were isolated in a REOF analysis of GPCP data. Their process consisted of using the GPCP dataset of rainfall from 1979 – 2007 perform a rotated empirical orthogonal function (REOF) to identify the dominant modes of spatial and temporal variability in precipitation. The analysis identified 3 distinct modes of variability that occurred over four different regions. These modes explained 35% of the variance in precipitation in the study region. Identifying these regions not only sets up the regions that we are going to study, but also sets up possible regional connections. Mean onset in the SACZ region appears to be closely tied to onset in the West region (Nieto-Ferreira and Rickenbach, 2010). Onset occurs first in the West region, so this suggests that SACZ onset could be a response to conditions that develop in the West region around onset.

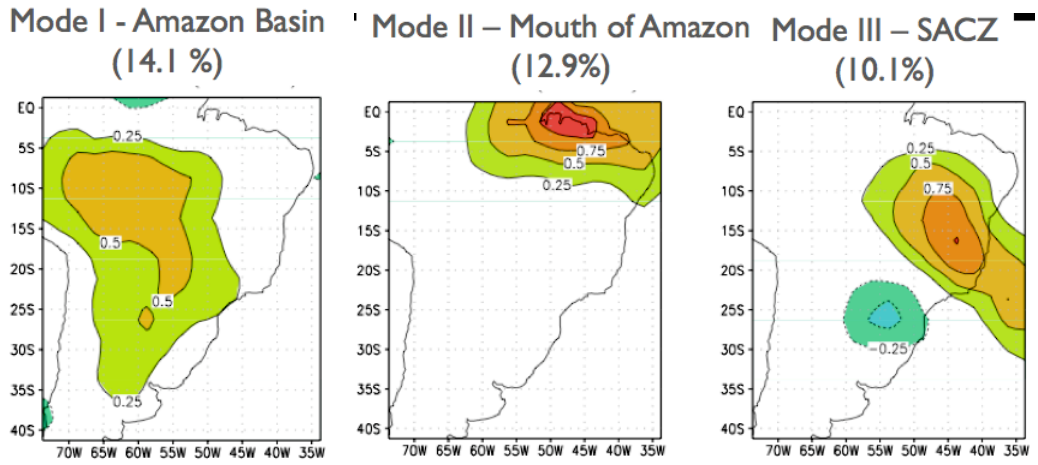

Figure 2.5: Three modes from the REOF of the GPCP-V2 pentad data from 1979-2007. Mode 1 – West region (annual cycle across Amazon), Mode 2 – East region (coastal squall lines and Atlantic ITCZ), and Mode 3 – SACZ and South regions (Frontal interactions and Thermodynamic forcing from Tropics) (from Nieto-Ferreira and Rickenbach, 2010)

The regions (Figure 2.5) consisted of the Amazon basin (where a strong annual cycle of precipitation exists), the mouth of the Amazon River (where there are coastal storms and also influence from the Atlantic ITCZ), the mean location of the SACZ (where fronts tend to stall

during the monsoon season), and finally the southern boxes (dominated by year round baroclinic waves) (Nieto-Ferreira and Rickenbach, 2010). Our analysis was centered on these different regions. Each region was analyzed individually and then select regions were compared and contrasted.

2.7 Data Analysis

The data for this research was primarily analyzed utilizing the computer software Interactive Data Language (IDL) (developed by ITT Visual Information Solutions) and SPSS (developed by IBM). IDL is a computer programming language, similar to FORTRAN and C++, which allows for the reading and manipulation of large datasets so that specific data can be analyzed in time and space. IDL was used to read in the PFDB, TRMM 3B42 files, NCEP data, and the PDF dataset. The data extracted using IDL was used to construct time series plots, frequency distribution histograms, and make precipitation images. The construction of these different sets of data were created in IDL, but primarily analyzed and viewed in Microsoft Excel. While most of the graphical analysis was preformed in Excel, some was done using the Grid Analysis and Display System (GRADS). GRADS is a graphical display software developed at the Center for Ocean-Land-Atmosphere Studies and allows for the easy manipulation and display of large datasets in many different formats (Doty, 1995). Data processed in GRADS is displayed on a 10-year average and monthly scale. Displaying data in this manner allowed the entire region to be viewed as a whole and not just a specific region.

Using the regions that were determined in the REOF analysis (Nieto-Ferreira and Rickenbach, 2010), time series were created for all of the previously discussed variables in the PFBD. Also, NCEP reanalysis variables were plotted in similar time series plots so that they could be integrated with the PFDB variables to identify correlations between variables in these

two completely independent datasets. All of the variables previously discussed in both the PFBD and NCEP reanalysis were averaged for their respective pentads over the 10-year period (1998-2007). These time series were instrumental in building a case for each region as to what the main differences at onset were between the regions. They also helped to identify trends in the data that aided in explaining how precipitation evolved over time in each region. These particular processes will be discussed in detail in the results.

The PFDB PDFs were also plotted to corroborate what the time series plots were indicating about each region. One of the strengths of the histograms is that they show the relative frequency of different variables as opposed to an absolute total. The relative frequencies allow us to separate the data into different range bins to see where the majority of storms occur during a particular part of the year, thus giving a more detailed look into the structure of convection at any given point. Knowing that a region averages a specific amount of rain over a pentad is useful, but being able to see how much rain fell per feature in a pentad is very useful in illustrating whether or not a region is dependent on a few large features or many small features to produce their rain. Histograms of 10-year averages, monthly averages, and seasonal averages (3-monthly) were plotted. Seasonal averages allow the partition of particular regions into their dry season and wet seasons to see when the frequencies of different variables are at their highest and lowest. Breaking down the PDF data into a 3 monthly time scale averaged over 10 years, allowed for the intraseasonal comparisons not only within a region, but also between other regions. This gives an indication again of what processes are at work during that time of the year in each region.

In order to identify statistical significance between two variables, SPSS, a statistical software package, was utilized to perform basic and advanced statistical functions ranging from linear analysis to multi-dimensional analysis. Correlation analysis between different variables in

the precipitation feature dataset and the NCEP reanalysis were performed to evaluate possibility of one variable being able to explain variability in another. Being able to determine these relationships provided evidence such as to what could be initiating precipitation in a particular region and how the process or processes changed over time.

Finally, in a combination of the TRMM data along with the precipitation feature dataset was analyzed centered on specific pentad onset dates on a yearly scale to resolve how these different variables behaved just before and just after onset. The TRMM 3B42 dataset was helpful in providing composite monthly, daily and even three hourly high-resolution images for rainfall in South America. One of the most critical uses of these images was identification of storm system size and movement through the region via animations. The TRMM 3B42 images provided conformation whenever data in the precipitation feature database time series or the PDFs looked strange and needed further investigation to verify that the data was accurate. An example of this would be if high variability was present in the time series, then we could look at the raw features in the 3B42 images to observe whether or not the variability matched what was really going on.

While all of these different analysis methods have their strengths and weaknesses, the main use of these individual methods was to combine them in the end to give the big picture. Showing how the monsoon evolves at onset in different regions, using different and sometimes independent data sources, was critical in keeping the results un biased and thus valid.

CHAPTER 3: RESULTS

The four regions in South America that were just identified (Figure 3.1) are analyzed here using a combination of time series, PDF, and statistical analysis. The time series plots were derived from the TRMM PFDB as well as NCEP Reanalysis data. The statistical analysis and the PDF analysis were also derived from the TRMM PFDB. All of the regions will be analyzed individually as a way of presenting what mechanisms are playing a role in driving precipitation in each region. Also, select regions will be compared and contrasted to better convey how the regions are dependant on one another or how they are fundamentally different, despite their close proximity.

Figure 3.1: South America with study regions (Nieto-Ferreira and Rickenbach, 2010) outlined in black. The outline of boxes represent where the monsoon regime is known to develop and exist. Colors show topography of South America, boxes represents a 5x5° grid used to divide the study region and boxes with black numbers represent land-based boxes

We expect to observe distinct regional differences, similar to those detailed in Nieto-Ferreira and Rickenbach (2010). Initial analysis of the 10-year means for the entire region introduced us to some of the regional trends and gave an important first look into regional

differences in convective properties. The analysis in Figure 3.2 was done for all features that contained a MCS for 1998 – 2007 and were averaged on a per pentad time scale.

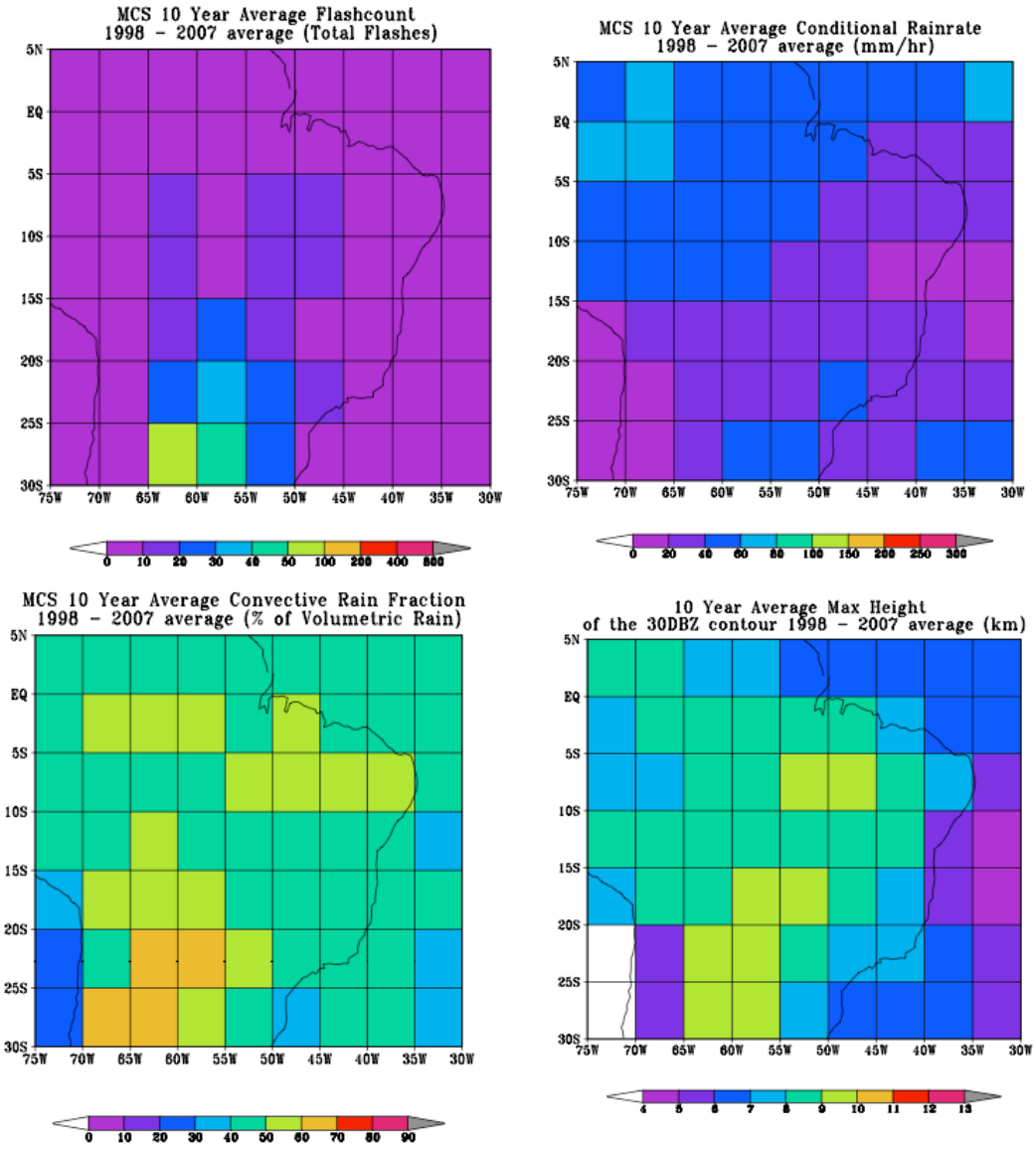

Figure 3.2: Region wide per pentad averages of 1) Lightning Flash Count, 2) Conditional Rain Rate, 3) Convective Rain Fraction, and 4) Maximum Height of the 30 dBZ contour, averaged 1998-2007

Being displayed in Figure 3.2 are average per pentad values for each box over a 10-year period. A trend that stands out is the largely convective regime that is present in the southern portion of the study region; however, all of the conditional rainfall is concentrated in the northern portion of the study region. This tells us that features with a MCS in the south region are more

convective as a group than those same features in the Tropics. Also, our SACZ region appears to be less convective than the South region and if the working hypothesis is that frontal interaction from systems moving from south to north are what is causing precipitation in the SACZ region then we need to identify what is causing frontal precipitation to be more convective in the south and less convective in the SACZ region. Another observation is that all of the convective boxes are inland in the continental regime, so that implies that coastal interactions suppress the convective nature of features. This will be important when comparing the West and East regions to see how a coastal regime differs from a continental regime, at approximately the same latitude.

3.1 The Tropics

This chapter will concentrate on the precipitation patterns and mechanisms that are present in the West and East regions. While part of the West region extends into the sub-Tropics, most of the region is in the Tropics and precipitation in this region responds primarily to forcing mechanisms that are typical of Tropical locations (thermodynamic forcing and the continental ITCZ). The East region is also a Tropical location that is heavily influenced by the Atlantic Ocean, but also is characterized in the pre-monsoon by Tropical processes such as increased sensible heat flux in the dry season driving convection. Both regions will be discussed individually and then will be compared and contrasted to expose how these relatively closely located regions vary.

3.1.1 West Region

The western region for our study was composed of 10 boxes that were located in the central Amazon River basin (Figure 3.1). This region is characterized by an annual cycle of rainfall, with the rainy season occurring between August and March, with March until July being

the dry season, as seen in Figure 3.3, which is a 10 year time series of conditional rain rate per pentad for features containing a MCS.

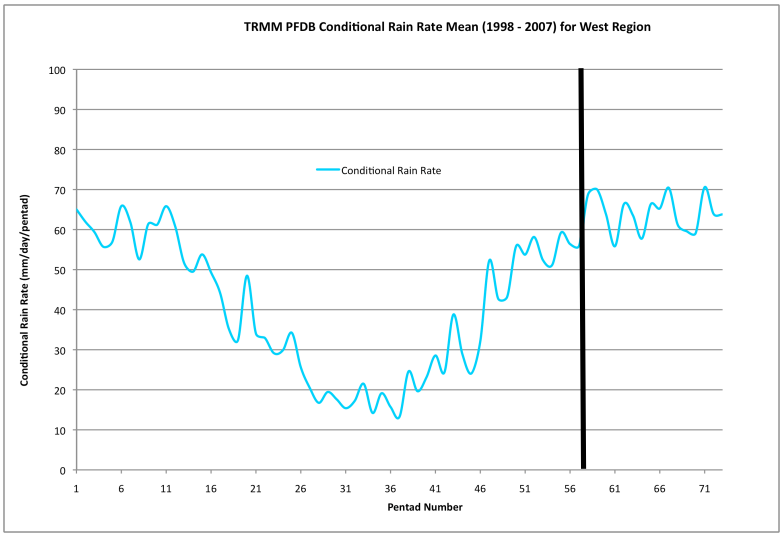

Figure 3.3: Conditional Rain Rate per Pentad for Features with a MCS, averaged 1998-2007 for the West Region

Onset, as defined by Nieto-Ferreira and Rickenbach (2010), occurs in mid-October (Pentad 58, Black line in time series) and has a standard deviation of 4 pentads. Monsoon onset occurred every year in the West for all of the years analyzed in this study.

Features with shallow convection

Figure 3.4 shows PFDB variables averaged over the 10-year period for the features with shallow convection. The number of features per pentad (red) and conditional rain rate per feature (blue), with latent and sensible heat flux are plotted. The decrease in number of features correlates well with the occurrence of the dry season in the South American winter. One variation to note, however, is that though the number of features varies throughout the year, the amount of rainfall per feature is constant, which means that features in this category rain consistently the same amount in this region year-round. Features with shallow convection build quickly after sensible heat flux has peaked and suggests that they thrive in the post-onset environment where features are driven by large-scale dynamics and not just local

thermodynamics. The nearly 100% (25 features to 50 features) increase in number of features around pentad 46 seems to correlate well with the initial downward turn in sensible heat flux and the upward turn in latent heat flux. The West region number of features with deep convection varies in sync with the annual cycle of rainfall as seen in Figure 3.4. This suggests that both shallow and deep convection could be caused by a similar mechanism(s).

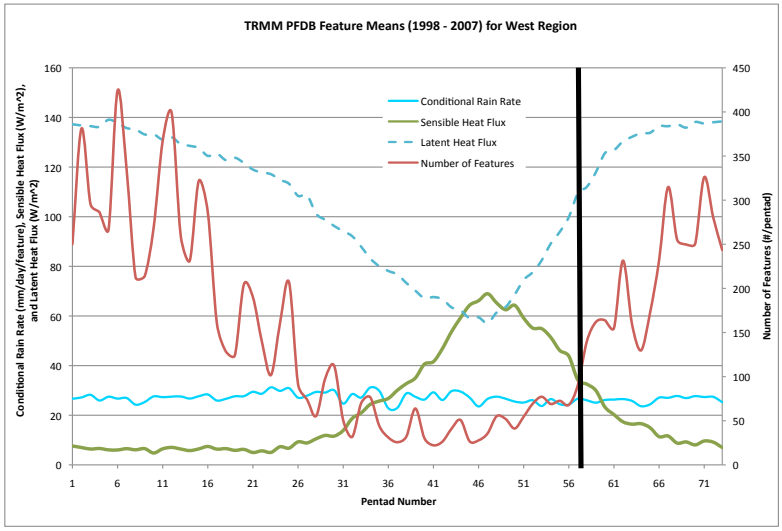

Figure 3.4: Variables from the PFDB for Features with shallow convection in the West Region. Conditional Rain Rate per feature (Blue), Number of Features (Red), Sensible Heat Flux (Green), and Latent Heat Flux (Blue dashed)

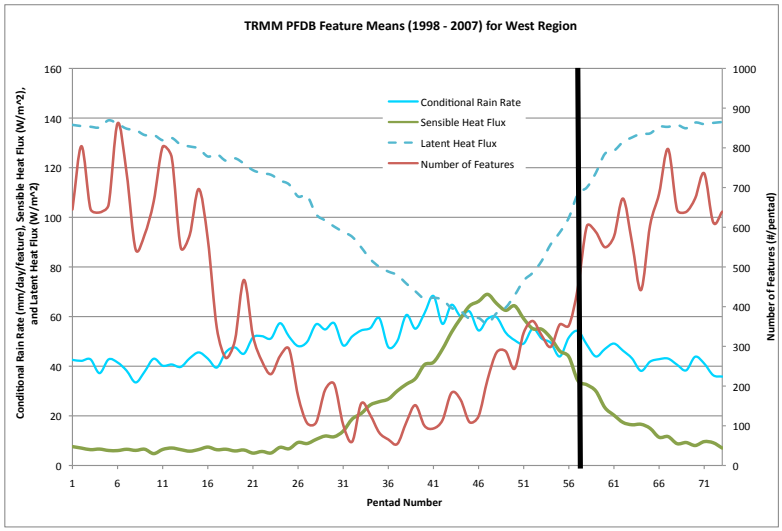

Figure 3.5: Same as in Figure 3.4, but for Features with deep convection

MCS Features

Compared to features without a MCS, features with a MCS rain over twice as much per feature on average, yet only account for a small percentage of the total amount of features in the West region. Previous research has noted that MCSs provide the least amounts of features of all the types, but provides the largest rain rates per feature as noted in previous research throughout the world and also in South America (Houze 1989, Negri et al. 2000, Nesbitt et al. 2000, Durkee et al.., 2008, and Zipser et al.., 2006). Furthermore, Fu et al (1999) suggests that 80% of the rainfall across the Amazon is a result of deep convection, including MCSs. One comparison between features with deep convection and features with a MCS is that their numbers per pentad typically begin to rise quickly as sensible heat flux at the surface starts to build. This suggests that deep convection that develops an ice scattering signature is contingent upon thermodynamic forcing because features with shallow convection do not begin to build quickly at the same time as sensible heat flux. On average MCSs in the West account for less than 5% of the total number of features at a given time; however, it is the large amounts of heat released by these storms that drive the monsoon circulations making them a vital player to the monsoon picture in this region.

The features categorized as large features with a MCS are those that are the largest in vertical structure and horizontal dimension of the three categories. Figures 3.6 and 3.7 show time series of variables that describe the convective nature of these features and include variables such as convective rain fraction per feature (black, Figure 3.6), lightning flash count per feature (red, Figure 3.6), number of Precipitation Radar (PR) pixels per pentad (green, Figure 3.7) and max height of the 30 dBZ contour per pentad (black, Figure 3.7).

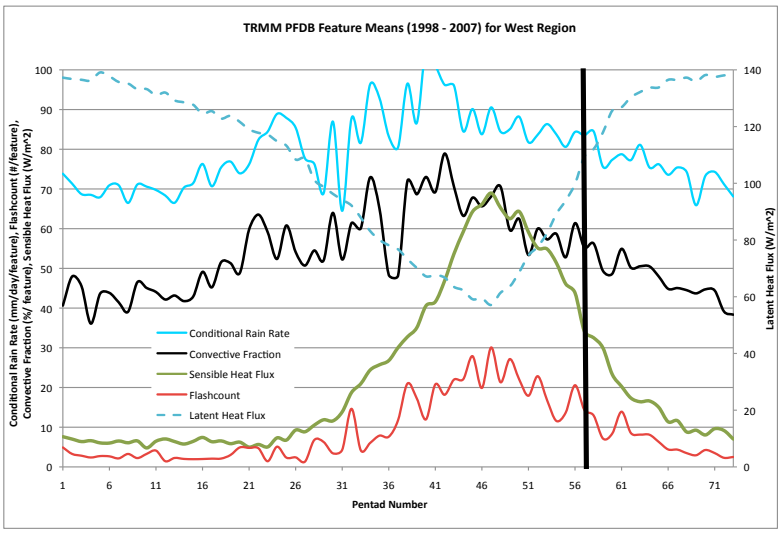

Figure 3.6: Variables from the PFDB for Features with a MCS in the West. Conditional Rain Rate (Blue), Lightning Flash Count (Red), Convective Rain Fraction (Black), Sensible Heat Flux (Green) and Latent Heat Flux (Blue dashed).

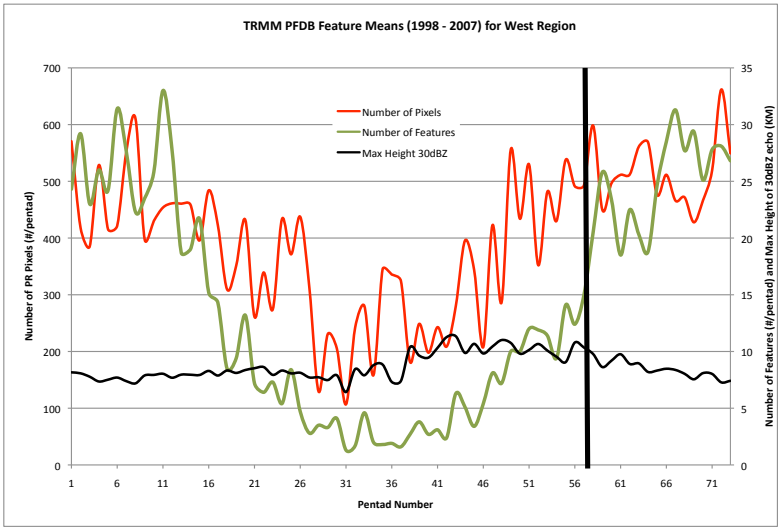

Figure 3.7: Variables from the PFDB for Features with a MCS in the West. Max Height of the 30dBZ contour (Black), Number of PR Pixels (Red), and Number of Features (Green).

Another tendency that stands out is the conditional rain rates per feature for features with a MCS are over 2 times higher than those for shallow and deep convection features. Also, the conditional rain rate per pentad for features with a MCS (Figure 3.3) shows a distinct annual cycle with a wet and dry season, which is not noticeable in the shallow and deep convection features. This same trend in rain rates to define the wet and dry season can also be seen in the conditional rain rate per feature PDF histogram (Figure 3.8).

The histogram is partitioned into DJF (December, January, February), MAM (March, April, May), JJA (June, July, August), and SON (September, October, November). The values are given as percentages of the total observed in each 3-monthly period. In the end of monsoon season/start of the dry season (MAM), there are a low percentage of features that occur with high rain rates, with the majority of features occurring toward the lower rain rates. As the dry season continues toward the pre-monsoon period (JJA) there are higher frequencies of features that occur in the high rain rates. However, Figure 3.9 illustrates that during this period that JJA is the time of the year when the fewest total features occur in the West.

However, once we move closer to onset (SON) feature frequency increases and the features begin to transition back toward more toward lower rates. Once the monsoon is in active phase (DJF) the feature frequency is even more so concentrated toward the lower rain rates, but this is also the time where the most features occur (Figure 3.9). These distributions imply that dry season convection tends to have a higher frequency of heavy rain rate features with less total features compared to the monsoon features, which contain lower rain rates and more total features.

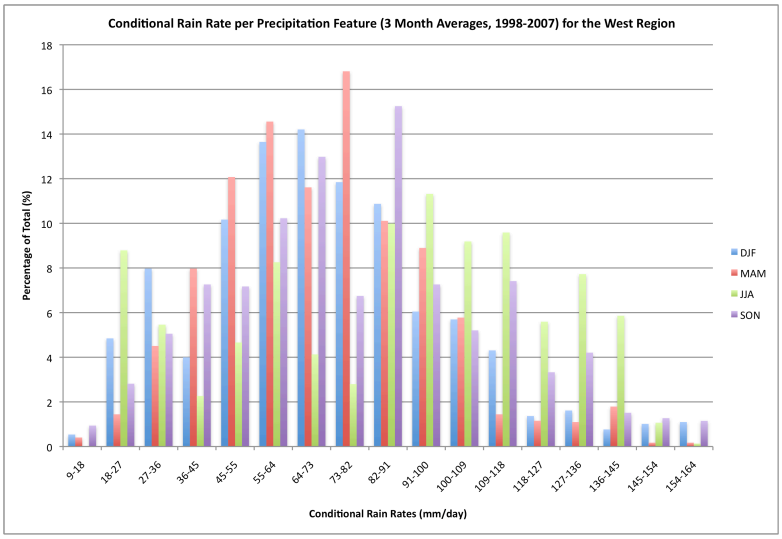

Figure 3.8: PDF of Conditional Rain Rates for 3-month periods, Percentage of Total Scale, averaged 1998-2007 for West Region

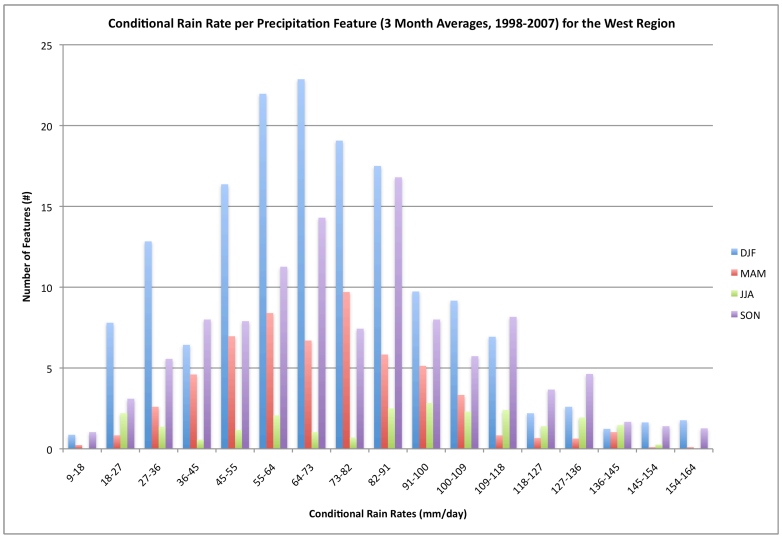

Figure 3.9: Same at Figure 3.8, but on a Number of Features Scale

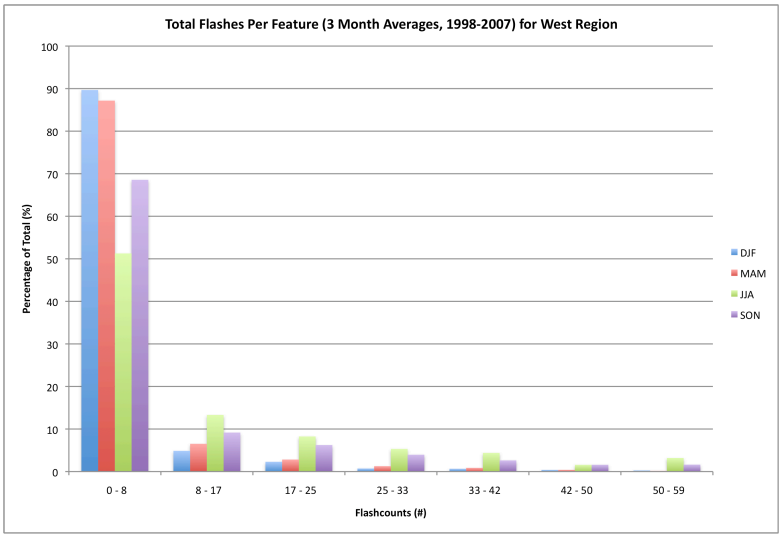

Figure 3.10: PDF of Lightning Flash Counts for 3-month periods on a Percentage of Total Scale, averaged 1998-2007 for West Region

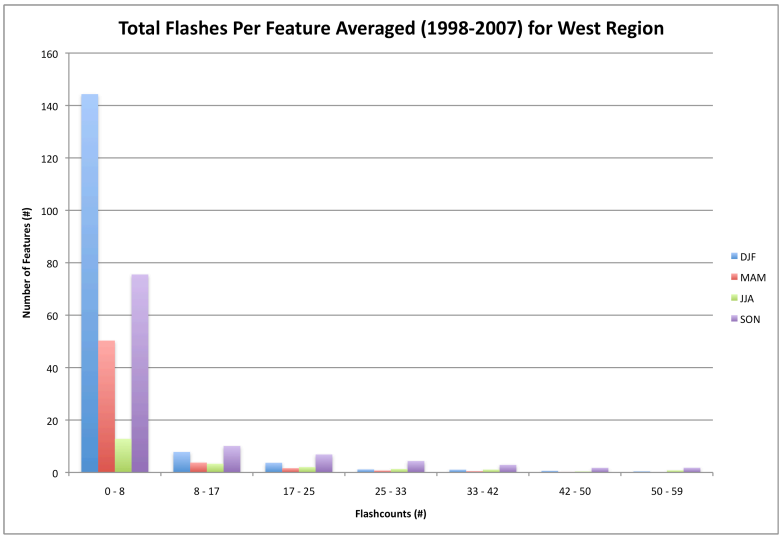

Figure 3.11: Same at Figure 3.10, but on a Number of Features Scale

On the same note, the convective fraction (Black, Figure 3.6) appears to vary in-sync with conditional rain rate (Blue, Figure 3.6) which makes it seem as though the more convective the storm the higher the rain rates, in agreement with Schumacher and Houze (2003) and their definition of convective rain fraction being with rain rates greater than 5 mm hr^{-1}. A field that helps to explain the convective nature of the precipitation features is the lightning flash counts per feature (Red, Figure 3.6). Relative to conditional rain rate and convective fraction, lightning flash counts per feature peaks just slightly later in the year. However, a variable that peaks in-sync with lightning flash count is the max height of the 30 dBZ contour (Black, Figure 3.7). This implies that the deeper (taller) convection occurs in conjunction with the peak in lightning flash counts and does not necessarily indicate features with heavy rain rates and large convective fractions.

To further illustrate this, histograms for lightning flash count per feature (Figure 3.10) and maximum dBZ at 6km (Figure 3.12) are presented to show trends in convective intensity. Of importance in these histograms are their trends relative to conditional rain rate (Figure 3.8). The highest rain rate per feature frequency occurs in JJA, which also is when the highest rates of

lighting flashes and strongest reflectivities occur as a percentage of the total (Figures 3.10 and 3.12, respectively). However, when compared total flashes (Figure 3.11), then we see that JJA is when the fewest total flashes occur and concurrently, this is the time of the year with the lowest rain rate per pentad (Figure 3.3). Also, storms in JJA, as a percentage of the total, have the strongest vertical intensity as indicted by the high frequency of features in Figure 3.12. So, JJA is when the strongest, rainiest, and more infrequent features occur with the lowest rain rates per pentad.

At the same time, other trends to draw from these convective histograms are that convection in the pre-monsoon and into active monsoon season trends toward lower flash counts based on percentage of lightning in the low flashes category and percentage of features with lower 6 km reflectivities. However, if the total number of features is taken into account, we notice that high values for these variables are achieved year round, but in the dry season the convection just tends to consist of the strongest features as opposed to large integration of weaker features, which is what occurs in the monsoon season. This transition from infrequent, strong, and high rain rate convection into more frequent, less vertically developed and overall rainier convection is typical of a monsoon climate and is present in the Western region.

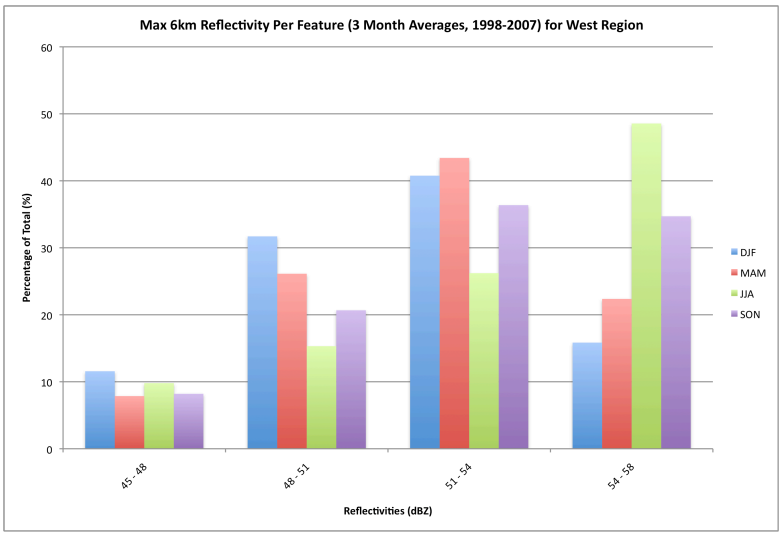

Figure 3.12: PDF of Max Reflectivity at 6km for 3-month periods on a Percentage of Total Scale, averaged 1998-2007 for West Region

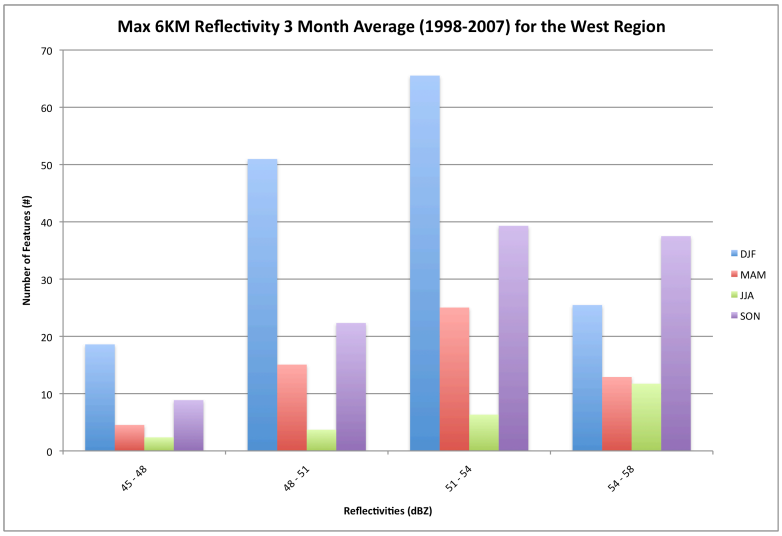

Figure 3.13: Same at Figure 3.12, but on a Number of Features Scale

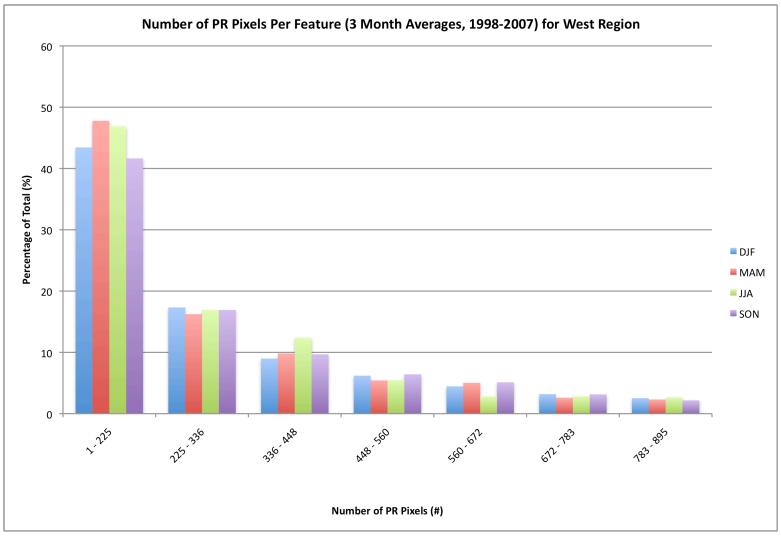

Figure 3.14: PDF of Number of PR Pixels for 3-month periods on a Percentage of Total Scale, averaged 1998-2007 for the West Region

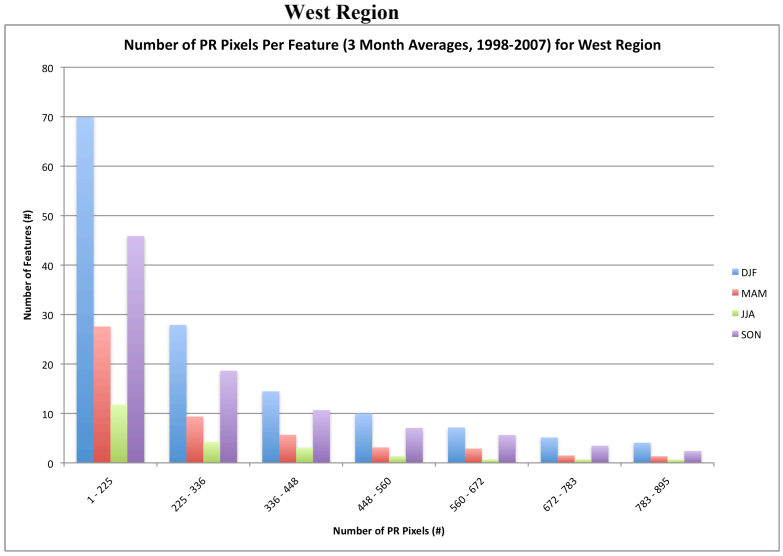

Figure 3.15: Same at Figure 3.14, but on a Number of Features Scale

Since we have established that the convection in the dry and wet seasons are different, an analysis of how and why they are different is needed. A reason for this observation could perhaps be due to the types of large convection that are occurring. Typically early in the dry season the West region experiences more isolated, large systems, while later into the season the systems can include coastal squall lines and more developed MCSs that propagate across the basin on a more consistent basis (Rickenbach, 2004).

This can be examined with time series analysis of latent and sensible heat flux, relative to other PFBD variables (Figure 3.16). Previous studies have argued that this region of South America is subject heavily influences by these fluxes, which act to provide the thermodynamic energy necessary to drive convection. In the case of the West region, the initial (Pentad 26) increase in sensible heat and decrease in latent heat, which later (Pentad 46) reverses in both variables, implies that the atmosphere is being initially driven by strong thermodynamic forcing from sensible heat flux and that once the low-level moisture builds (Fu and Li, 2003), latent heat initiated processes and a larger scale mechanism take over.

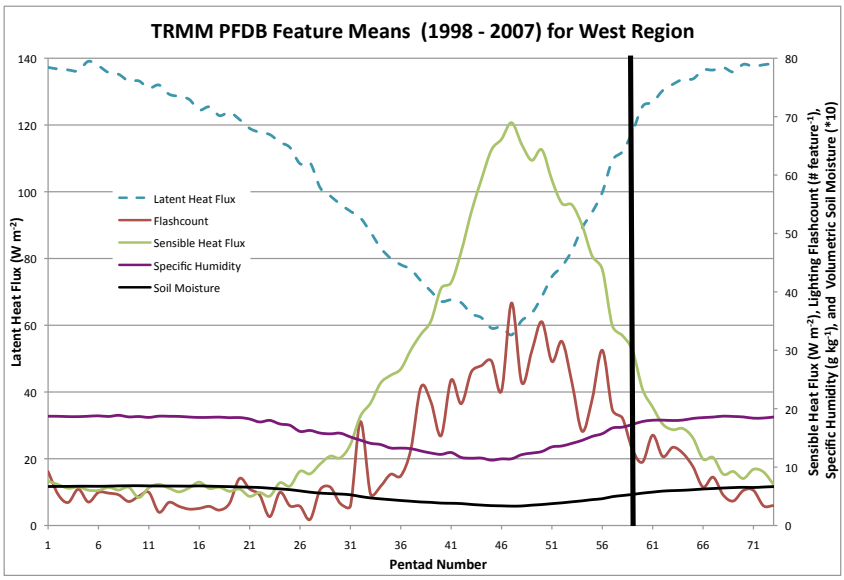

Figure 3.16: Variables from the PFDB and NCEP Reanalysis averaged 1998-2007 for West Region. Latent Heat Flux (Blue, dashed), Sensible Heat Flux (Green), Lightning Flash Count (Red), Specific Humidity (Black), and Volumetric Soil Moisture (Black)

In the pre-onset, there is a significant build up of sensible heat, starting at pentad 21 and peaking at pentad 46. This is the time of the year when we see peaks in lighting per feature, conditional rain rate per feature, convective fraction per feature, and 30 dBZ height (Figures 3.6 and 3.7). In fact, a correlation analysis preformed between flash count per feature and sensible heat flux returned a correlation coefficient of .94. This is very significant because implies that 94% of the variance in lightning flash count is explained by variations in sensible heat flux and is consistent with previous work (Fu and Li, 2003, and Fu et al.., 1998) that suggest that sensible heat flux at the surface acts to destabilize the atmosphere and creates a favorable environment for the development of convection. Also, sensible heat flux has a .63 correlation with max height of 30 dBZ, which again serves to imply that sensible heat is a player in driving dry season convection.

At the same time, correlations between flash count and specific humidity and soil moisture were -.766 and -.854, respectively. So as humidity and soil moisture increase, the amount of lightning decreases. Again, negative correlations here show that lightning thrives in

drier seasons of the year, when sensible heat has time to build at the surface to drive convection. Also, the argument that was presented earlier for increased lightning activity due to the presence of many small CCN that could be lofted high into the atmosphere is valid as well. We see a drop off in lightning activity as we approach onset (Pentad 58) possibly due to the moistening of the region driving sensible heat down and latent heat flux up. Latent heat increasing implies a moist surface in a relatively dry environment and also the presence of clouds that inhibit the heating of the surface to drive sensible heat flux.

Figures 3.17 through 3.20 represent the average rainfall in each respective month from July (Dry Season) to October (Onset). Of note here is the lack of rainfall in the central Amazon in July and August, which corresponds with the peak observed in sensible heat flux. Following this gap in rainfall, September and October show an increase of rainfall across the basin and is in line with the rise in latent heat seen in the time series plots. It is the solar radiation that helps drive the thermodynamic processes in the pre-monsoon season; however, once local thermodynamic processes cannot support the continued high rain rates the larger scale precipitation mechanism that takes over is the continental ITCZ. This mechanism acts to combine large-scale convergence with available moisture that is fed southward by the eventual southward turning of the low-level easterlies in the central Amazon (Zhou and Lau, 1998 and Fu et al. 1999). Moisture advection and also the advection of more unstable air that acts to destabilize the lower troposphere, by altering the low level lapse rates and increasing the amount of CAPE, is transported through this wind reversal from the Tropics into the higher latitudes (Fu et al., 1999).

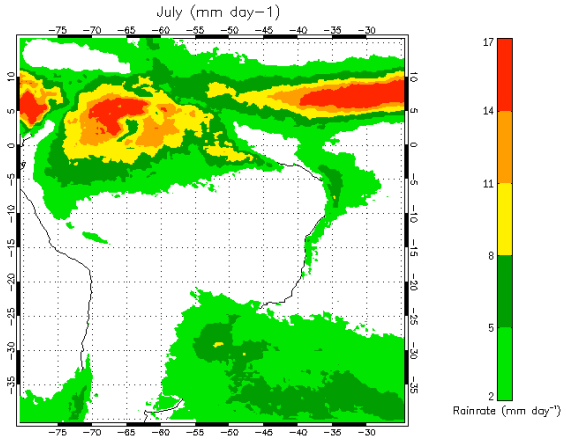

Figure 3.17: 3B42 average rainfall (mm/day) for the month of July, averaged 1998-2007

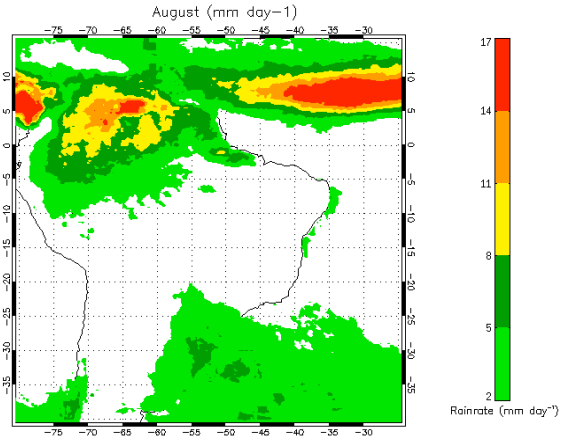

Figure 3.18: Same as Figure 3.17, but for August.

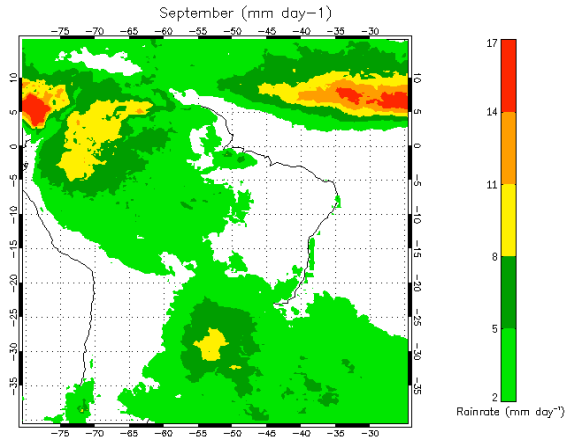

Figure 3.19: Same as Figure 3.17, but for September.

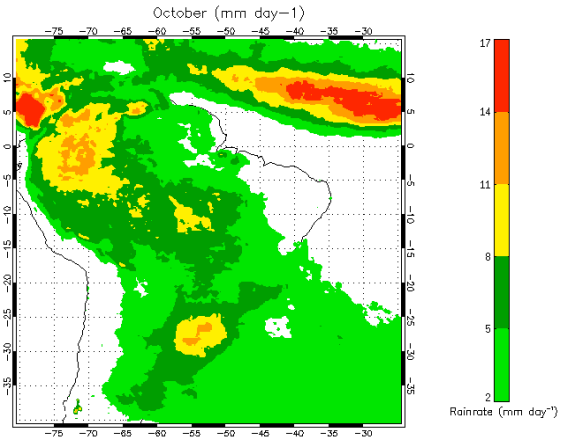

Figure 3.20: Same as Figure 3.17, but for October.

Based on the results presented so far, it is understood that in the West the drivers of precipitation change as the monsoon season approaches. The 10-year and 3 monthly averages illustrate how these variables vary over longer periods of time, but to gain a better picture of their variability as it relates to onset, then one must isolate each variable and how it varies before and after local onset on a year-to-year basis. Table 3.1 is a composite of the listed variables for the West region 10 pentads before and 10 pentads after onset. This provides a look at how these variables change in the roughly two months prior to and two months after onset has occurred.

	East	West	South	SACZ
Average Flash count Before (#/pentad)	15.18	26.1	43.13	13.79
Average Flash count After (#/pentad)	5.32	9.37	41.57	7.33
% Change	**-64.89**	**-64.08**	**-3.56**	**-46.84**
Average Cond. Rain Before (mm/hr/pentad)	49.13	54.68	50.60	46.29
Average Cond. Rain After (mm/hr/pentad)	67.17	63.04	52.04	55.41
% Change	**36.71**	**15.29**	**2.85**	**19.69**
Mean Pre-onset Conv. Fraction (%/pentad)	45.86	55.34	51.50	47.93
Mean Post-onset Conv. Fraction (%/pentad)	47.34	48.05	52.35	45.4
% Change	**3.22**	**-13.16**	**1.66**	**-5.23**
Mean Pre-onset max 30DBZ Height (km)	6.54	9.65	8.68	8.57
Mean Post-onset max 30DBZ height (km)	7.05	8.41	9.29	8.10
% Change	**7.74**	**-12.85**	**7.02**	**-5.41**

Table 3.1: Precipitation Feature Statistics for Features with a MCS for 10 pentads prior to local onset and 10 pentads after local onset, averaged 1998-2007 for all four regions

Most of these changes were observed in the time series plots, but being able to quantify them close to onset lets us analyze which ones have the most significant changes. For example, lightning activity in the West region decreases by 64% after onset and max 30 dBZ heights decrease almost 13%, while conditional rain rate increases 15%. This shows that the rainfall in the West region before onset is dependent on these electrified and vertically developed storms, whereas after onset storms are not as dependant on these storms being strong and vertically developed in order to produce high rainfall rates. These changes further corroborate the initial

observations that convection prior to onset and after onset are fundamentally different and quite possibly driven by different mechanisms.

Regimes of winds just above the surface have been shown to be associated with the change in convection as referenced in previous studies (Petersen et al. 2002, Halverson et al. 2002, and Rickenbach et al. 2002). A 10-year time series of the lower level winds shows a post onset shift in wind direction (Figure 3.21). Throughout the dry season, the winds are stronger and easterly/northeasterly (easterly wind regime). However, after monsoon onset, there is on average a 5-10 pentad shift to average westerly/northwesterly flow (westerly wind regime). Before onset, when winds are more easterly, the convection is more isolated, stronger, and contains heavier rain rates (Petersen et al. 2002). After onset, when the mean winds shift is when convection typically becomes more widespread with less intensity and lighter rain rates (Rickenbach et al. 2002). Thus, the shift in mean wind direction is a signal of the transition into a monsoon regime in the West region.

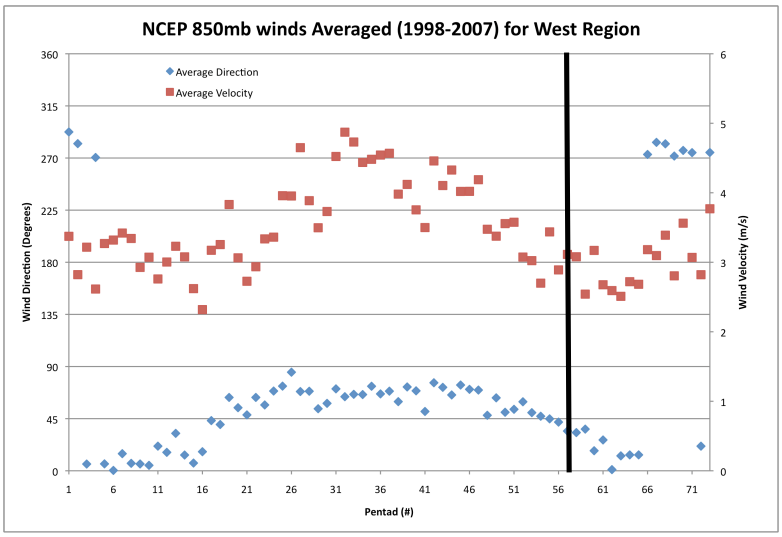

Figure 3.21: NCEP Reanalysis winds for West region averaged 1998-2007. Wind Direction (Blue) and Wind Velocity (Red).

These shifts in winds are in line with both the PFDB and other NCEP fields that characterized precipitation in the pre-onset period as deep convection with high rain rates, while

post-onset precipitation tends to consist of weaker systems that on average rain less per feature. The appearance of this shift in the 10-year average further shows how important the wind shift truly is. The shift of winds from easterly to westerly helps drive moisture into the West region and allows the larger scale ITCZ to become the dominate driver of precipitation as opposed to the local and isolated efforts of thermodynamic forcing, aided by sensible and latent heat fluxes at the surface.

The West region is characterized by shifts in both the mechanisms that drive precipitation around onset and the types of precipitation that each mechanism favors. Before onset the convection is stronger, more intense, and driven by local forcing mechanisms like heat fluxes. While after onset the precipitation is driven by the larger scale continental ITCZ and due to the development of the SALLJ along the Andes, moisture transport is transported into the Amazon Basin. Convection after onset is typically more widespread, with features becoming less rainy due to the eradication of the thermodynamic forcing mechanisms present in the pre-onset period. The East region experiences a similar pattern like the West, but due to its location its precipitation is governed by a slightly different mechanism.

3.1.2 - East Region

The Eastern region is located in the Northeast part of the study region, around the mouth of the Amazon River. This region has an annual cycle of rainfall, but does not have a significant "dry" season, with rain rates per pentad only dropping to around 30 (mm/day) (Figure 3.22). Monsoon onset occurs later in the East with an average onset pentad of 68 (Nieto-Ferreira and Rickenbach, 2010), which is in early December. The East region is the last of our four regions to reach monsoon onset and with that, it is also the last to have the monsoon season end, which is around April or May. The standard deviation of onset pentad for this region is 4 pentads

(Nieto-Ferreira and Rickenbach, 2010) and in all of the years studied, onset as defined by the precipitation threshold occurred in each but one.

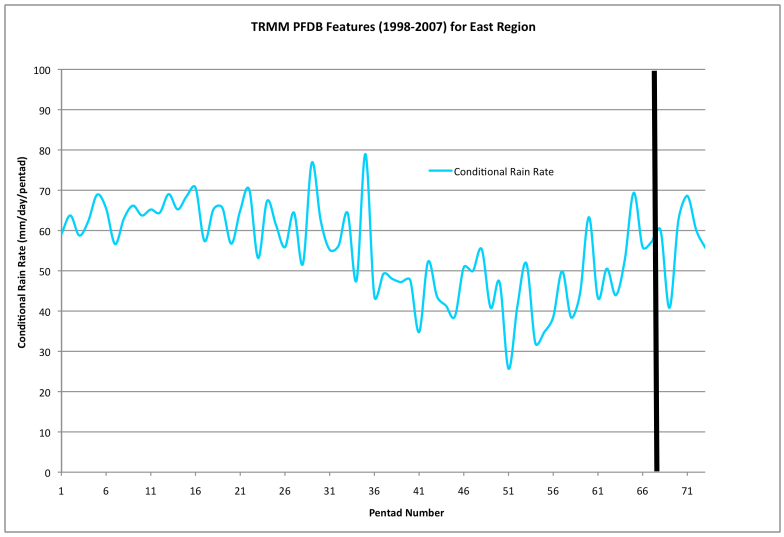

Figure 3.22: Conditional Rain Rate per Pentad for Features with a MCS, averaged 1998-2007 for the East Region

Features with shallow convection

These features in the East region give the first indication that precipitation features here are occurring later in the year. The number of features (Red, Figure 3.23) reaches a minimum late in the year, around September and increase rapidly through the average onset date. Increase in the number of features begins as the sensible heat flux (Green, Figure 3.23) has peaked and is trending downward. Figure 3.23 also introduces us to the latent heat and sensible heat fluxes in this region and the first thing that should stand out is the relative constant nature of the latent heat flux. The lack of variability is most likely attributed to the influence of the ocean on these boxes. With a constant source of moisture, the surface humidity level should stay consistently high, while atmospheric humidity levels will fluctuate with evaporation due to solar radiation. The mean signal is one of elevated latent heat flux. Sensible heat flux in the East region is tied closely to the presence cloud cover and evaporative cooling. The clouds are present due to the steady onshore flow for most of the year, and when they are not observed to be as pronounced

(Figures 3.19 and 3.20), sensible heat flux is observed to rise in the pre-onset period. Also, evaporative cooling due to constant presence of moisture can cool the atmosphere to mirror the surface temperature, which would act to limit the sensible heat flux.

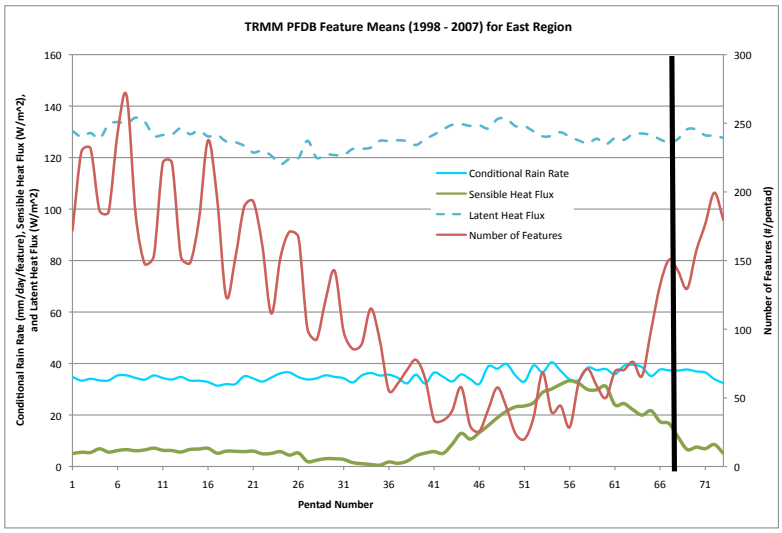

Figure 3.23: Variables from the PFDB for Features with shallow convection in the East Region. Conditional Rain Rate (Blue), Number of Features (Red), Sensible Heat Flux (Green), and Latent Heat Flux (Blue dashed)

Features with deep convection

For features with deep convection, the trends in the number of features are the same as in features with shallow convection, including the relative numbers. One noticeable difference between the two is that features with deep convection are rainier per feature and this trend begins once the monsoon is winding down, all the way until the average onset occurs. Sensible heat seems to not have much effect on when rain rates per feature (Blue, Figure 3.24) start to increase, but the number of features appears to be inversely proportional to rain rate between pentads 31 to 66. This could be similar to what is seen in the West region where there are less total storms that are more intense overall.

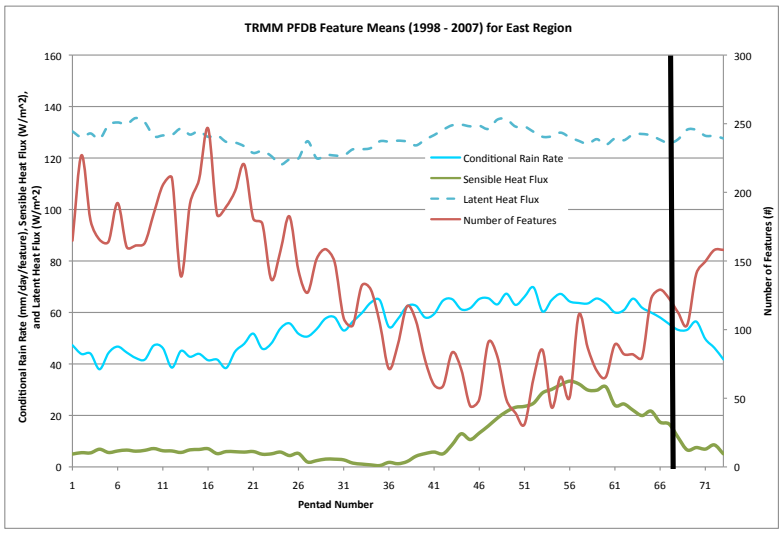

Figure 3.24: Same as in Figure 3.23, but for Features with deep convection

Features with a MCS

The largest noticeable difference between features with and without a MCS is that the number of features with a MCS in the east region are dramatically fewer than the others. The highest average number of features with a MCS occurs after onset and is only 11-12 features per pentad on average, compared to approximately 450 features per pentad on average for features without a MCS. An interesting observation also is that the rainfall per feature in this region does not vary as dramatically as it does in the West. Rainfall per feature for those with deep convection and also those with a MCS follow roughly the same trend through out the year. Features with deep convection (no MCS) have just slightly lower rain rates; however, those without a MCS are also not as variable as those with a MCS.

The East region is yet another region where before onset thermodynamics are driving precipitation, whereas after onset there is a large scale mechanism that takes over, similar to what is observed in the West. Lightning flash counts (Red, Figure 3.25) are relatively low and constant throughout most of the year, however, in the later part of the dry season (pentad 41) flash counts begin to increase and become a little more variable. Interestingly, this trend occurs

in conjunction with the sudden increase in sensible heat flux. The max height of the 30 dBZ contour time series varies similarly to flash count, which signals that features containing higher flash counts are more vertically developed. Based on the East region 10 year time series features in the dry season are rainier per feature and are more convective as a function of the total feature. Another important observation is that onset here occurs late in the year, well into the South American summer, and is apparent by many of the variables peaking in the late part of the year. The fact that the Atlantic ITCZ is slow moving due to heat capacity differences in water causing it to migrate slower contributes to it lingering in the region well into the fall. This prevents the region from drying out and limits sensible heat flux from increasing and eventually playing a role in the development of more rigorous convection.

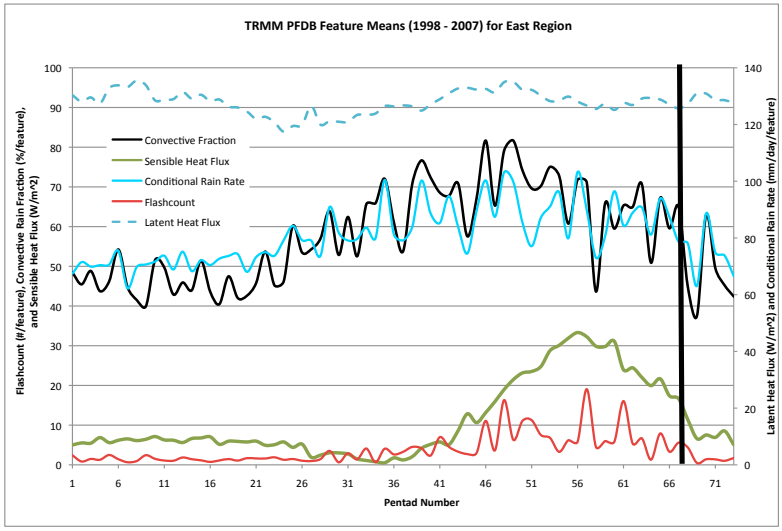

Figure 3.25: Variables from the PFDB for Features with a MCS in the East. Conditional Rain Rate (Blue), Lightning Flash Count (Red), Convective Rain Fraction (Black), Sensible Heat Flux (Green) and Latent Heat Flux (Blue dashed).

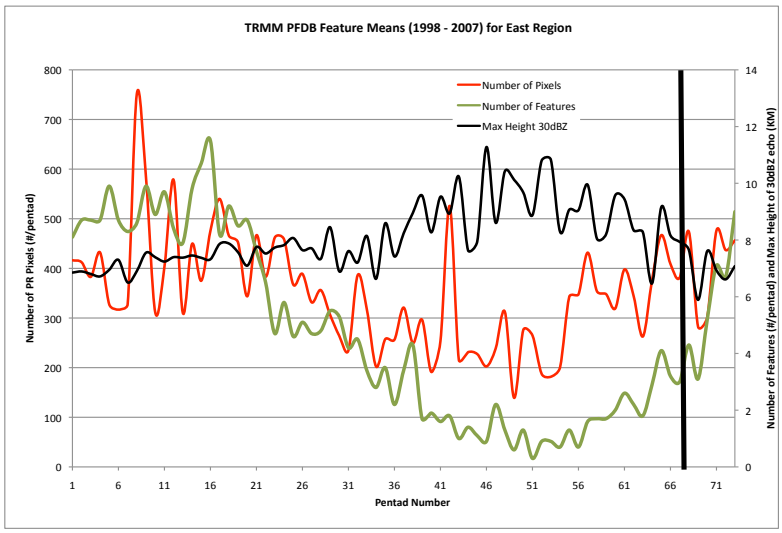

Figure 3.26: Variables from the PFDB for Features with a MCS in the East. Max Height of the 30dBZ contour (Black), Number of PR Pixels (Red), and Number of Features (Green).

The observation of rainier features in the dry season is further confirmed with PDFs of conditional rain rates per feature. Figures 3.27 and 3.28 show the conditional rain rates per feature on a percentage of total features and total number of features basis averaged over 10 years. These PDFs show that the highest percentage of heavily raining features does occur in JJA and SON (Green and Purple bars, respectively); however, these are also the 3 month periods with significantly less total features when compared to the other 6 months of the year.

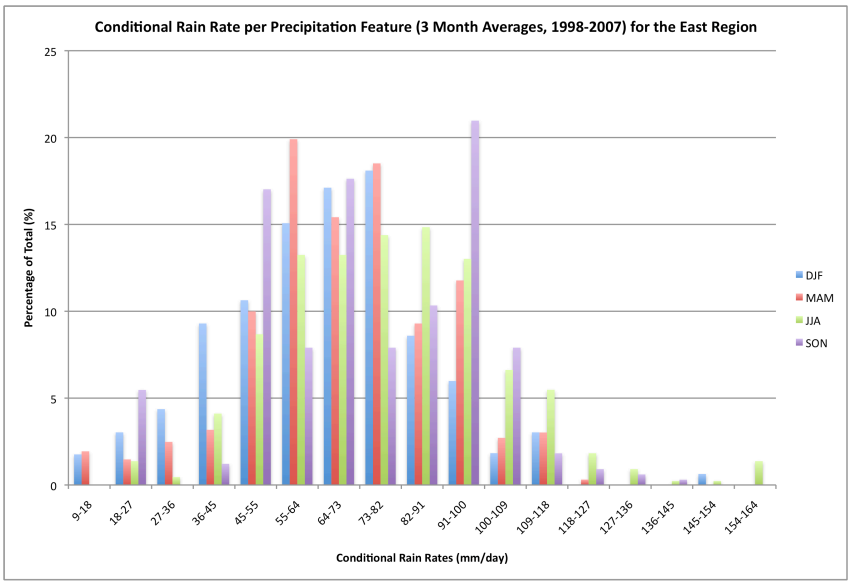

Figure 3.27: PDF of Conditional Rain Rates for 3-month periods, Percentage of Total Scale, averaged 1998-2007 for East Region

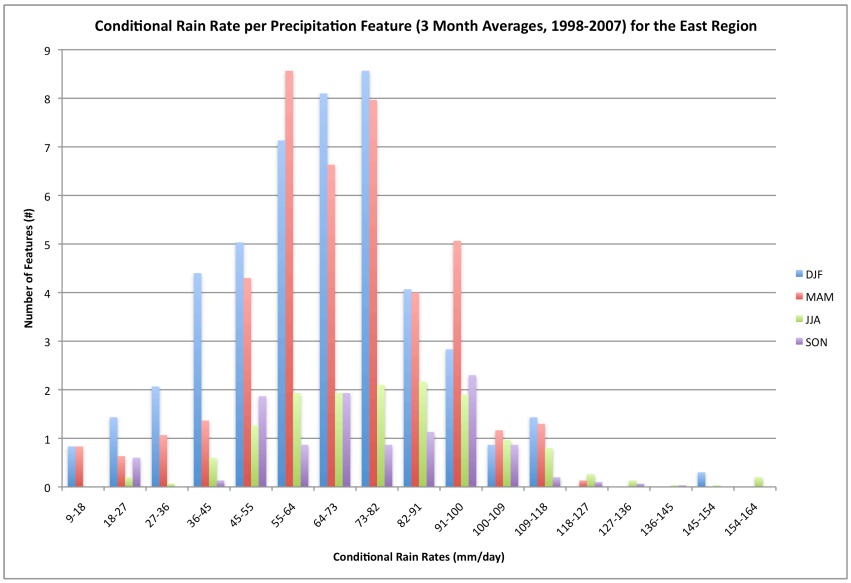

Figure 3.28: Same at Figure 3.27, but on a Number of Features Scale

This does not specifically mean that in the dry season that it rained more than in the wet season, but what it does suggest is that when it does rain in the dry season on average the rain rates are much larger than in the wet season. There are heavily raining features in the wet season, but the majority of them were contained within the lower rain rates and this fact poses the question of whether or not the conditions that are driving the precipitation are vastly different from JJA/SON into DJF/MAM.

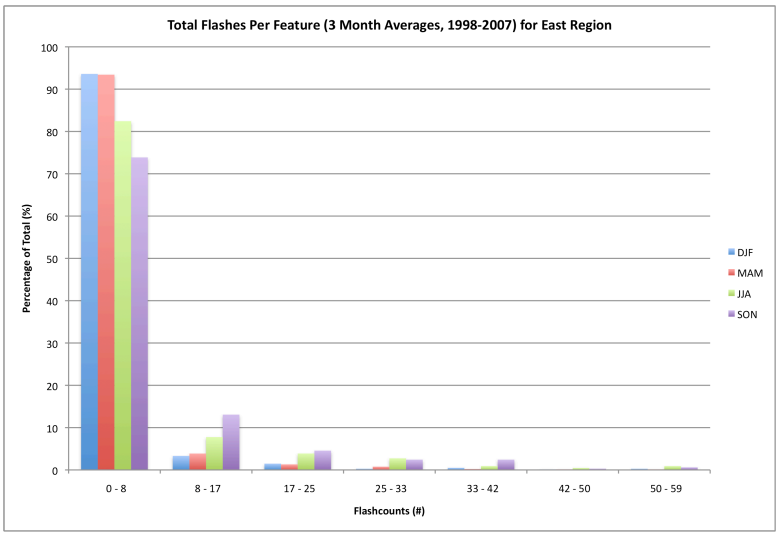

Figure 3.29: PDF of Lightning Flash Counts for 3-month periods on a Percentage of Total Scale, averaged 1998-2007 for East Region

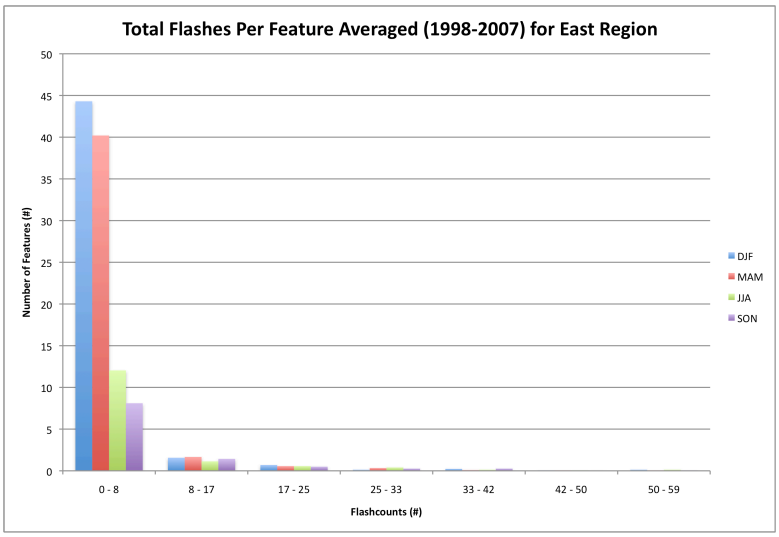

Figure 3.30: Same at Figure 3.29, but on a Number of Features Scale

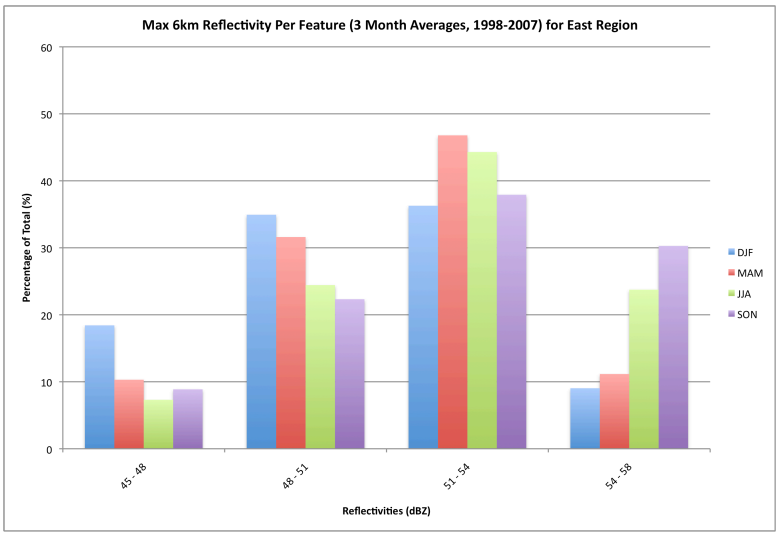

Figure 3.31: PDF of Max Reflectivity at 6km for 3-month periods on a Percentage of Total Scale, averaged 1998-2007 for East Region

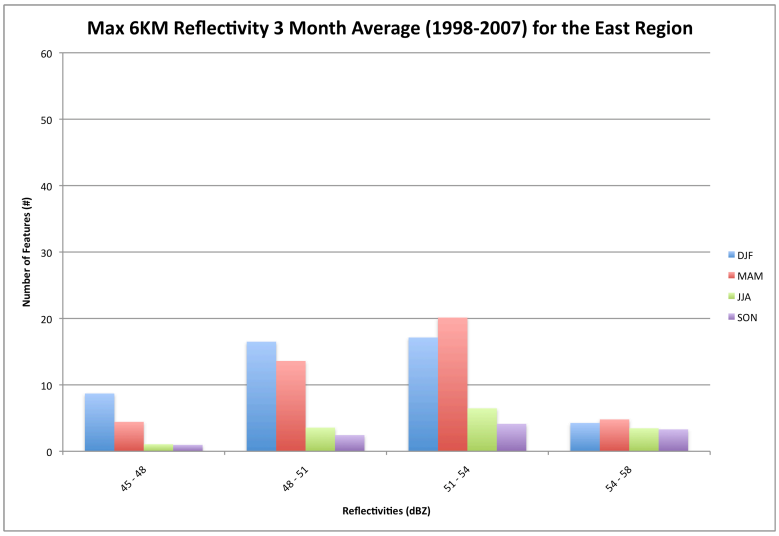

Figure 3.32: Same at Figure 3.31, but on a Number of Features Scale

To further illustrate that dry season features are more convective, Figures 3.29 and 3.30 show PDFs of lightning flash counts. As a percentage of the totals, Figure 3.29 shows that SON and JJA (to a lesser extent) contain more features with higher flash counts. As was the case with conditional rain rate, the total number of features in this time period is significantly less than the rainy season. When looking at the total numbers (Figure 3.30), there are actually just as many features occurring on the higher end of the flash counts in every 3 month period, but where the difference lies is that the rainy season contains the majority of low flash count features.

In conjunction with the flash counts PDFs, max reflectivity at 6km (Figures 3.31 and 3.32) is another proxy for vertical intensity. Again, the observation of fewer and more vertically developed features in the JJA/SON period as compared to the DJF/MMA period is evident. Simply put, features in all of these ranges for all of these variables occur year round in the East region; however, on a per feature basis, it is more common for the dry season features to contain a higher percentage of the "strong" convection relative to the wet season.

Correlations between different variables can give insight into a relationship that can help explain why the convection varies from season to season. Figure 3.33 is a time series of conditional rain rate per pentad, sensible heat flux per pentad, and lightning flash count per feature (per pentad values of flash count were approximately the same).

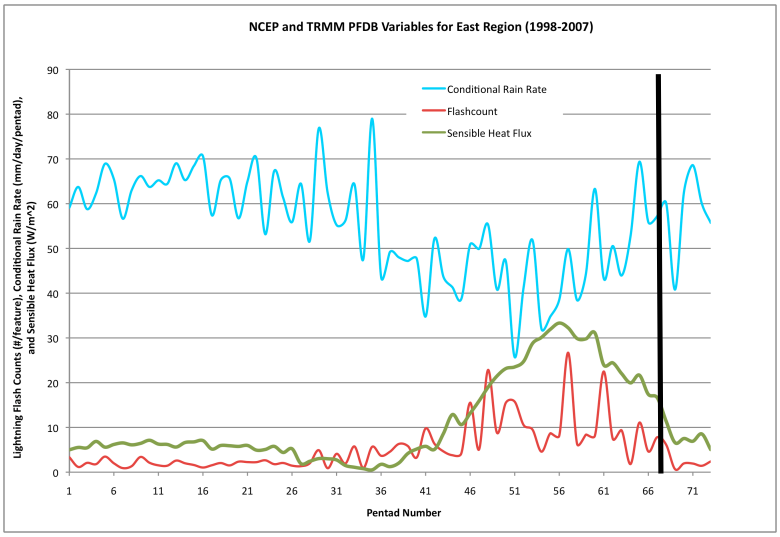

Figure 3.33: Variables from the PFDB and NCEP Reanalysis averaged 1998-2007 for Features with a MCS in the East Region. Conditional Rain Rate (Blue), Sensible Heat Flux (Green), Lightning Flash Count (Red)

What is important is to note that there is a .539 correlation between flash count and sensible heat flux and at the same time flash count has a -.558 correlation with soil moisture (not shown on graph). Basically this illustrates that features that have high flash counts occur in times where sensible heat flux is high, which include times where there is very little blocking direct

solar warming of the surface and also when the ground is dry and the suns energy does not have to go into evaporating moisture, which acts to lower the temperature difference between the ground and surrounding air and thus lowers the surface sensible heat flux (Figures 3.18, 3.19, and 3.20). These features represent the time of year when the East region is transitioning from the winter (dry season) in to the spring (pre-onset season). These images reveal that there is constantly rain (clouds) present in the northern East box, but in the southern sections, there is a brief retreat of cloud cover and it is during this time that solar radiation is able to heat and dry out the surface and increase the sensible heat flux.

This is significant because it suggests that thermodynamic forcing due to high levels of sensible heat possibly drives electrified features. These levels are high prior to onset and explain the sudden increase in features (Figure 3.25) and rain rates (Figure 3.22). Another correlation that is important is between conditional rain rate per pentad and sensible heat flux, which turns out to be -.517. Sensible heat is high during the dry season when convection is observed to be more intense per feature, but also more infrequent. So this relationship just confirms that when sensible heat builds there are few and more intense features, compared to other times in the year when sensible heat is basically negligible. Once conditional rain rates start to increase again, more clouds and moisture are present and sensible heat flux begins to decrease (Figure 3.20).

The next question to address is why is it that dry season convection seems to contain mainly high rain rate and electrified features, while wet season features are less electrified, but rain more per pentad than their dry season counterparts. Figures 3.34 and 3.35 are PDFs that represent the percentage of total and total numbers for the number of PR pixels. This variable is used as a proxy for the size of the features due to the fact that if more pixels are filled with radar returns that represent precipitation, then the features will be larger in horizontal dimension. One

initial observation to take from these PDFs is that in the dry season months JJA/SON is when the highest percentage of low pixel count features occurs. JJA/SON contain a higher percentage of PR pixels, compared to the other periods, until the 3rd pixel count bin is reached. This bin is when the higher percentage of the number of PR pixels becomes dominated by the wet season months. This suggests that in the dry season, features typically contain low pixel counts relative to the wet season when there are a higher percentage of features in the larger pixel count bins. Total counts (Figure 3.35) also shows that while the wet season features are concentrated in the lower end, there are also a significant number of features as the bin sizes increase. On the other hand, the dry season (JJA/SON) counts are concentrated toward the lower end and then quickly drop off as the bin sizes increase.

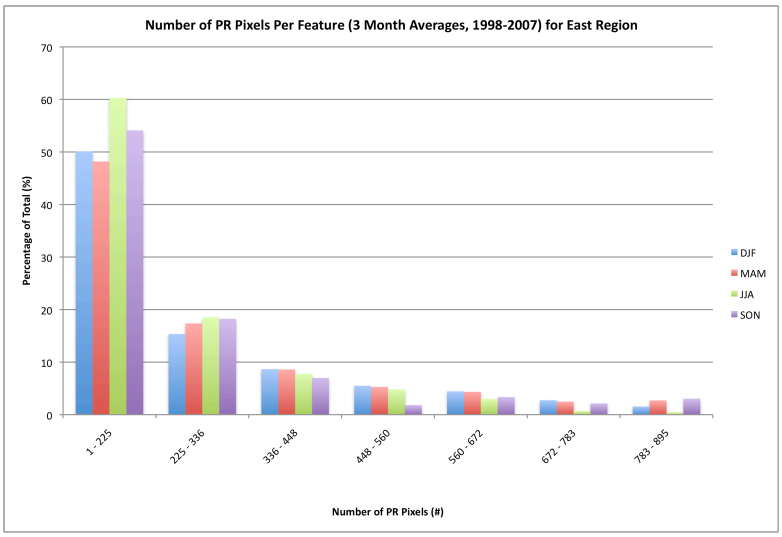

Figure 3.34: PDF of Number of PR Pixels for 3-month periods on a Percentage of Total Scale, averaged 1998-2007 for East Region

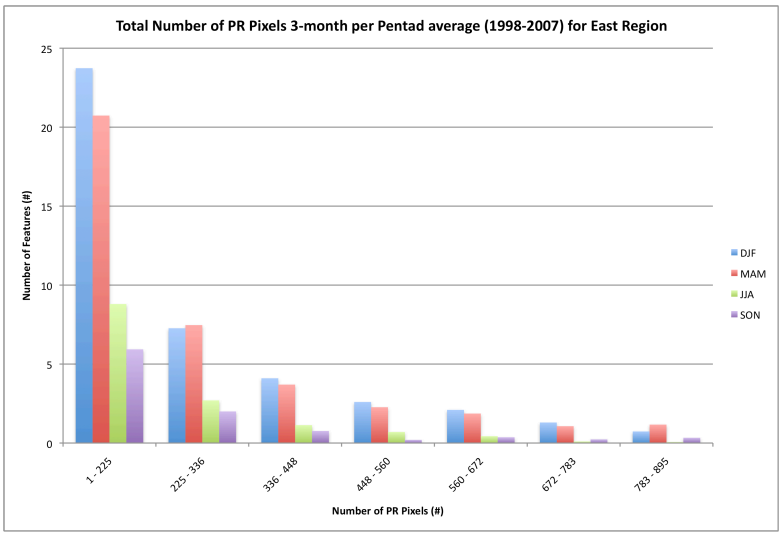

Figure 3.35: Same at Figure 3.34, but on a Number of Features Scale

In the East region, dry season convection is characterized by the presence of few features and of these features, most contain more intense rain rates, are more electrified, and do not occupy a large horizontal domain as a percentage of the total number as compared to the wet season convection. On the other hand, during the wet season, there are more total features and these features typically contain more features in the high and low ends of variable bins. However, due to the larger numbers of features, their tendency is to be weaker because there are significantly more features concentrated toward the lower bins than is observed in the dry season. Being able to see how these variables act around onset should give insight into whether or not the storms are truly much different from the dry to wet season.

As was seen in the time series, flash counts noticeably drop off after onset by 65% (Table 3.1). This is consistent with the working hypothesis that pre-onset features are more electrified than their counterparts after onset. Also, post onset rain rates are higher by 37% and this is expected because it is the formal transition into the rainy season. However, one interesting observation here is the subtle increase in convective parameters while the electrification variable denotes a negative trend. One explanation of this is that while features are more vertically

developed after onset, they are not as electrified because more destabilized atmosphere that is available in the presence of high sensible heat flux does not exist after onset and thus limits the extent by which electrified convection can develop.

The mean wind speed and direction at 850 mb in the East region (Figure 3.36) do not explain why the dry season storms are more electrified, but what they do show the persistent influence that the ocean has on the local environment. Persistent easterlies in the East region provide a steady supply of low-level moisture, which helps to maintain the steady level of latent heat that is observed in the time series. As mentioned before, this limits the amount of sensible heat that can build at the surface to be the main driver of the atmosphere thermodynamically. Also, easterlies serve to usher in oceanic convection in the post-onset period, which is typically not vertically developed and more stratiform in nature (Petersen and Rutledge, 2001). This assists in explaining the relatively stable levels in the vertical intensity fields before and after onset. Conditional rain rate per pentad levels rise after onset because the ITCZ settles in the region and steady easterlies serve to move more oceanic systems associated with the ITCZ onshore. These are not available year round, thus the per-pentad values increase when present.

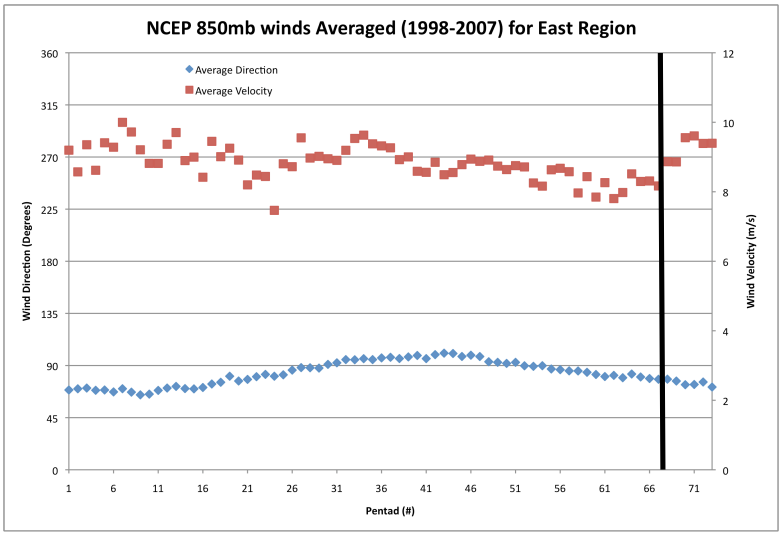

Figure 3.36: NCEP Reanalysis winds for East region averaged 1998-2007. Wind Direction (Blue) and Wind Velocity (Red).

The East region is unique in that monsoon onset here does not occur until well after onset in most of South America and also because it lasts much longer than the monsoon in other regions. The pre-onset environment here is characterized by the thermodynamic forcing of precipitation, caused by latent and sensible heat fluxes. After onset, the principal precipitation mechanism is the Atlantic ITCZ. The slow migration southward into the East region is the reason why monsoon onset here occurs later in the year and is also why the season takes longer to transition out of the monsoon period. Although the East region is located relatively close to most of the West region, the two regions are very much different when it comes to the types of precipitation features that affect each respective region, both in feature magnitude and defining characteristics.

3.1.3 - West vs. East

The West and East regions are being compared because the mechanisms that are responsible for initiating their monsoon season are similar, yet vastly different. These regions are subject to similar a similar buildup in instability due to sensible heat flux, while at the same time being driven after onset by a large scale mechanism. In both cases, the movement of the sun dictates when onset occurs and when the large-scale drivers take over. In the West, continental heating allows for onset to occur early in the season, while in the East, the ocean not only prevents the quick build up of sensible heat flux, but also delays the migration of the Atlantic ITCZ due to the slow heating of the ocean compared to the land. These interactions will be further explored through an in depth comparison of each of these regions.

Both of these regions are located in the Tropics and Amazon Basin region of South America. However, monsoon onset in these regions differs in two ways. One way is the time of

the year when onset occurs and the second way are the mechanisms that dictate when and how it happens. When looking at the raw onset averages (Nieto-Ferreira and Rickenbach, 2010), the average onset pentads for these regions are 58 (Black line in time series) for the West and 68 (Red line in time series) for the East (both with standard deviations of 4 pentads), so this fact alone sets them apart. Yet, it is how the precipitation feature variables contrast in relation to each other that shows the fundamental differences between precipitation in each region. These trends are seen more clearly when comparing precipitation features time series' presented earlier for each region.

Conditional rain rate (Figure 3.37) is the clearest indicator that there is an offset between onset between the West and East regions. The West region reaches its precipitation minimum around pentad 36, whereas the East region does not reach this point until pentad 51. Also, an important observation is that in the East the rain rates stay higher for longer, which implies that there is something driving continual precipitation deep into the Southern Hemisphere Autumn. In the West, the rain rates drop off rapidly around pentad 15 and continue to fall for another 4-5 months. Pre-onset precipitation in both regions, according to the presented research, is driven by the destabilization of the atmosphere due to surface heat fluxes. The delays in conditional rain rate changes imply that the build up of these surface heat fluxes are slower to occur in the East region than in the West region. This observation will be addressed shortly.

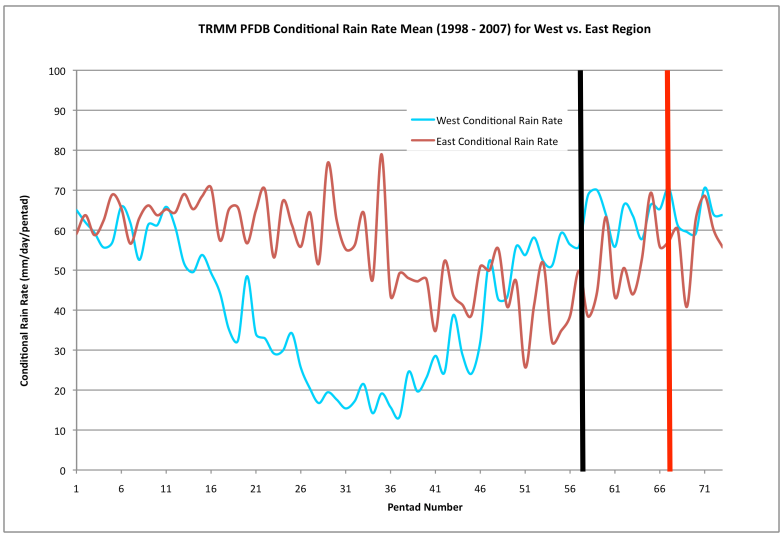

Figure 3.37: Conditional Rain Rate per Pentad for Features with a MCS, averaged 1998-2007. West Region (Blue) and East Region (Red)

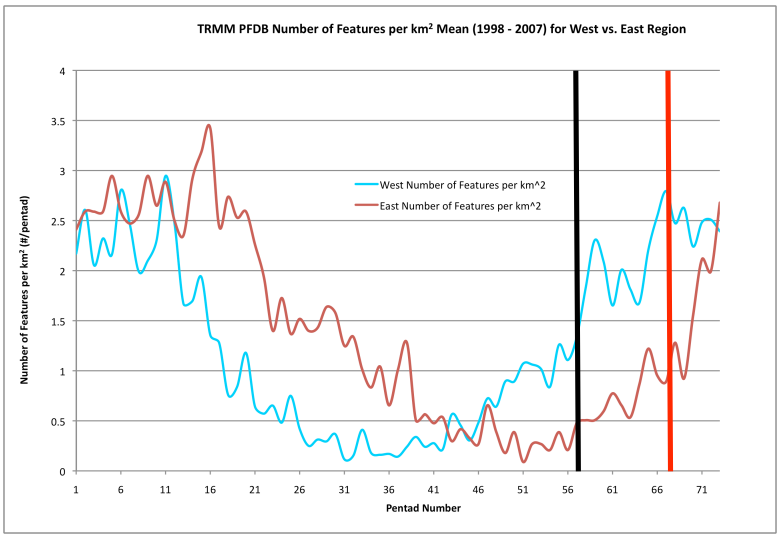

Figure 3.38: Number of Features per km^2 per Pentad for MCS Features averaged 1998-2007. West Region (Blue) and East Region (Red)

In conjunction with rain rates, the number of precipitation features (Figure 3.38) also shows an offset between the East and West regions. This time series shows the number of features in each region, relative to their respective sizes so that the West region, which covers over 200% more area than the East region will not dominate the time series. The number of features behaves very similar to variability in the conditional rain rates in that the West region reaches a minimum in both approximately half way through the year, with the East region reaching a minimum much later in the year, again in both. Something interesting to note is how

the West recovers from the dry season much earlier than the East, which implies that a pre-onset mechanism of tropospheric destabilization through the rapid increase in sensible heat flux in the West region is driving this rapid increase in the amount of features. The increase in sensible heat in the East is not nearly as dramatic, but it is present, occurs later in the year, and is consistent with the observed increase in the number of features in that region as well. Both regions are being influenced by fluxes of sensible heat, but the only difference is the timing and the magnitude by which they are affected.

Lightning flash counts (Figure 3.39) shows another aspect of this offset. This field shows the relative difference between the most convective times of the year in each region, which can also serve to confirm when distinct mechanisms of precipitation are at work. In the West, this time of the year builds from pentad 31 to a peak around pentad 46. The East has a similar trend; however, lightning here builds much more slowly than in the West with a start at pentad 36 and a peak at pentad 56. So, the West reaches a maximum in intensity in roughly 3 months, while there is about a 4 month build up in the East.

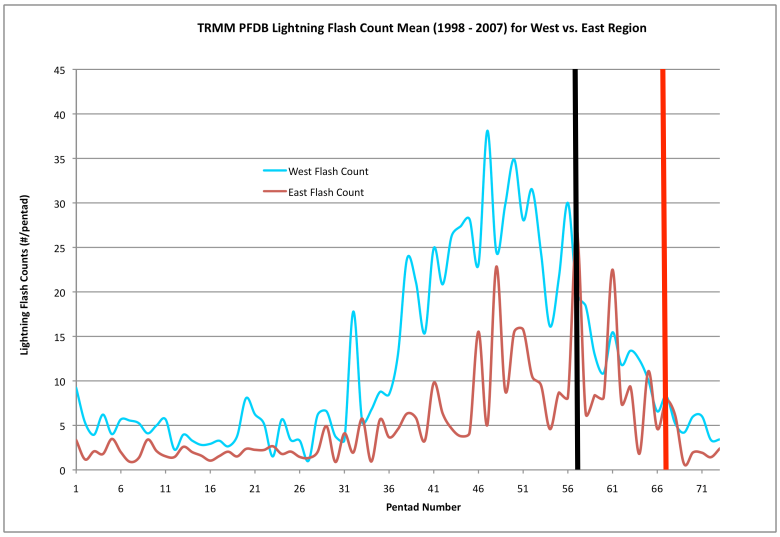

Figure 3.39: Lightning Flash Counts per Pentad for Features with a MCS, averaged 1998-2007. West Region (Blue) and East Region (Red)

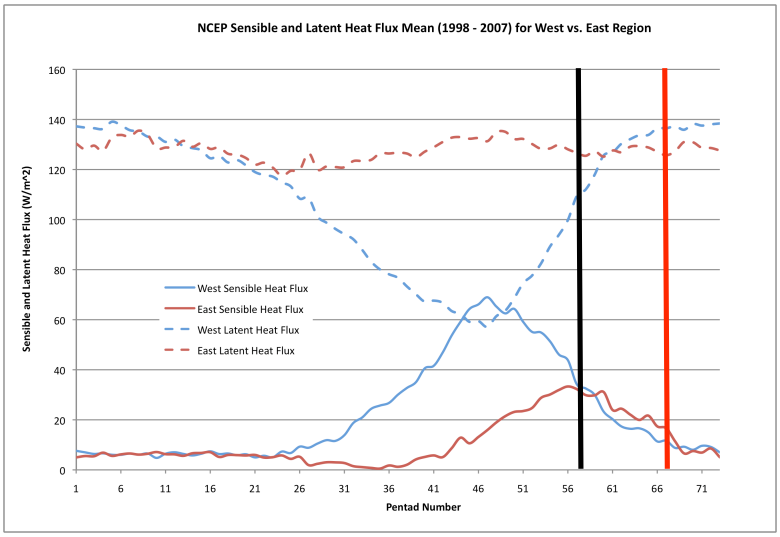

Figure 3.40: NCEP Heat Fluxes per Pentad. Latent Heat Fluxes (Red dashed, East and Blue dashed, West) and Sensible Heat Fluxes (Red, East and Blue, West)

Lighting flash counts (Figure 3.39) in both regions reach a maximum during the same period of time when sensible heat flux (Figure 3.40) is reaching its maximum. As was discussed in the West region section, this region is subject to a quick build up of sensible heat due to relatively clear skies and low moisture content (latent heat). At the same time, the East region is confined in its ability to build up sensible heat like the West region. The East region is subject to constant flow of moist, oceanic air inland through out the year. This moist air can limit daily temperatures through two processes: cloud cover and also evaporational cooling. Sensible heat flux is largely driven by a significant difference between the surface temperature and the local air temperature, so with a moist air mass limiting the amount of solar radiation that can be used to heat the surface, sensible heat flux is not able to build as efficiently as it does in the West region, where abundant moisture is not as readily available.

When it comes to latent heat flux, the specific humidities of the surface and the local atmosphere are contrasted. In the East (Figure 3.36), the wind speed is constant throughout the year, so from the equation for latent heat flux, it is also assumed that the observed difference

between surface and air humidities are roughly similar year round as well since latent heat flux in the East is constant (Figure 3.36). However, in the West there is a depression in latent heat flux in the dry season and (Figure 3.40) with a quick rebound in the pre-onset period. When compared to the winds for the region (Figure 3.21), there is a drop in wind speeds in conjunction with the initial rise in sensible heat flux, which implies that this is a time of the year when the difference in temperature between the surface and the air is most substantial. This is in agreement with the lack of cloud cover in the region during the dry season that allows solar radiation to directly hit the surface of the earth and also in agreement with the increase in thermodynamically driven convection in this region in the dry season.

Trends in lightning flash counts in both regions are highly correlated with sensible heat flux, so we are able to conclude that the pre-onset period both regions have convection that are influenced by increases in sensible heat flux. However, the intensity of the convection varies between the regions. Another key difference between these regions is that in the West region lighting flashes occurs earlier and are also regulated sooner than in the East. Regulation of lightning in the West most likely has to do with the build up of latent heat (dashed blue, Figure 3.40) caused by the dry season convection and also the quick migration southward of the continental ITCZ. In the East region, the suppressed sensible heat flux, which has been shown to lower the localized thermodynamic instability (Fu and Li, 2004 and Fu et al, 1999), limits the amount of electrified features that can form. However, like in the West region, once sensible heat decreases another mechanism becomes the dominant driver of precipitation. This mechanism is the Atlantic ITCZ, which moves at a much slower rate than its continental counterpart, due to the larger amount of time it takes to heat the ocean versus the land. The oceanic ITCZ arrives here

later and lingers here longer, which is why there is a late onset in this region and also why the rainy season lasts longer than in the West (Figure 3.37).

Table 3.1 shows the West region next to the East region and what is apparent is that the type of convection in the West prior to onset is much stronger than the convection in the East prior to onset. The same observation can be claimed for post-onset convection. Both the convective fraction of the precipitation features and the max height of the 30 dBZ contour are telling of a regime in the West region that supports much deeper and convective convection, relative to the East. Another interesting observation when comparing the local onset statistics is the 8% increase in the max height of the 30 dBZ contour in the East. It would be expected that after onset that this value would actually decrease, like was observed in the West, but here it increases and there is really no clear explanation for this observation.

Local thermodynamic processes drive precipitation in both the West and the East. This acts to prime these regions in the pre-onset period for the introduction of larger scale mechanisms at and after onset. Also, both regions are influenced by the ITCZ, the continental version in the West and the oceanic version in the East. The delay in onset in the East is due to the ITCZs slow migration, while the quick onset of the monsoon in the West is in line with the timing of the continental ITCZ and its ability to stay in sync with the movement of the sun. Differences between these two regions are unique, however, other difference do exist across other regions in South America.

3.2 The Subtropics

This chapter will concentrate on the shift of precipitation to regions that are included in the transition from the Tropics into the sub-Tropics. While the SACZ region is technically part of the Tropics, interactions with the sub-Tropics make this region respond to both forcing that is

present in the Tropics and sub-Tropics. The South region is almost purely a sub-Tropical region as it is primarily subject to interactions with forcing mechanisms that originate from high/mid latitude storm systems. These regions will be discussed individually and then we will compare the SACZ region to the West region to observe how Tropical regions interact with sub-Tropical regions as a way of intensifying the monsoon across the entire region.

3.2.1 South Atlantic Convergence Zone (SACZ) Region

The SACZ region is the result of frontal systems stalling across the region and influencing precipitation from the coast into the Amazon Basin (Lenters and Cook, 1999 and Garreaud and Wallace, 1998). The 10-year averaged annual time series of conditional rain rates (Figure 3.41) show that there is an annual cycle, with a relatively short dry season from pentads 26-36 on average. Frontal interactions cause the high variability in conditional rain rates to exist. The time series is a 10-year mean, which implies that the pentad averages exhibit local maximums and minimums due to times with high precipitation and times with little or no precipitation. On average, onset occurs at pentad 62 (Black line in time series), with a standard deviation of 4 pentads (Nieto-Ferreira and Rickenbach, 2010).

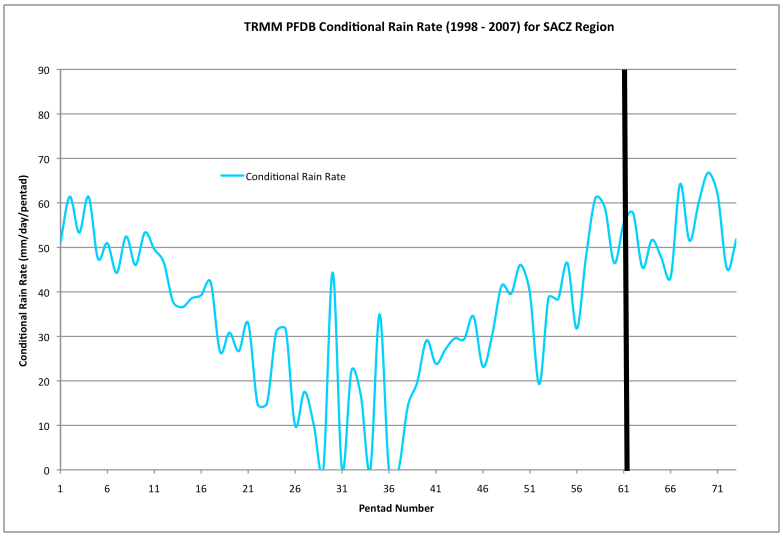

Figure 3.41: Conditional Rain Rate per Pentad for Features with a MCS, averaged 1998-2007 for the SACZ Region

Features with shallow and deep convection

Shallow and deep convection (Figures 3.42 and 3.43, respectively) illustrate again how the SACZ region experiences a dry season, illustrated by the annual cycle in precipitation features (red). Also, the trends in the number of features follow the trends in both sensible and latent heat flux. In the dry season, it seems as if the increase in features is tied to the increase in sensible heat flux, but as that flux drops off, the rise in latent heat flux seems to rise at the same time as the number of features. This would argue that in the dry season local thermodynamic processes dominate producing isolated convective clouds, while after near onset large-scale processes such as fronts drive precipitation.

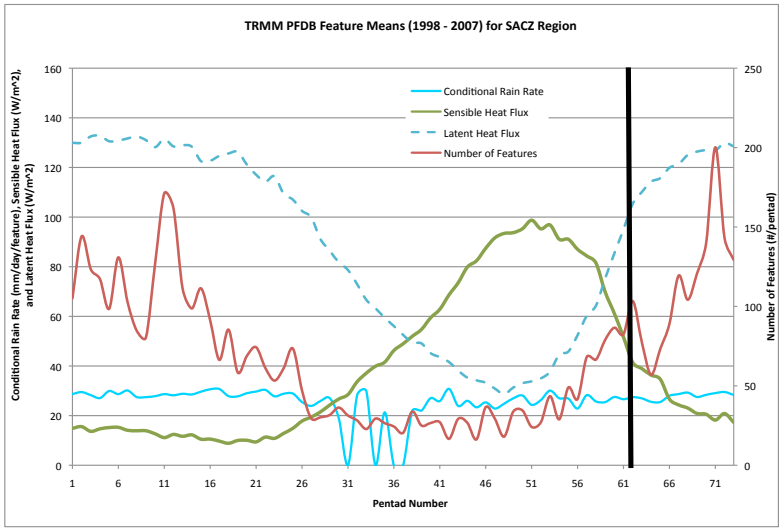

Figure 3.42: Variables from the PFDB for Features with shallow convection in SACZ Region. Conditional Rain Rate (Blue), Number of Features (Red), Sensible Heat Flux (Green), and Latent Heat Flux (Blue dashed)

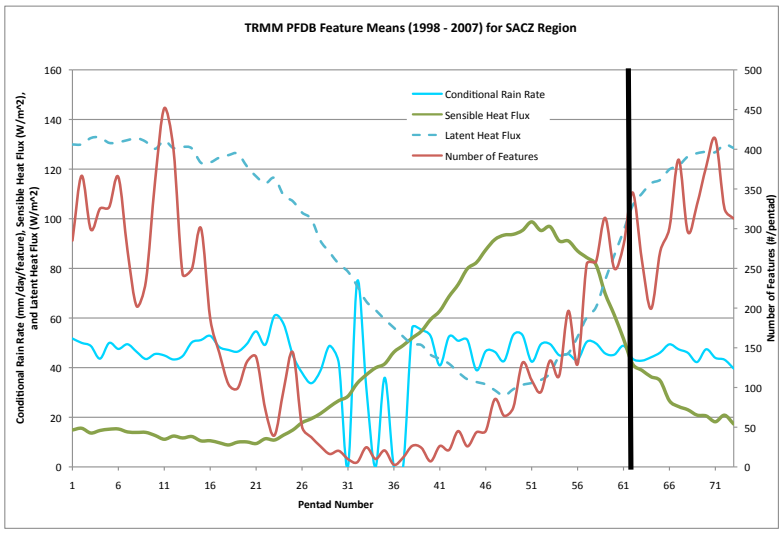

Figure 3.43: Same as in Figure 5.2, but for Features with deep convection

Features with a MCS

The largest difference between the previous set of features and the ones with a MCS is that ones with a MCS only account for a very small portion, on average, of the total number of features in the SACZ region. Also, features with a MCS are significantly rainier per feature than those with shallow convection and those with deep convection that do not contain a MCS. The amount of lightning flashes are dominated by features with a MCS, primarily due to their associated rigorous vertical intensity associated with their development into a feature in this classification. Flashes are very infrequent in the other features, which is why lighting flashes were not included in their time series analysis.

One of the first observations that we made about the SACZ region based on time series analysis is that the pattern is very noisy over the 10-year means in just about every variable. This region is subject to frontal passages for most of its precipitation. Given that their frequency is on the weekly time scale, the 5 day means will be noisy. Fronts in South America are similar to North America in that they are transient in the wintertime, propagating through a region very quickly with a small band of precipitation. However, in the summer time they have a tendency to

move slower and stall out across a particular region (Garreaud 2000 and Garreaud and Wallace, 1998). In the United States this area is usually Florida and along this boundary there is enhanced convergence and storms forming for sometimes days at the time (Hodanish et al., 1997). In South America this occurs in Southeastern Brazil extending into the Atlantic Ocean and is called the SACZ.

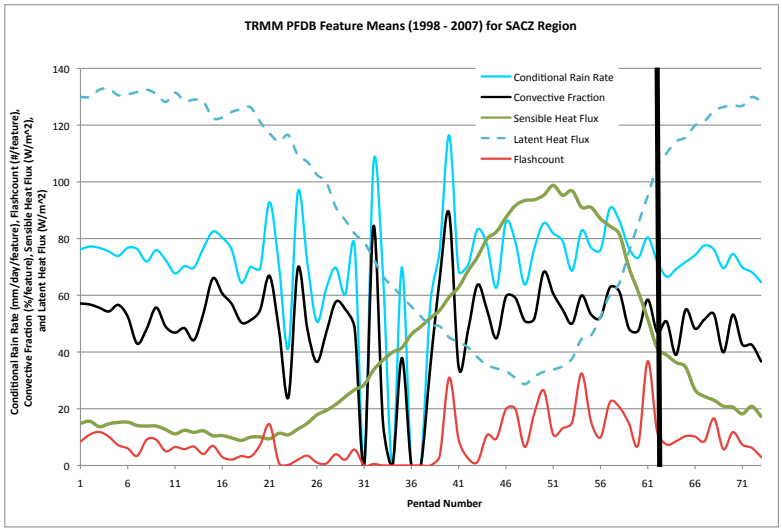

Figure 3.44: Variables from the PFDB for Features with a MCS for the SACZ Region. Conditional Rain Rate (Blue), Lightning Flash Count (Red), Convective Rain Fraction (Black), Sensible Heat Flux (Green), and Latent Heat Flux (Blue dashed).

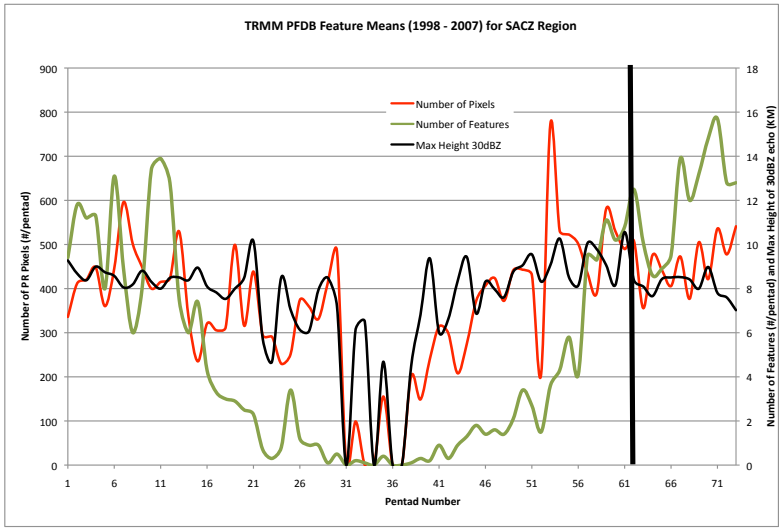

Figure 3.45: Variables from the PFDB for Features with a MCS for the SACZ Region. Max Height of the 30dBZ contour (Black), Number of PR Pixels (Red), and Number of Features (Green).

The time series of PFDB variables shows some interesting variability in this region (Figure 3.44). For instance, conditional rain rate per feature varies similarly to convective fraction and lightning flash count, in the 2nd half of the year. This suggests that fewer features dominate the 10-year means and that the characteristics of these features are relatively similar and thus the variables that describe them vary concurrently. Aside from this, there is a definite separation between the wet and dry seasons in the SACZ. During the fall and winter months (first half of the year), lightning activity is at its lowest, while the 2nd half of the year (spring into summer) is when lighting activity tends to increase slightly.

Other variables (Figure 3.45) that do not show much of any trend are the vertical intensity variables of convective fraction and maximum height of the 30 dBZ contour. Throughout the year, these variables are relatively stable, with the only real variability seemingly being caused by baroclinic interactions later in the year. None of the vertical intensity variables show any correlation with sensible heat flux, except lighting, which has a .348 correlation coefficient with sensible heat. Lightning flash count does seem as if it becomes larger in magnitude once sensible heat flux increases, but there is not a perfect correlation that would suggest that the atmosphere is being solely driven by thermodynamics. Instead, it appears as if dynamic triggers are predominantly driving the atmosphere. The main evidence of this is the increased variability of the PFDB variables prior to onset and also the steady rise in conditional rain rate per pentad (Figure 3.41). Frontal systems on average move across South America in 1-2 weeks (Garreaud, 2000), while summertime fronts move quicker and cover the same region in 5 days on average (Garreaud and Wallace, 1998). The increase in frontal speed in the summer helps explain the higher variability in the time series and also provides the reasoning for increases in rain and number of features in all dimensions that are observed in the time series.

PDFs of these variables also show how much the frequency of these features varies season to season. Figures 3.46-3.49 show (in order) absolute values of conditional rain rate, flash count, max 6km height, and number of PR pixels. What stands out in all of these PDFs is that the months of SON and DJF are when the majority of features occur in the SACZ region. This time of the year is also when onset is occurring in the West region and is followed by onset in the SACZ region. Onset in the West is influenced by the buildup of instability due to thermodynamic forcing and previous work has suggested that these conditions in the West region (Amazon Basin) facilitate the intrusion of the dynamical trigger (fronts) into the SACZ region and eventually farther into the Amazon, drawing the more moist and unstable air southward (Nieto-Ferreira and Rickenbach, 2010). The presence of the South American Low-Level Jet (reversal of winds in the West region after onset) has been associated with increased development of MCSs in the sub-tropics (Salio et al., 2006), which also helps explain the increase in features with a MCS, observed after SACZ onset. Combining the quicker moving fronts (Garreaud and Wallace, 1998) and the favorable conditions present in the West region (Nieto-Ferreira and Rickenbach, 2010 and Salio et al., 2006) to assist convergence and precipitation, it is understandable how the PDFs identify DJF (SACZ post-onset) to be more active than any other 3-month period in the SACZ region of South America. The favorable conditions that are supplied by increased frontal activity and NW flow also allow for the formation of convection between frontal passages.

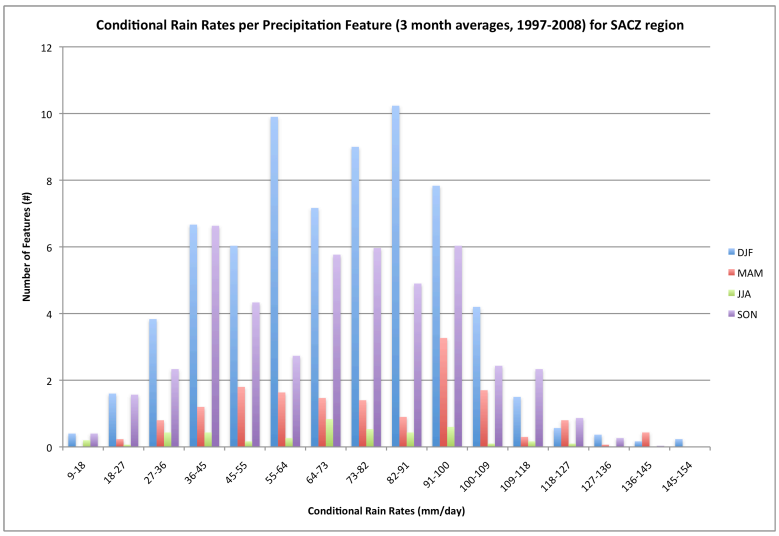

Figure 3.46: PDF of Conditional Rain Rates for 3-month periods Number of Features Scale, averaged 1998-2007 for SACZ Region

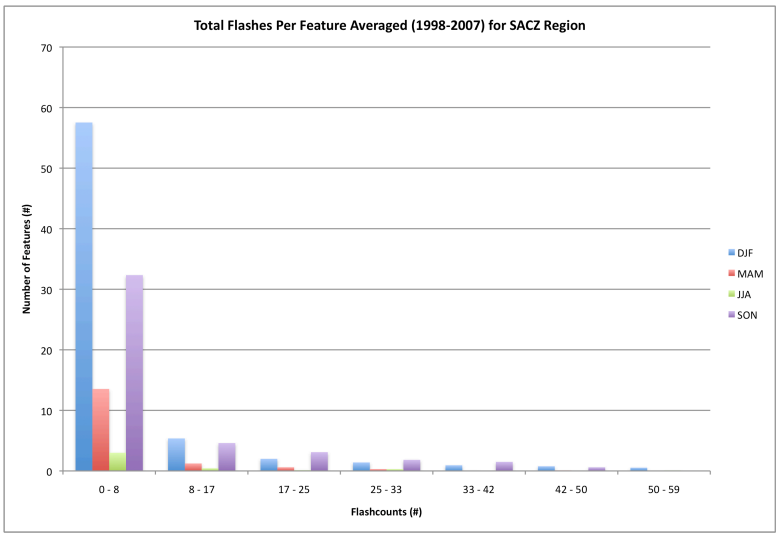

Figure 3.47: PDF of Lightning Flash Counts for 3-month periods Number of Features Scale, averaged 1998-2007 for SACZ Region

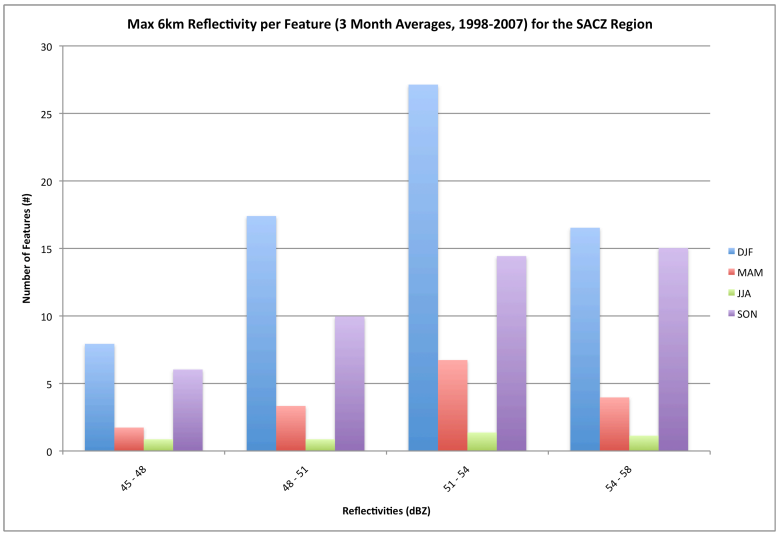

Figure 3.48: PDF of Max Reflectivity at 6km for 3-month periods Number of Features Scale, averaged 1998-2007 for SACZ Region

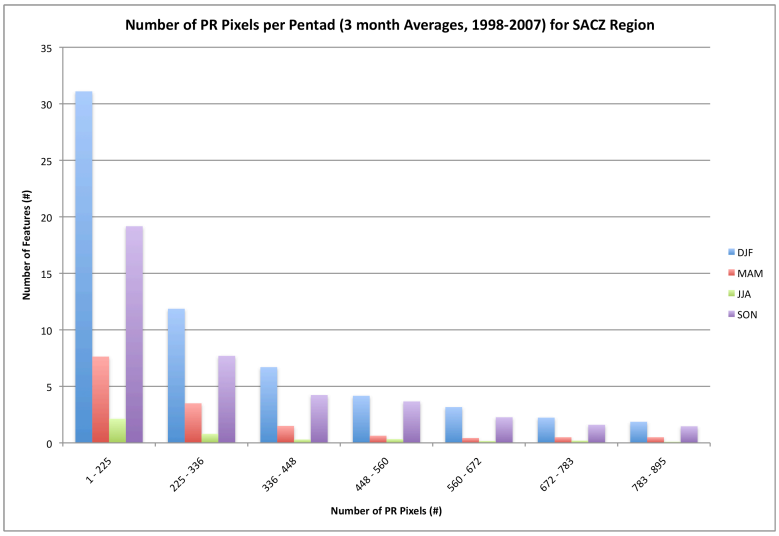

Figure 3.49: PDF of Number of PR Pixels for 3-month periods Number of Features Scale, averaged 1998-2007 for SACZ Region

The next result to take from these graphs is whether or not the type of convection varies much from season to season. Here we looked for fundamental differences between 3-month periods that could be explained by other mechanisms influencing convection. While SON and DJF have the most features over the 4, 3-month periods, the percentages of the totals show that there is really not much of a difference between the convection in the winter (dry) months and the summer (wet) months (Figure 3.50-3.53).

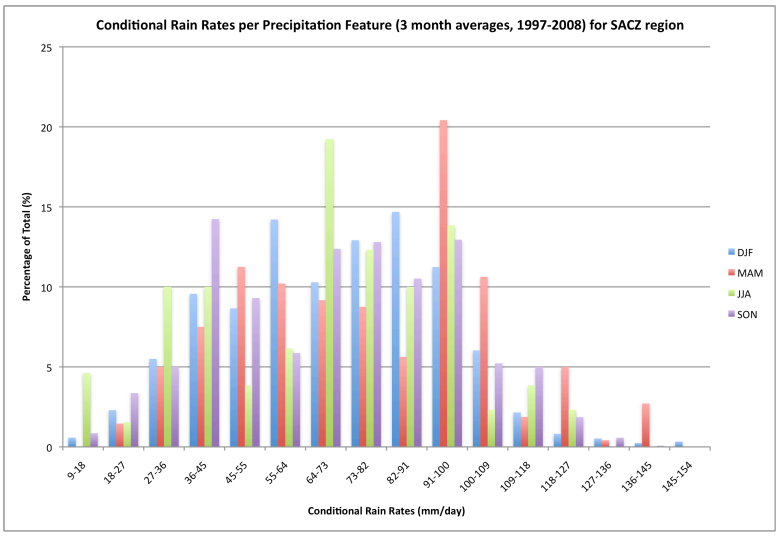

Figure 3.50: PDF of Conditional Rain Rates for 3-month periods Percentage of Total Scale, averaged 1998-2007 for SACZ Region

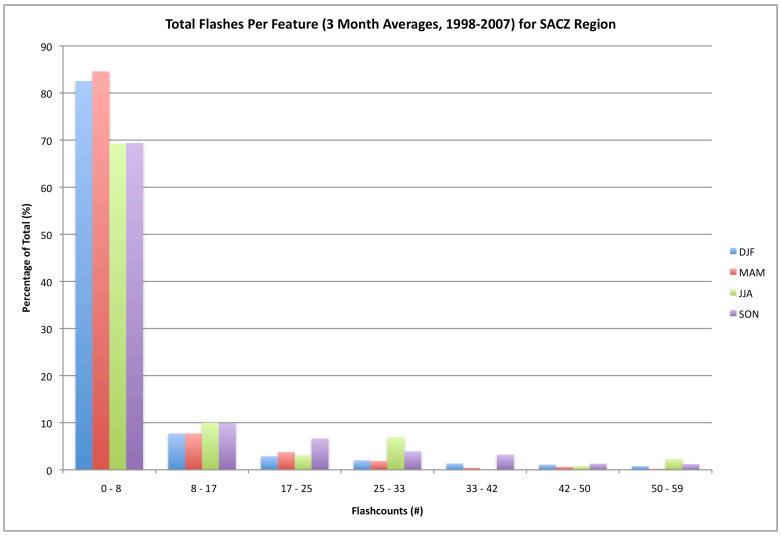

Figure 3.51: PDF of Lightning Flash Counts for 3-month periods Percentage of Total Scale, averaged 1998-2007 for SACZ Region

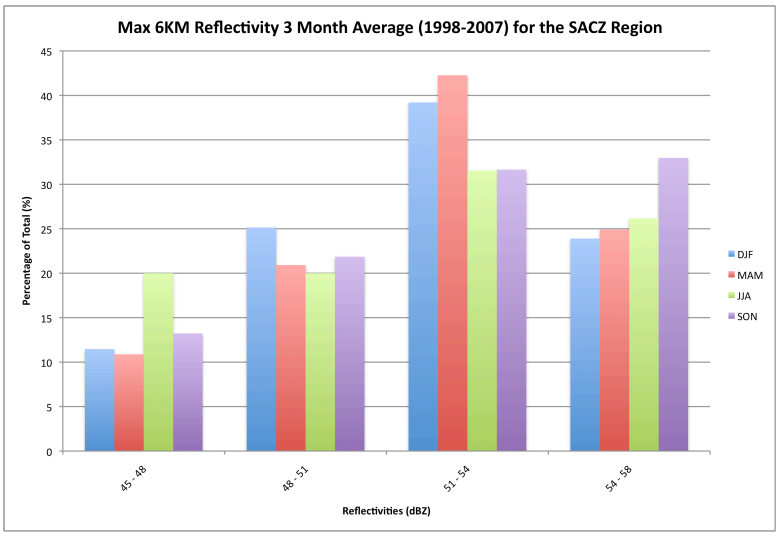

Figure 3.52: PDF of Max Reflectivity at 6km for 3-month periods Percentage of Total Scale, averaged 1998-2007 for SACZ Region

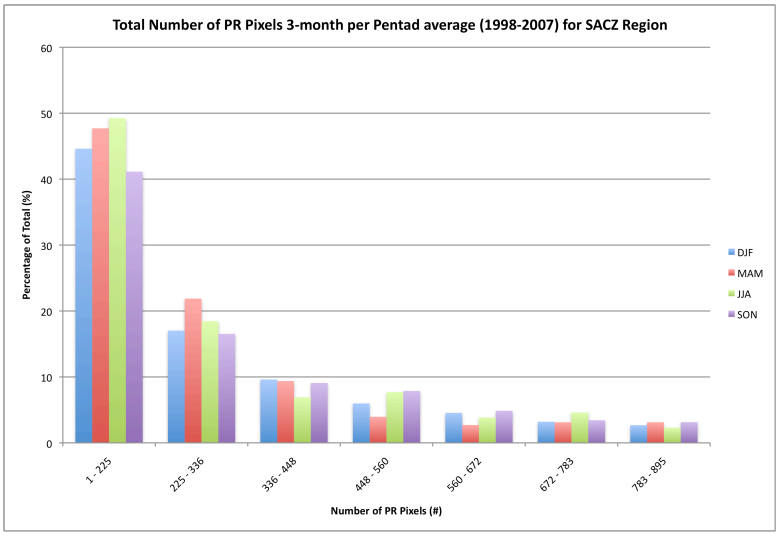

Figure 3.53: PDF of Number of PR Pixels for 3-month periods Percentage of Total Scale, averaged 1998-2007 for SACZ Region

The only contradictions to uniformity here that could be argued occur in the JJA/SON months when there are a higher percentage of storms with more lighting (Figure 3.51) and higher 6km reflectivity (Figure 3.52). This could be caused by either by fewer, but stronger features or stronger features due to decreased stability from an increase in sensible heat flux. This is the time of the year when there are fewer features, so with only a few features there might be a few strong ones that cause the percentages to exaggerate the non-homogeneity of features. The other explanation could be that this is the time of the year when the sensible heat flux is highest and

thus there is more available energy to produce stronger features. Aside from this argument, convection here is homogenous year round and is more than likely all due to the characteristics that are associated with frontal precipitation systems.

To further assert that the SACZ region convection does not change much, statistics in Table 3.1 characterize how the variables respond prior to and after onset. The one statistic that sticks out here and contradicts a change in vertical structure is the 47% decline in lighting activity after onset. There are two issues with this value. One of them is that a drop from 13 flashes per pentad to 7 flashes per pentad is not as significant as a larger change in value would be, and also the raw data make this variable misleading. Before onset in this region, there were not always storms containing lightning, so a few features are sometimes driving the values in the lightning field in the pre-onset period as opposed to having a lighting feature in every pentad, 10 pentads before and 10 pentads after onset. Other fields were also subject to this issue, but not as badly as lightning due to the fact that the others can be calculated in the absence of lighting.

The increase in conditional rain rate after onset is expected because that is the simple definition of monsoon and wet season. Though, the increase is marginal and nothing extremely significant. Finally, the vertical intensity fields of convective fraction and 30 dBZ heights slightly decrease, but not by any factor that suggests a fundamental change in the mechanisms of precipitation. Thus, uniformity prevails with the increase in features per pentad being the explanation for why the rainfall per pentad increases after onset.

The SACZ region is observed to be a transition region between precipitation mechanisms in the tropics and ones in the sub tropics. The pre-onset period is dominated by high variability from slow moving frontal systems that occur on a week to two-week time scale. Pre-onset thermodynamic forcing as interpreted from sensible heat flux interactions with convective

characteristics appears to be minimal; however, increased lightning activity before onset suggests that pre-onset features may harness some of this energy to form deep convection and this may play a role in the evolution of onset.

As onset approaches, the frontal frequency increases and the variability decreases. This increase in frontal activity appears to be closely tied with increasing thermodynamic conditions in the West region, seeing as onset in the SACZ region occurs on average only a few pentads after the West region. Also, the wind reversal observed in the West region (shift from easterly to northwesterly around SACZ onset) servers to usher more moist and unstable air into the SACZ region and aids in the formation of precipitation. The SACZ region is very much driven by frontal interactions, however, without the influences from the West region and also the pre-onset thermodynamic build up within the region, the establishment of the SACZ and onset in this region might be completely different.

3.2.2 South Region

Our South region is located in southeast Brazil and is primarily influenced by frontal systems that pass through the region year round. Onset here occurs on average around pentad 57 (Black line in time series) (early October) and has a standard deviation of 5.5 pentads. Identifying onset in this region is tricky because solely following the objective precipitation algorithm will sometimes not conclude a definitive onset date because it is raining year round and the thresholds are not triggered like they are in other regions. Year round rain is illustrated in Figure 3.54, which shows conditional rain rates per pentad for dimension 3 features.

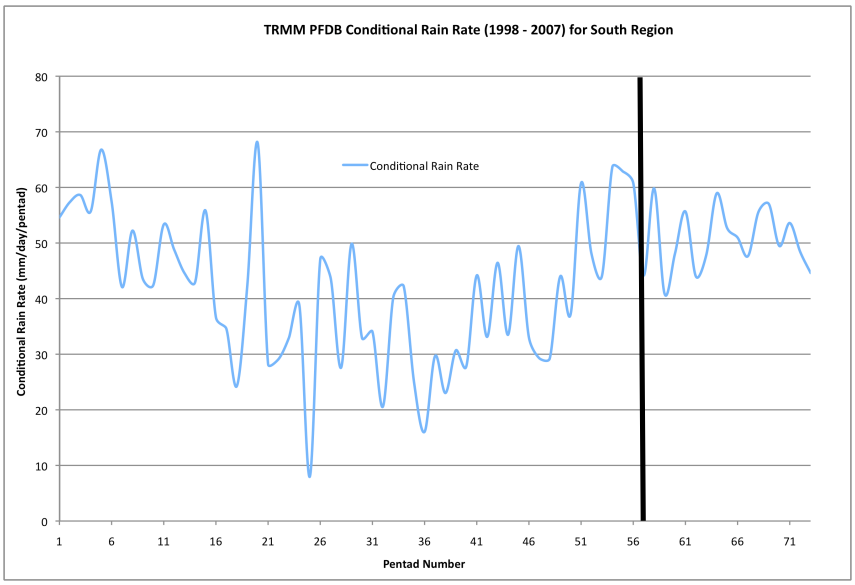

Figure 3.54: Conditional Rain Rate per Pentad for Feature with a MCS, averaged 1998-2007 for the South Region

Features with Shallow and Deep convection

The number of features with shallow and deep convection (Red, Figures 3.55 and 3.56) attempt to show some resemblance of an annual cycle, but high variability due to transient frontal systems results in a well defined annual cycle being hard to identify. These time series' show that more features in these dimensions occur in the summer months, with their minimum points occurring in the winter time. The best-defined annual cycle in the south is seen in the number of features per pentad. This field is highest in the wet season (summer), lowest in the dry season (winter), which is expected based on the increased frequency of frontal activity in the wet season as compared to the dry season (Garreaud, 2000 and Garreaud and Wallace, 1998). As for rain rates, there is little variability in the rates of features with shallow convection; however, features with deep convection begin to show some variability. The time series of feature variables appears noisier and leads us to infer that features with deep convection are more closely tied to frontal interactions than those features with shallow convection.

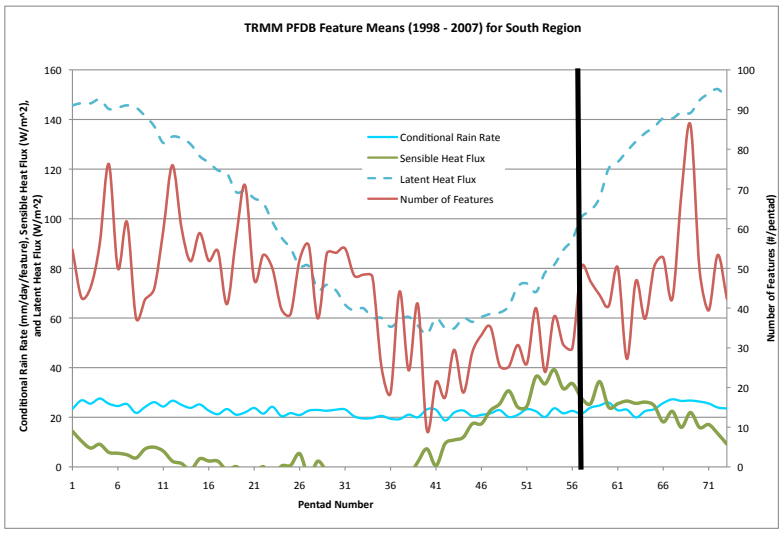

Figure 3.55: Variables from the PFDB for Features with shallow convection in South Region. Conditional Rain Rate (Blue), Number of Features (Red), Sensible Heat Flux (Green), and Latent Heat Flux (Blue dashed)

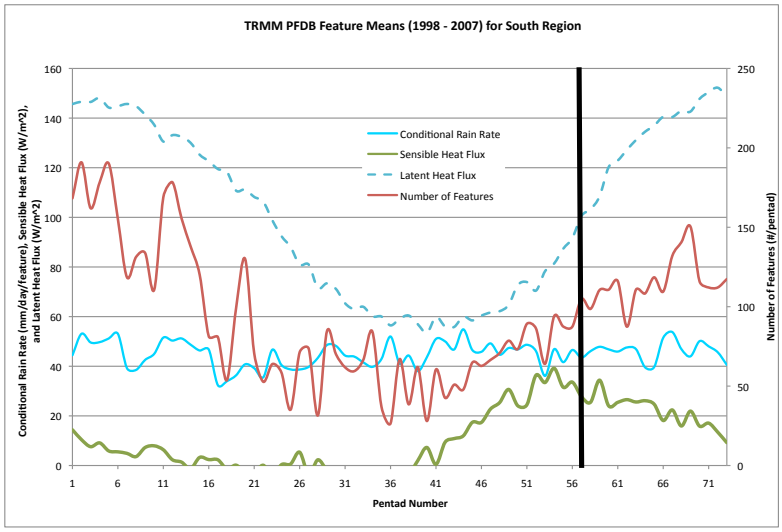

Figure 3.56: Same as in Figure 2, but for Features with deep convection

Features with a MCS

As was the case in the SACZ region, the South region has vastly more features without a MCS than those that are MCSs. However, again MCSs in the South account for more rain per pentad and per feature than the other feature types. This observation is nothing new because it has been shown that MCSs account for a small percentage of the storms around the world, but account for a high percentage of the total precipitation (Houze 1989, Negri et al. 2000, and

Nesbitt et al. 2000). Another difference between MCS features and the other two is that MCS features appear to increase with the increase in sensible heat flux, while the others do not. This suggests that thermodynamic forcing could drive MCS features and that this forcing plays little in the formation of the features without a MCS.

In the South region, features with a MCS are very noisy when it comes to their 10-year mean time series plots. This extreme variability in the South region is no doubt a result of baroclinic systems, which are present year round. Looking at each variable individually, as opposed to how they vary in relation to other variables, reveals trends that cannot be readily identified within noise of all the variables. By eliminating the temptation to observe relationships that may not exist, we are able to concentrate on the raw trends in the data. The main result that can be drawn from Figures 3.57 and 3.58 is that rain rates and lightning on average are highest between pentads 41 and 56. Coincidentally, this coincides with their springtime and in this region they are subject to storms similar to what is experienced in the Midwest of the United States during the spring and summer (Velasco and Fritsch, 1987 and Nieto-Ferriera et al., 2003, Durkee et al., 2009). These large systems called MCCs (Mesoscale Convective Complexes) are large complexes of convection that encompass and produce rain over a large lateral area. MCCs are common this time of the year and could be one explanation of why rain rates and lightning peak in this time of the year on average.

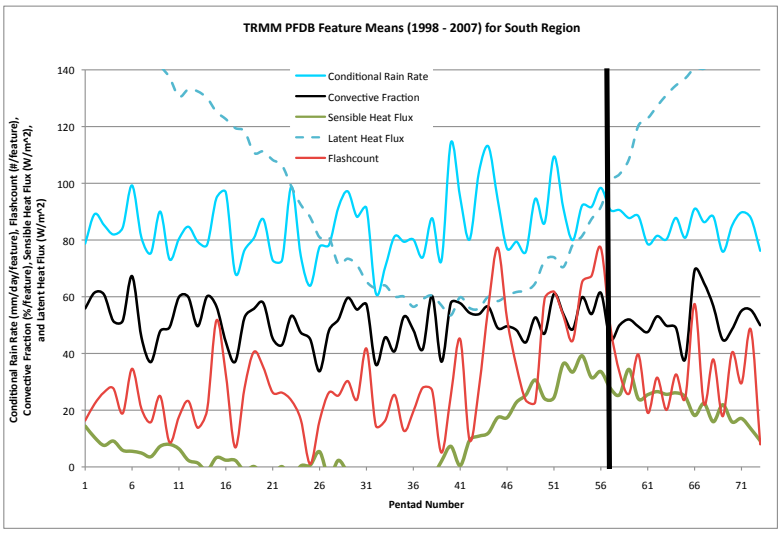

Figure 3.57: Variables from the PFDB for Features with a MCS in the South Region. Conditional Rain Rate (Blue), Lightning Flash Count (Red), Convective Rain Fraction (Black), Sensible Heat Flux (Green), and Latent Heat Flux (Blue dashed).

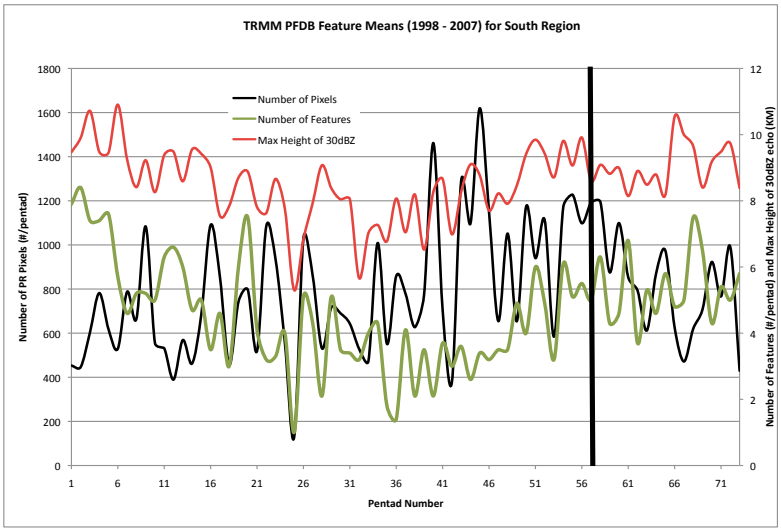

Figure 3.58: Variables from the PFDB for Features with a MCS in the South Region. Max Height of the 30dBZ contour (Black), Number of PR Pixels (Red), and Number of Features (Green).

One might expect that these MCCs would also cause a spike in the convective fraction of features, just because these storms produce high rain rates does not necessarily mean they are dominantly convective in nature. These storms are massive from a cloud top perspective, but from the PR perspective, the stratiform cloud shield that is produced through the ejection of precipitation out of the updraft, from enhanced vertical wind shear, is much larger than the inner convective core (Nesbitt et al., 2006). This is why convective fraction remains relatively constant

through the spring. Another trend is a trivial increase in max height of the 30 dBZ contour and how it correlates with slight increases in sensible heat flux. The increase in surface sensible heat flux could provide the extra energy necessary to build larger storms when the influence of frontal systems is present, but overall the increase is not too drastic.

Since the precipitation in the South region is predominately affected by frontal systems, variability in the number of features here is also closely tied to frontal activity. Taking a looking at features per season, as a percentage of the total is more useful that looking at the total number of features on average, since each season receives roughly the same number of features. This will show how storms during different seasons differ overall from features in other seasons. Figures 3.59 – 3.60 show PFDB variable PDFs on a percentage of the average total observed.

The conditional rain rate in the South region (Figure 3.59) shows a very spread out distribution of values which suggests that it does rain here all year round and throughout the year there is very little variation in the distribution of precipitation feature rain rates. This observation is further verified by the -.564 correlation coefficient between conditional rain rate and sea level pressure. This number emphasizes the role the fronts have on the rain in the region by showing that 56% of the variation in rain rates is explained by SLP changes or frontal systems. There are a few spikes in different 3-month periods, but overall there is no one season that dominates the higher or lower rain rates.

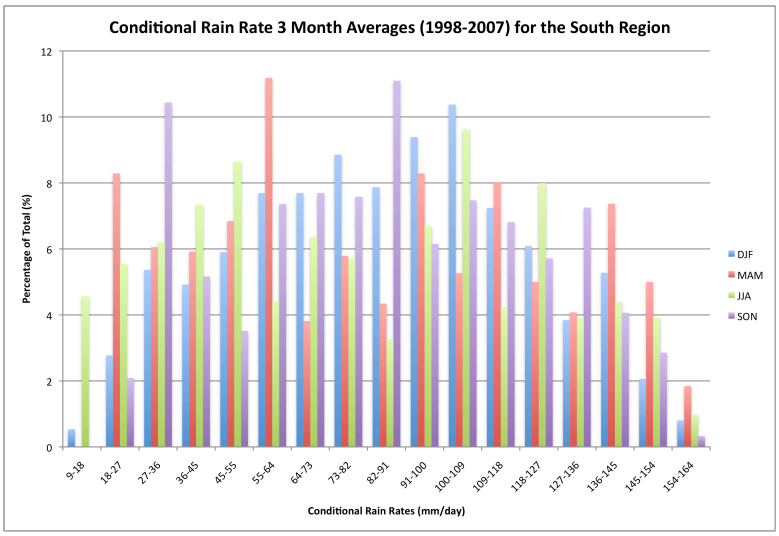

Figure 3.59: PDF of Conditional Rain Rates for 3-month periods Percentage of Total Scale, averaged 1998-2007 for South Region

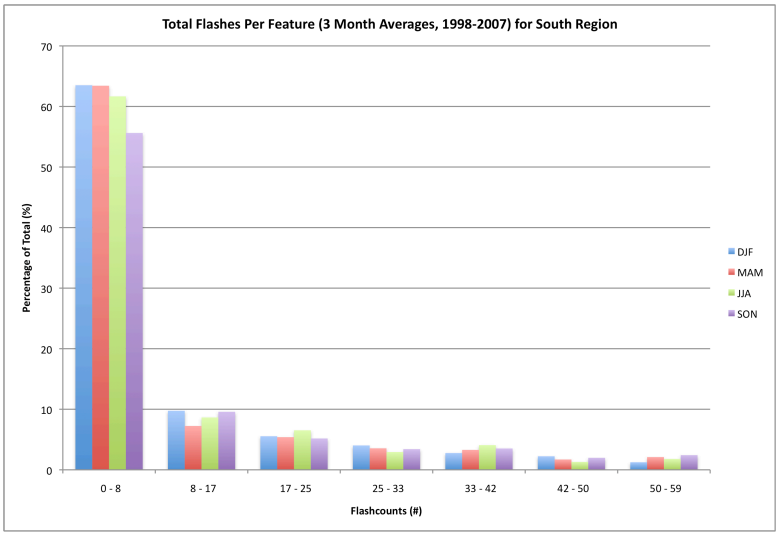

Figure 3.60: PDF of Lightning Flash Counts for 3-month periods Percentage of Total Scale, averaged 1998-2007 for South Region

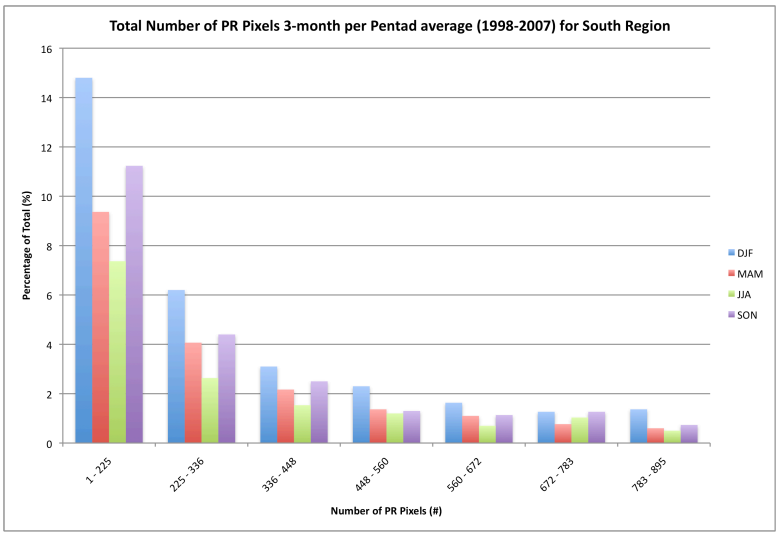

Figure 3.61: PDF of Number of PR Pixels for 3-month Percentage of Total Scale, averaged 1998-2007 for SACZ Region

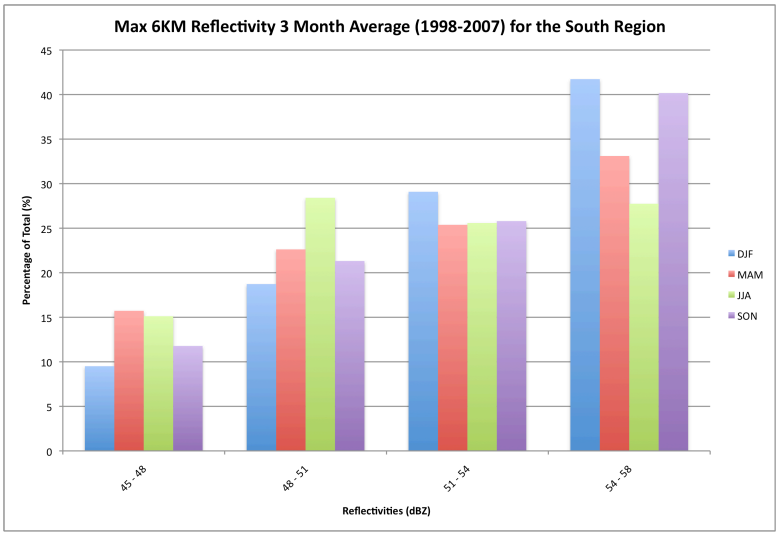

Figure 3.62: PDF of Max Reflectivity at 6km for 3-month periods Percentage of Total Scale, averaged 1998-2007 for SACZ Region

Lightning flash counts (Figure 3.60) also resemble a pretty uniform distribution of features throughout each season. There are slightly more higher frequency lightning flash counts in JJA, but if we refer back to the dimension 3 time series (Figure 3.57), this is the season where the mean flash counts tend to spike, so this result is in line with the 10-year mean. Also, the time series shows the lowest flash counts occur in the start of the year and concurrently the PDF for flash count shows the same thing with the DJF and MAM seasons having the highest concentration of low flash counts.

The number of pixels (Figure 3.61) shows yet another field where there is little variation throughout the year. Although, there is one pattern that can be drawn from this chart and it is that JJA and SON on average have a just slightly higher percentage of large storms compared to the other periods. This would be in line with larger springtime MCCs, but overall, there is little variation in storm size. However, there is something to be drawn from the max 6km reflectivity field (Figure 3.62). In JJA, the "dry" season, most of the storms are not as convective on average as storms in the wet season. Pre-onset and post-onset (SON and DJA respectively) have the highest percentage of storms with the most vertical development, which implies that this time of the year is when the most frontal influence is present and the conditions are also prime for these fronts to drive taller convection (increase in sensible heat flux). While storms this time of the year are taller, Figure 3.57 shows that this does not affect the rainfall per feature or even rainfall per pentad (Figure 3.54) too much.

The point that South region convection does not vary much at all is further exemplified in the pre and post-onset statistics. Table 3.1 shows that there is very little change before and after onset. There are some minor changes, but nothing to suggest that there is a different mechanism causing precipitation before or after onset. The only change that seems to be meaningful is the slight increase in vertical intensity (+7% in 30 dBZ height), which could suggest that as the summer time approaches, frontal system convection is driven to be more vertical, so the features could begin to contain higher rain rates. This is somewhat corroborated in the 2% increase in conditional rain rate per pentad, but again it is nothing more than a trivial increase.

The South region is subject to primarily baroclinic systems year round, with some enhancement from increases in sensible heat flux in the springtime. Convection before and after

onset it rather homogenous and does not reveal influences from other mechanisms that could drive precipitation.

3.2.3 West vs. SACZ

While these two regions are at the same latitude, they both are influenced by different mechanisms that cause the onset of the monsoon. At the same time, interactions between both regions also help intensify and sustain the monsoon regime through out the rainy season. The West region onset is primarily driven initially by thermodynamic forcing in the form of sensible heat flux at the surface. This increase in sensible heat flux is also present in the SACZ region prior to onset; however, the SACZ region is mostly driven by an increased frequency in frontal activity, along with an increase in stationary fronts. These stationary fronts also aid in the reversal of winds in the West region that draw tropical moisture south and into the sub-Tropics. It appears as if SACZ onset due to stationary fronts is partially due to the reversal of winds in the West region being able to supply more moist and unstable air into the region. This section attempts to compare and contrast these regions to draw on these connections to see whether or not they are as connected as they appear to be.

The West region and the SACZ region are both located at approximately the same range in latitudes, however, the SACZ region is more prone to direct influence from baroclinic waves compared to the West which is typically more affected by these waves after onset when they become stationary and extend deep into the Amazon (Rickenbach et al., 2002 and Halverson et al. 2002). Onset occurs relatively early in both regions, with the West occurring around pentad 58 (Black line in time series) and the SACZ around pentad 61 (Red line in time series), on average. Though onset occurs at roughly the same time, one major difference between the two regions is the mechanisms that facilitate precipitation before and after onset.

A comparison of the conditional rain rates per pentad (Figure 3.63) shows that the two regions for the most part are similar in how rain rates vary throughout the year. The number of features (Figure 3.64) uncovers another field with a similar trend to conditional rain rate. Again, similarly to the East region, the SACZ region is smaller in physical size compared to the West, so we plotted the number of features as a function of region size to give an accurate comparison. What is evident when this is done is that most of the time there are more features per sq. km in the West than in the SACZ region.

While these figures served to show some similarity between the regions, they did not supply evidence for fundamental differences between the two regions. Figures 3.65 and 3.66 on the other hand offer more insight into how the West and SACZ differ. The comparison of the heat fluxes (Figure 3.66) shows that in both regions there is a buildup of sensible heat (solid lines), while at the same time a decrease in latent heat (dashed lines) is occurring. While these trends are important, the most revealing evidence here is the difference in the peaks in sensible heat. The peak in the West region takes place a few pentads before the peak in the SACZ region. This is significant because the offset in peaks is similar to the difference between the average onset dates. On average, monsoon onset happens three pentads later in the SACZ region, so the "delayed" build up of sensible heat could be responsible in delaying the priming of the atmosphere, which is necessary for significant rain to begin, and thus onset to be triggered.

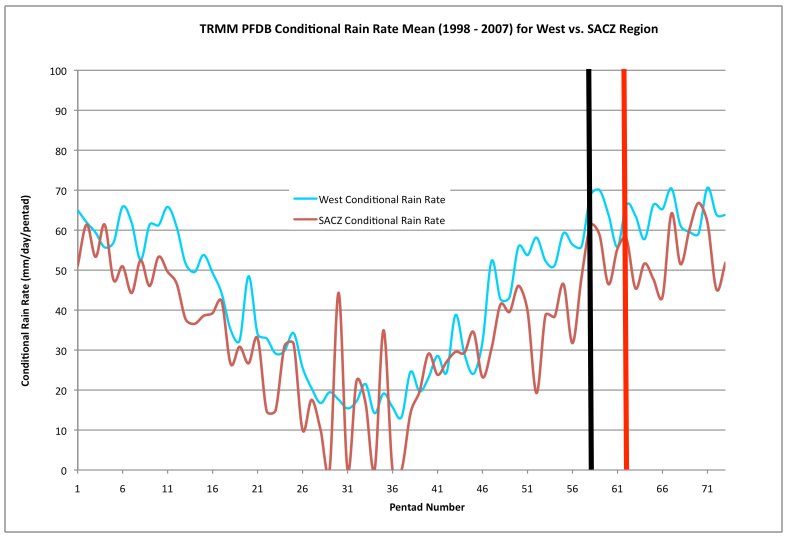

Figure 3.63: Conditional Rain Rate per Pentad for features with a MCS, averaged 1998-2007. West Region and SACZ Region

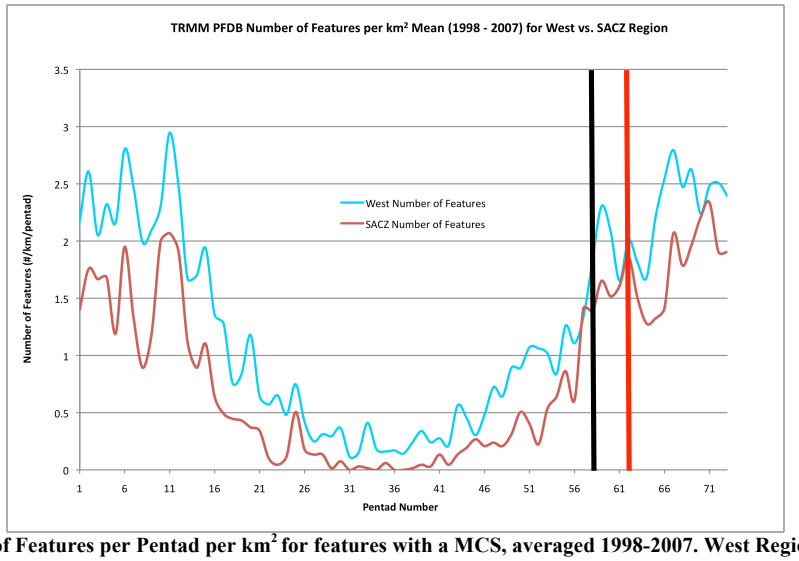

Figure 3.64: Number of Features per Pentad per km^2 for features with a MCS, averaged 1998-2007. West Region and SACZ Region

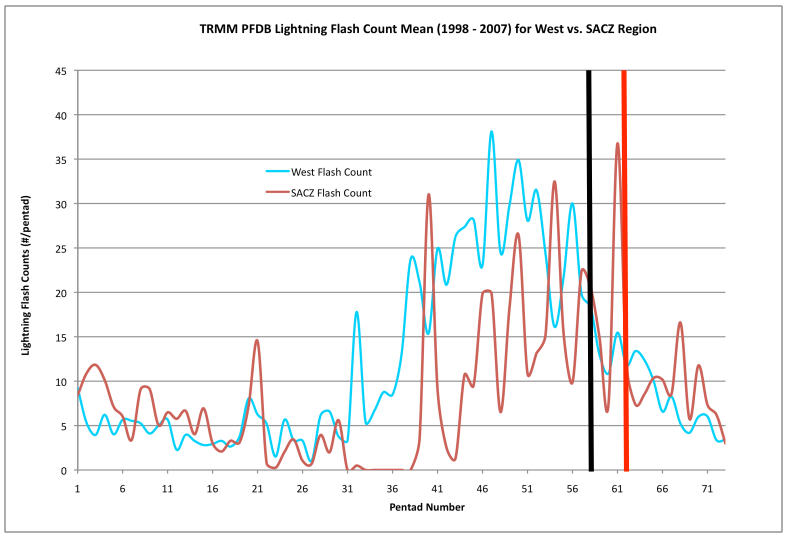

Figure 3.65: Lightning Flash Counts per Pentad for features with a MCS, averaged 1998-2007. West Region and SACZ Region

Figure 3.66: NCEP Heat Fluxes per Pentad. Latent Heat Fluxes (Red dashed, SACZ and Blue dashed, West) and Sensible Heat Fluxes (Red, SACZ and Blue, West)

Lightning flash counts further substantiate the observation of a slight delay in onset in the SACZ region compared to the West region (Figure 3.65). Flash counts in the West region (Blue) are on average reaches a maximum just ahead of the SACZ flashes (Red). As was explained in sections 3.1 and 5.1, there are positive correlations between lightning flashes and sensible heat (.933 for West and .348 for SACZ). Previous research has shown how these heat fluxes can prime the atmosphere prior to onset (Fu and Li, 2004, Li and Fu, 2004, and Fu et al., 1999)

through large, vertically developed and electrified storms, but the lower correlation in the SACZ leaves one wondering whether or not that is necessarily the case here. It seems to be the case in the West where sensible heat helps dictate pre-onset lightning; however, the SACZ could be modulated by a combination of pre-onset mechanisms such as build up of sensible heat in the absence of complete cloud cover and also the increase in low level moisture and unstable air that is provided via the South American Low-level Jet, once the wind reversal occurs in the West (Rickenbach et al., 2002, Salio et al., 2006 and Nieto-Ferreira and Rickenbach, 2010). Increasing flow from the northwest has been shown to increase the occurrence of MCSs in the SACZ region (Salio et al., 2006), so this increase, which typically occurs relatively close to the average SACZ onset date of pentad 61 (based on Figure 3.21), along with in situ sensible heat fluxes may be responsible for pre-onset lightning. This combination may also explain why sensible heat only explains 35% of the variance in lighting flashes in the SACZ, compared to 93% of the variance in lighting in the West region where thermodynamic forcing pre-onset is the dominant forcing mechanism.

The main known difference between the West and SACZ, aside from the sensible heat increasing later in the SACZ region, is the fact that the SACZ region is mainly affected by baroclinic systems whereas the West region is not directly affected by fronts until they stall and establish the SACZ, which can extend well into the Tropics (Rickenbach et al. 2002 and Halverson et al. 2002). This baroclinic interaction in the SACZ region is seen especially in Figures 3.63 and 3.65 where there is high variability in the SACZ in the conditional rain rates and lighting flash counts. Conversely, the same period of time in the West does not reveal the same variability, which leads one conclude that the high variability is associated with periodic

passage of fronts (Garreaud, 2000) and then the increased frequency of frontal passage as onset approaches (Garreaud and Wallace, 1998).

While fronts are not the primary driver of precipitation in the West region, there is a tendency for frontal systems, especially after onset, to penetrate the region and drive convection along the SACZ well into the Amazon Basin. This is especially seen in 850 mb winds (Figure 3.21) where after onset there is a tendency for the average wind direction in the West region to be from the northwest.

The average flow throughout the year is from the northeasterly and easterly. However, only after onset, and more importantly after SACZ onset, does the wind tend to change. This change in direction can be directly associated with the fact that SACZ onset is closely tied to fronts and their tendency to stall, extend into the West, and draw wind and moisture from the northwest down through the West region (Rickenbach et al. 2002 and Halverson et al. 2002). This feature is well documented in previous research and is understood to be a vital source of moisture for precipitation in the SACZ region.

The final comparison between the two regions is how they vary before and after onset. Table 3.1 summarizes these statistics and shows how the two regions compare mainly when it comes to convective intensity. Both have a decrease in lighting and vertical intensity after onset, while at the same time increasing the total rain rate. The one major difference that is present here is the lighting in the SACZ. Sensible heat flux in the SACZ region is much higher than in the West, despite its smaller physical size (Figure 3.66). This would lead one to assume that if it were closely tied to electrification then the lighting in the pre-onset period would be higher than in the West. The fact is that pre-onset lightning in the SACZ region is almost 50% lower than the pre-onset lightning in the West and leads one to think that thermodynamic priming here may not

be as big of a player as it is in the West. Thermodynamic forcing surly plays a role in the SACZ region, but perhaps the forcing is not as vital to priming the atmosphere as it is in the West, since the SACZ region is primarily affected by fronts in one way or another year round.

While these two regions are next to each other, the timing of onset, pre-onset mechanisms of precipitation, and main drivers of precipitation after onset are different. The temporal offset in the maxima of heat fluxes and flash counts illustrate how late peaks in these variables were in line with each regions respective onset dates. However, while these were in line with onset dates, the extent by which these fluxes seemed to influence each region varied heavily as seen in the correlations. The SACZ is a baroclinic zone year round, so fronts are always influencing this region, unlike in the West where thermodynamics driven by sensible heat flux is unimpeded by other mechanisms in the pre-onset period. It is only after onset when the West region is driven by a combination of thermodynamics and diurnal convection, squall lines, and occasionally frontal intrusions, whereas the SACZ region is almost entirely driven by fronts.

CHAPTER 4: CONCLUSIONS

This work presents a case for the regional variability in mechanisms of onset in the South American Monsoon System. Each of the four regions identified in South America have distinct mechanisms driving the monsoon both before and after onset. The TRMM satellite and different products derived from the data gathered by TRMM and other weather satellites, along with daily surface data, allowed us to analyze an uninterrupted 10-year time frame. These products allowed us to build time series as well as build a statistical analysis of different variables, which characterize convection. These feature-defining characteristics were the basis of the identification of types of convection, which were then related to a particular forcing mechanism that was identified to be driving the convection during that period of time. Identification of these specific regional mechanisms have to potential to immediately impact those that depend on seasonal rain for their livelihood, as well as a longer term goal of incorporating these mechanisms into global climate models to better model their impacts on global circulations.

Thermodynamic forcing via sensible heat flux at the surface appears to be an important mechanism in most of the regions in our study for pre-onset convection. Sensible heat flux at the surface, from direct solar radiation and stronger wind flow, allows for the destabilization of the troposphere and the formation of deep convection. The rise in sensible heat was documented in the 10-year analysis of sensible heat flux at the surface from the NCEP Reanalysis data for both the West and East regions. Also, this is the time of the year when the Precipitation Feature Dataset time series analysis identified that features were fewer in number, but were more electrified and on average rained more per feature than those that occurred in the monsoon season. Features under this regime were more convective (based on convective fraction) and also the height of the 30 dBZ contour.

A conceptual model of South America when sensible heat flux is increasing in the West based on NCEP time series analysis of sensible heat flux (Figure 4.1) and in the East (Figure 4.2) is presented to illustrate the progression of precipitation mechanism in these regions, as indicated by PFDB time series and PDF analysis of flash counts and conditional rain fall. The sensible heat flux is able to initially build in the West region, due to a mostly cloud free regime. While in the East this flux is able to build because of the absence of the Atlantic ITCZ and its slow migration southward.

Figure 4.1: Conceptual model for South American Monsoon evolution for the month of August. Sun (solar radiation, resulting in increase in sensible heat flux), lightning (convective/electrified storms), clouds with rain (rain), cold front (transient fronts), L (low pressure driving frontal movement), aarow (flow behing front), and Blue box (approximate location of Atlantic ITCZ.

Figure 4.2: Same at Figure 4.1, but for average October.

These figures also present another important observation that our study identified and that was the noticeable offset in onset dates between the West and the East. All forms of analysis from the objective onset definition, TRMM 3B42 rain analysis, PFDB time series, and NCEP reanalysis data confirm that onset in the East region occurs later than in the West. We identified

the main cause of this offset to be because of the fundamental difference between a continental regime and an oceanic regime. The continental regime has a much quicker response to solar radiation than an oceanic regime. The quick response of the West region to solar radiation is what we hypothesize to eventually drive the continental ITCZ and produce rainfall throughout the region. At the same time, the East region build up pre-onset is thought to be not nearly as important to the evolution of the monsoon season since the Atlantic ITCZ's migration is not contingent upon a favorable environment, such as the case in the West region. Instead it is contingent upon the heating of the surface of the ocean and this is hypothesized to be the mechanism that drives the delay between the regions.

Another important mechanism that was identified was cold fronts and the dynamical forcing of precipitation, primarily in the sub-Tropics. However, these systems also played roles in precipitation in the Tropics. High variability in the PFDB time series analysis initially indicated that the SACZ region and South region were both influenced by frontal activity, but upon further analysis of TRMM 3B42 precipitation composites, it was evident that fronts were the primary driver of precipitation in these regions.

What we identified was that in the pre-onset in the SACZ region, baroclinic systems that originated in the mid-latitudes would move into the region and then depart quickly, with a very small footprint of precipitation (Figure 4.3) as indicated by PFDB time series analysis. These systems in the dry season were more transient and result in rainfall that was more sporadic and not as organized. PFDB per feature conditional rain rate as well as number of features illustrated that these dry season features rained more on average, but were much less frequent. As the summer time approached, however, these fronts began to slow down and eventually stall across the SACZ region (Lenters and Cook, 1999 and Garreaud and Wallace, 1998), providing a source

of convergence and accordingly precipitation, which can at times extend into the West region (Figure 4.4).

Figure 4.3: Same at Figure 4.1, but for average September.

Figure 4.4: Same at Figure 4.1, but aarow represents establishmend of SALLJ, stationary front (stalled frontal systems present), and for average November.

The eventual stalling of these fronts also helped us identify another mechanism that contributes to precipitation in the form of the South American Low-Level Jet (SALLJ) (Figure 4.4) (Ferreira et al., 2003). This feature was identified in an NCEP time series of average 850 mb wind in the West region and only occurred once both the West and SACZ regions reached the objectively determined average monsoon onset dates. This feature acted to enhance precipitation in the West region as well as contribute to precipitation in the sub-Tropics by providing necessary moisture and lifting (Rickenbach et al. 2002 and Halverson et al. 2002).

By December the South American Monsoon System was in full raining mode, with all regions achieving onset by this time (based on objective onset algorithm) (Figure 4.5). Features that were heavily influenced by the Atlantic ITCZ controlled the East region, while in the West,

continental scale precipitation that was enhanced by the Bolivian High. Also frontal intrusions and the establishment of the SALLJ played a role in the West. This precipitation extended southeastward into the SACZ region, where stationary fronts provided a steady source of convergence and lift to perpetuate the monsoon season deep into the summer months.

Figure 4.5: Same at Figure 4.1 and 4.4, but for average December.

Each region of South America is unique in its own way. Some of these regions even share common bonds with other regions; however, the overall trend is that each region is fundamentally different. The tropical regions are primarily forced in the pre-onset period by thermodynamic forcing, while in the post-onset period they were driven by larger scale entities of the ITCZ. The SACZ region is mainly affected by remnant frontal systems from the subtropics, with some influence from thermodynamics early on and influence from the moisture rich tropics after onset. In the South region, there is not much variability in what drives the precipitation, but

the true variability here lays in the frequency of frontal systems. Some pre-onset convection could be enhanced by thermodynamics, but the majority is driven by baroclinic energy.

Overall, the South American monsoon system is complex at best, but by identifying these four regions and revealing their pre and post onset precipitation mechanisms; perhaps it will provide a better understanding of the monsoon so that its predictability can be improved upon in the future. Furthering this research into a more applicable form would be the next logical step. This should include extensive modeling to determine if current models can verify the trends and variability that are presented in this paper, including their relative timing and interactions between the regions. From this, integration of this information into climate models as a way of improving the predictability of not only the monsoon itself, but also improving global circulations, which are highly affected by strong heat release from precipitating systems in the tropics, such as the South American Monsoon System.

REFERENCES

Cecil, D.J., S.J. Goodman, D.J. Boccippio, E.J. Zipser, and S.W. Nesbitt, 2005: Three Years of TRMM Precipitation Features. Part I: Radar, Radiometric, and Lightning Characteristics. *Mon. Wea. Rev.*, **133**, 543–566.

Christian H. J., and Coauthors, 1999: The Lightning Imaging Sensor. *Proc. 11th Int. Conf. on Atmospheric Electricity,* Huntsville, AL, NASA, 746–749.

DeMott, C.A., and S.A. Rutledge, 1998: The Vertical Structure of TOGA COARE Convection. Part I: Radar Echo Distributions. *J. Atmos. Sci.*, **55**, 2730–2747.

Doty, B., 1995. The grid analysis and display system. GRADS Manual, 148pp

Durkee, J.D., T.L. Mote, and J.M. Shepherd, 2009: The Contribution of Mesoscale Convective Complexes to Rainfall across Subtropical South America. *J. Climate*, **22**, 4590–4605.

Dye, J. E., W. P. Winn, J. J. Jones, and D. W. Breed (1989), The Electrification of New Mexico Thunderstorms 1. Relationship Between Precipitation Development and the Onset of Electrification, *J. Geophys. Res.*, ***94***(D6), 8643–8656.

Ferreira, R.N., T.M. Rickenbach, D.L. Herdies, and L.M.V. Carvalho, 2003: Variability of South American Convective Cloud Systems and Tropospheric Circulation during January–March 1998 and 1999. *Mon. Wea. Rev.*, **131**, 961–973.

Fu, R., B. Zhu, and R.E. Dickinson, 1999: How Do Atmosphere and Land Surface Influence Seasonal Changes of Convection in the Tropical Amazon? *J. Climate*, **12**, 1306–1321.

Fu, R., and W.H. Li, 2004: The influence of the land surface on the transition from dry to wet season in Amazonia. *Theoretical and Applied Climatology,* **78,** 97–110

Garreaud, R.D., 2000: Cold Air Incursions over Subtropical South America: Mean Structure and Dynamics. *Mon. Wea. Rev.*, **128**, 2544–2559.

Garreaud, R.D., and J.M. Wallace, 1998: Summertime Incursions of Midlatitude Air into Subtropical and Tropical South America. *Mon. Wea. Rev.*, **126**, 2713–2733.

Grimm, A.M., and M.T. Zilli, 2009: Interannual Variability and Seasonal Evolution of Summer Monsoon Rainfall in South America. *J. Climate*, **22**, 2257–2275.

Halverson, J.B., T. Rickenbach, B. Roy, H. Pierce, and E. Williams, 2002: Environmental Characteristics of Convective Systems during TRMM-LBA. *Mon. Wea. Rev.*, **130**, 1493–1509.

Hodanish, S., D. Sharp, W. Collins, C. Paxton, and R. E. Orville, 1997: A 10-yr monthly lightning climatology of Florida: 1986–95. *Wea. Forecasting*, **12**:439–448.

Horel, J. D., A. N. Hahmann, and J. E. Geisler, 1989: An investigation of the annual cycle of convective activity over the tropical Americas. *J. Climate,* **2,** 1388–1403.

Houze R.A. Jr., 1989. Observed structure of mesoscale convective systems and implications for large-scale heating. *Q. J. R. Meteorol. Soc.* **115**: 425-461.

Huffman, G.J., R.F. Adler, D.T. Bolvin, G. Gu, E.J. Nelkin, K.P. Bowman, Y. Hong, E.F. Stocker, and D.B. Wolff, 2007: The TRMM Multisatellite Precipitation Analysis (TMPA): Quasi-Global, Multiyear, Combined-Sensor Precipitation Estimates at Fine Scales. *J. Hydrometeor.*, **8**, 38–55.

Janssen, M. A., 1993: An introduction to the passive microwave remote sensing of atmospheres. *Atmospheric Remote Sensing by Microwave Radiometry,* M. A. Janssen, Ed., John Wiley & Sons, 1–35.

Kalnay, E., M. Kanamitsu, R. Kistler, W. Collins, D. Deaven, L. Gandin, M. Iredell, S. Saha, G. White, J. Woollen, Y. Zhu, A. Leetmaa, R. Reynolds, M. Chelliah, W. Ebisuzaki, W. Higgins, J. Janowiak, K. Mo, C. Ropelewski, J. Wang, R. Jenne, and D. Joseph, 1996: The NCEP/NCAR 40-Year Reanalysis Project. *Bull. Amer. Meteor. Soc.*, **77**, 437–471.

Keenan, T. D. and Carbone, R. E. 1992 A preliminary morphology of precipitation systems in tropical northern Australia. *Q. J. R. Meteorol. Soc.* , **118**, 282-326

Kousky, V.E., 1985: Atmospheric Circulation Changes Associated with Rainfall Anomalies over Tropical Brazil. *Mon. Wea. Rev.*, **113**, 1951–1957.

Kousky, V. E., 1988: Pentad outgoing longwave radiation climatology for the South American sector. *Rev. Bras. Meteor.,* **3,** 217-231

Kummerow, C., W. Barnes, T. Kozu, J. Shiue, and J. Simpson, 1998: The Tropical Rainfall Measuring Mission (TRMM) Sensor Package. *J. Atmos. Oceanic Technol.*, **15**, 809–817.

Lenters, J.D., and K.H. Cook, 1997: On the Origin of the Bolivian High and Related Circulation Features of the South American Climate. *J. Atmos. Sci.*, **54**, 656–678.

Lenters, J.D., and K.H. Cook, 1999: Summertime Precipitation Variability over South America: Role of the Large-Scale Circulation. *Mon. Wea. Rev.*, **127**, 409–431.

Li, W., and R. Fu, 2004: Transition of the Large-Scale Atmospheric and Land Surface Conditions from the Dry to the Wet Season over Amazonia as Diagnosed by the ECMWF Re-Analysis. *J. Climate*, **17**, 2637–2651.

Marengo, J.A., B. Liebmann, V.E. Kousky, N.P. Filizola, and I.C. Wainer, 2001: Onset and End of the Rainy Season in the Brazilian Amazon Basin. *J. Climate*, **14**, 833–852.

Mohr, K.I., J.S. Famiglietti, and E.J. Zipser, 1999: The Contribution to Tropical Rainfall with respect to Convective System Type, Size, and Intensity Estimated from the 85-GHz Ice-Scattering Signature. *J. Appl. Meteor*., **38**, 596–606.

Negri, A. J., E. N. Anagnostou and R. F. Adler, 2000: A 10-yr climatology of Amazonian rainfall derived from passive microwave satellite observations. *J. Appl. Met.,* **39**, 42-56.

Negri, A.J., T.L. Bell, and L. Xu, 2002: Sampling of the Diurnal Cycle of Precipitation Using TRMM. *J. Atmos. Oceanic Technol.*, **19**, 1333–1344.

Nesbitt, S. W., E. J. Zipser and D. J. Cecil, 2000: A census of precipitation features in the Tropics using TRMM: Radar, ice scattering, and lightning observations. *J. Climate*, **13**, 4087-4106.

Nesbitt, S.W., R. Cifelli, and S.A. Rutledge, 2006: Storm Morphology and Rainfall Characteristics of TRMM Precipitation Features. *Mon. Wea. Rev.*, **134**, 2702–2721.

Nieto-Ferreira, R. and T. Rickenbach, 2010: Regionality of monsoon onset in South America: a three-stage conceptual model. Accepted, *Int. J. of Clim.*

Petersen, W.A., S.A. Rutledge, and R.E. Orville, 1996: Cloud-to-Ground Lightning Observations from TOGA COARE: Selected Results and Lightning Location Algorithms. *Mon. Wea. Rev.*, **124**, 602–620

Petersen, W. A. and S. A. Rutledge, 2001: Regional variability in tropical convection: Observations from TRMM. *J. Climate*, **14**, 3566-3586.

Petersen, W.A., S.W. Nesbitt, R.J. Blakeslee, R. Cifelli, P. Hein, and S.A. Rutledge, 2002: TRMM Observations of Intraseasonal Variability in Convective Regimes over the Amazon. *J. Climate*, **15**, 1278–1294.

Ramage, C. S., 1971: *Monsoon Meteorology*. Academic Press, 269 pp.

Rao, G. V., and S. Erdogan, 1989: The atmospheric heat source over the Bolivian Plateau for a mean January. *Bound.-Layer Meteor.*, **46**, 13-33.

Rickenbach T. M., R. N. Ferreira, J. B. Halverson, D. L. Herdies, and M. A. F. Silva Dias, 2002: Modulation of convection in the southwestern Amazon basin by extratropical stationary fronts. *J. Geophys. Res.*, **107**

Rickenbach, T.M., 2004: Nocturnal Cloud Systems and the Diurnal Variation of Clouds and Rainfall in Southwestern Amazonia. *Mon. Wea. Rev.*, **132**, 1201–1219.

Rickenbach, T., R. Nieto-Ferreira, D. Herdies, and S. Nesbitt, Regional differences in South American Monsoon onset: Implications for onset predictability, *American Meteorological Society 28th Conference on Hurricanes and Tropical Meteorology*, Orlando, Florida, April 2008.

Rinehart, R. E., 1997: RADAR for meteorologists. Fourth edition. Rinehart Publications, Grand Forks, North Dakota, USA

Roberts, G. C., Nenes, A., Seinfeld, J. H., and Andreae, M. O., 2003: Impact of biomass burning on cloud properties in the Amazon Basin, J. Geophys. Res., **108**.

Salio, P., M. Nicolini, and E.J. Zipser, 2007: Mesoscale Convective Systems over Southeastern South America and Their Relationship with the South American Low-Level Jet. *Mon. Wea. Rev.*, **135**, 1290–1309.

Schumacher, C., and R.A. Houze, 2003: Stratiform Rain in the Tropics as Seen by the TRMM Precipitation Radar. *J. Climate*, **16**, 1739–1756.

Silva Dias, P.L., W.H. Schubert, and M. DeMaria, 1983: Large-Scale Response of the Tropical Atmosphere to Transient Convection. *J. Atmos. Sci.*, **40**, 2689–2707.

Sorooshian, S., X. Gao, K. Hsu, R.A. Maddox, Y. Hong, H.V. Gupta, and B. Imam, 2002: Diurnal Variability of Tropical Rainfall Retrieved from Combined GOES and TRMM Satellite Information. *J. Climate*, **15**, 983–1001.

Steiner, M., R. A. Houze Jr., and S. E. Yuter, 1995: Climatological characterization of three-dimensional storm structure from operational radar and rain gauge data. *J. Appl. Meteor.* 34, 1978–2007.

Velasco I., and J. M. Fritsch, 1987: Mesoscale convective complexes in the Americas. *J. Geophys. Res*, **92**, 9591–9613.

Wallace, J. M., 1975: Diurnal variations in precipitation and thunderstorm frequency over the conterminous United States. *Mon. Wea. Rev.*,103, 406–419.

Wallace, J. M. and P.V. Hobbs, 2006: Atmospheric Science: An Introductory Survey, Academic Press, 2nd edn., pp.

Zhou, J. and K. M. Lau, 1998: Does a monsoon climate exist over South America? *J. Climate*, 11, 1020-1040.

Zipser, E.J., and K.R. Lutz, 1994: The Vertical Profile of Radar Reflectivity of Convective Cells: A Strong Indicator of Storm Intensity and Lightning Probability? *Mon. Wea. Rev.*, **122**, 1751–1759.

Zipser E. J., D. J. Cecil, C. Liu, S. W. Nesbitt, and D. P. Yorty, 2006: Where are the most intense thunderstorms on Earth? *Bull. Amer. Meteor. Soc.*, **87**, 1057–1071.